INVESTIGATION AND CONTROL OF THE STATIC ELECTRIFICATION IN POLYPROPYLENE

A THESIS SUBMITTED TO

THE GRADUATE SCHOOL OF ENGINEERING AND SCIENCE

OF BILKENT UNIVERSITY

IN PARTIAL FULFILLMENT OF THE REQUIREMENTS FOR

THE DEGREE OF

MASTER OF SCIENCE

IN

MATERIALS SCIENCE AND NANOTECHNOLOGY

By

Zelal Yavuz

August 2016

INVESTIGATION AND CONTROL OF THE STATIC ELECTRIFICATION IN POLYPROPYLENE

By Zelal Yavuz

August 2016

We certify that we have read this thesis and that in our opinion it is fully adequate, in scope and in quality, as a thesis for the degree of Master of Science.

_____

H. Tarık Baytekin (Advisor)

_____

Tamer Uyar

_____

Gülay Ertaş

Approved for the Graduate School of Engineering and Science:

_____

Levent Onural

Director of the Graduate School of Engineering and Science

ABSTRACT

INVESTIGATION AND CONTROL OF THE STATIC ELECTRIFICATION IN POLYPROPYLENE

Zelal Yavuz
M.Sc. in Materials Science and Nanotechnology
Advisor: Hasan Tarık Baytekin
August 2016

The electrostatic charging of polymers due to friction is such a common phenomenon in daily usage of polymers that can be a problematic issue for various applications, such as in electronic devices, textile, space industry and so on. Hence, understanding and controlling of the mechanism behind the static electrification, which is basically because of the charge accumulation on the material, is an important subject in terms of the applications.

In the way to understand static electrification of bulk materials, examining the physical and morphological properties is crucial. On the other hand, when the physical properties are considered, the structure of polymer plays a significant role, yet there is a lack of knowledge in the literature about the relation between these structural properties and triboelectricity. As a reason of this, it can be pointed out that in the proposed mechanisms about the frictional electrification the structure-property relation could not get sufficient attention so far. In this thesis, the crystalline structure of polymer, which plays a crucial role in the determination of physical properties of polymeric materials, was studied and by using different treatment techniques, such as microwave radiation and mechanical stress, and the relation between the degree of

crystallinity and triboelectric charging was investigated. Due to its economical cost and heat-sensitive degree of crystallinity that can be changed in a significant way polypropylene (PP) which is a semi-crystalline polymer was used in this study. Hence, by utilizing different spectroscopic and microscopic techniques the relation between physical properties and triboelectrification of polypropylene was investigated in detail. In order to understand the physical and chemical changes taking place in untreated and treated polypropylene X-ray Photoelectron Spectroscopy (XPS), Raman Spectroscopy, X-ray Diffraction (XRD), Atomic Force Microscopy (AFM), Differential Scanning Calorimetry (DSC) are the techniques that were employed.

In this study, by considering the mechanism behind static electrification the potential link between electrification and degree of crystallinity was designated. Furthermore, the generation of charge on the surface of mechanically treated polypropylene film was observed for the first time by this current work. The results lead to the fact that it is possible to convert mechanical energy into electrical energy without any contact between the objects by introducing physical forces onto the insulating materials and the reasons behind non-contact electrification was investigated. Therefore, in the light of the results obtained from this study, more efficient triboelectric generators can be designed to harvest electrical energy from mechanical energy.

Keywords: physical properties, crystallinity, polypropylene, static electrification, triboelectric charging, triboelectrification.

ÖZET

POLİPROPİLENDE STATİK ELEKTRİKLENMENİN İNCELENMESİ VE KONTROL ALTINA ALINMASI

Zelal Yavuz
Malzeme Bilimi ve Nanoteknoloji Programı, Yüksek Lisans
Tez Danışmanı: Hasan Tarık Baytekin
Ağustos 2016

Polimerlerin gündelik hayatta dokunma ve sürtünme sonucu elektriksel yük ile yüklenmeleri sonucu açığa çıkan statik elektriklenme olayı oldukça sık karşılaşılan bir durum olmakla birlikte, bu durum polimerlerin kullanıldığı birçok alanda, örneğin elektronik cihazlarda, tekstil sanayisinde ve uzay endüstrisinde sorun yaratabilmektedir. Bu sebeple, ani elektriksel yük birikmesi ve yük boşalması sonucu ortaya çıkan statik elektriklenmenin mekanizmasını anlamak ve kontrol altına alabilmek uygulamalar açısından son derece önemli bir konudur.

Yalıtkan ve büyük ölçekli malzemelerin statik elektriklenmesini anlamaya çalışırken, fiziksel ve morfolojik özellikleri incelemek kritik bir rol oynamaktadır. Öte yandan, fiziksel özellikleri ele alındığında polimerlerin yapısının önem arz ettiği görülmekte olup bu yapısal özellikler ile triboelektriklenme arasındaki ilişki hakkında literatürde çok sınırlı miktarda bilgi yer almaktadır. Bunun nedeni olarak sürtünme elektriklenmesinin aydınlatılması konusunda şu ana kadar önerilen mekanizmaların yapı-özellik ilişkisini genellikle göz ardı etmiş olması gösterilebilir. Bu tez çalışmasında, polimerlerin fiziksel özellikleri ele alındığında önemli bir faktör olan kristallenme üzerinde çalışılarak, farklı muamele teknikleriyle (örneğin, mikrodalga

ışıması, mekanik gerilme) değiştirilen kristallik derecesi ile triboelektrik yüklenme (yada yük oluşumu) arasındaki ilişki çalışılmıştır. Yarıkristal özelliğe sahip olan polipropilen (PP) hem ekonomik değerinden dolayı hem de kristallenme derecesinin ısısal işlem sayesinde oldukça farklı değerler alabilmesi nedeni ile seçilmiş ve bu tezde farklı spektroskopik ve mikroskopik teknikler kullanılarak PP in fiziksel özellikleri ve triboelektriklenme özellikleri arasındaki ilişki detaylı bir şekilde ortaya konulmaya çalışılmıştır. Muamele edilmiş ve edilmemiş polipropilende meydana gelen fiziksel ve kimyasal özelliklerindeki değişimleri anlayabilmek için X-ışınlı Fotoelektron Spektroskopisi (XPS), Raman Spektroskopisi, X-ışını Saçılma Difraktometresi (XRD), Atomik Kuvvet Mikroskobu (AFM), Diferansiyel Tarama Kalorimetresi (DSC) tekniklerinden yararlanılmıştır.

Bu çalışmanın ilk bölümünde öncelikle statik elektriklenmenin mekanizması göz önünde bulundurularak elektriklenme olayı ile polimerlerin fiziksel özelliklerini belirleyen en önemli faktörlerden biri olan kristallenme derecesi arasında var olduğu düşünülen ilişkiler belirlenmiştir. Çalışmanın ikinci bölümünde ise, mekanik gerilime maruz kalan bir polipropilen film yüzeyinde elektrik yükü oluştuğu da ilk defa olarak bu çalışmada gözlemlenmiştir. Bu sonuçlar, yalıtkan malzemelere fiziksel kuvvetler uygulayarak, etkili bir şekilde mekanik enerjiyi elektrik enerjisine dönüştürmenin cisimler arasında dokunma olmadan da mümkün olduğunu göstermiştir. Bu olayın sebepleri açıklanmaya çalışılmıştır. Bu çalışmadan elde edilen bilgiler ışığında mekanik enerjiden elektrik enerjisi elde edebilen daha verimli triboelektrik jeneratörlerin tasarlanabileceği düşünülmektedir.

Anahtar Kelimeler: fiziksel özellikler, kristallik, polipropilen, statik elektriklenme, triboelektrik yük, triboelektriklenme.

Acknowledgement

First and foremost, I would like to express the deepest gratitude to my advisor Asst. Prof. H. Tarık Baytekin. He enabled me to gain a broad scientific perspective and scientific enthusiasm. He taught me how to found a laboratory with hard working and patience. I learned a lot in this research group thanks to my advisor and his valuable advices. In the first place, I learned not to give up in any case since there is a light at the end of the tunnel if we insist enough. I would like to thank my advisor for his knowledge, supervision, encouragement, patience, and guidance throughout my studies.

I want to express my thanks to our research group members Umar Gishiva Musa and Doruk Cezan for their valuable help and support in the lab.

I would like to thank the National Nanotechnology Research Center (UNAM) and Bilkent University for their support and for providing the researchers with pleasant facilities and high-tech modern equipments.

I present my special thanks to the precious friends from UNAM, especially to the members of 3rd floor. They became my group members as well during all the time in my master's period.

I want to express my special thanks to Ebru Şahin Kehribar, Elif Duman Ergül, and Tuğçe Önür for their valuable companionship, support, and friendship that I hope will last in the future.

During all the time in Bilkent, I have been very pleased and felt privileged to be with you Canan Erdoğan, Aybegüm Samast, Merve Tohumeken, Şehmus Tohumeken, Çisil Karagüzel, and Merve Alabak. We shared lots of memories which will not be forgotten.

I want to thank my little cousins Zeynep Duru and İsa Eren for their lovely support during my thesis period.

I would also like to express my gratitude to TÜBİTAK (Project number: 214M358) for the financial support during my studies.

Last but not least, I present my special thanks to my dear family. I am so grateful for your continuous support and encouragement in all my life. More than anything, thank you for your unconditional love.

To My Sister

Contents

List of Figures

List of Tables

List of Abbreviations

PP	**:**	Polypropylene
ESD	**:**	Electrostatic discharge
TENG	**:**	Triboelectric nanogenerator
T_m	**:**	Melting temperature
T_g	**:**	Glass-transition temperature
PE	**:**	Polyethylene
LDPE	**:**	Low-density polyethylene
HDPE	**:**	High-density polyethylene
L_o	**:**	Gauge length
L	**:**	Total length
W	**:**	Width
POM	**:**	Polarized Optical Microscope
AFM	**:**	Atomic Force Microscope
KPFM	**:**	Kelvin Probe Force Microscope
XRD	**:**	X-ray Diffraction
DSC	**:**	Differential Scanning Calorimetry
XPS	**:**	X-ray Photoelectron Spectroscopy
Q	**:**	Charge
nC	**:**	Nanocoulomb
ms	**:**	Millisecond
s	**:**	Second

h	**:**	Hour
σ_y	**:**	Yield strength
σ	**:**	Stress
ε	**:**	Strain
EL	**:**	Elongation
Cu	**:**	Copper
RH	**:**	Relative humidity
CE	**:**	Contact electrification
SE	**:**	Separation electrification
I_c	**:**	Convergent induction
I_d	**:**	Divergent induction

Chapter 1

Introduction

1.1 Overview of problem in triboelectricity

Tribology focuses on the friction, lubrication and wear of the interacting surfaces which are in a relative motion. [1] One very closely related field to this well-known engineering and science concept is tribocharging or triboelectricity. [2] Tribocharging is a very common phenomenon and it is observed very often in our daily lives e.g. a piece of wool is get charged and attracts some other materials when it is rubbed, or an air balloon attracts other materials or can be held by the ceiling for some time when it is rubbed against e.g. a piece of paper or hair especially in a dry day. However, generation of charges during the tribocharging event by some mechanical means such as sliding, rubbing, or contact is not fully understood and many questions have not been answered yet regarding clarification of the charge generation mechanism. For example, the source of electrons in tribocharging is still unclear if the mechanism is based on the electron transfer for insulating materials? what is the fundamental reason for a better charging in a dry atmosphere? why the charging is very low in an inert atmosphere? how is it possible to light a lamp without electrons regarding ion-transfer mechanism? why different materials charge differently? Nevertheless, various research groups working on this field indicated that physical, chemical and mechanical properties of the materials and external conditions effect the tribocharge formation. Therefore, we believe that the investigation of the physical properties of the materials and the correlation between these properties and

triboelectric charge generation would be a very good starting point to understand the fundamentals of the problem in tribocharging.

1.1.1 Historical Development of Triboelectricity

When two materials are brought into physical contact and separated, charging occurs and this phenomenon is called as ‘contact electrification’. [3-15] Albeit, it is more obvious for the contact of insulator materials owing to their ability to retain the charge for a long time. Without considering the contact electrification, the practical applications of friction appears in pre-historical times when the man use the frictional heat for lighting of fires. [16] On the other hand, the origin of tribology studies is based on the experiments of Thales of Miletus, a pre-Socratic Greek philosopher, showing that the electrostatic charging is caused by rubbing amber against wool, and this is the preliminary demonstration of ‘triboelectric’ effect that means ‘rubbing amber’ in Greek. [2] Later, William Gilbert (1544 – 1603) focused on the ‘amber effect’ and he found out that different materials other than amber attract each other when they are rubbed. After the first indications on electrostatic charging related with the charging behavior of amber as a result of friction, Gilbert states "There is in amber something flame-like, or having the nature of the breath and this, when the paths are cleared by friction of the surface, is emitted and attracts bodies" as a quotation from Plutarch (c46-120) who was another Greek philosopher. [17] Then, with the observation of Gilbert around 1600, this effect was called as ‘electric’ coming from *elektra*, which is used for ‘amber’ in Greek. [18] As it was hypothesized in seventeenth century by Cabeo, Digby, Gassendi, Descartes, Boyle, and Newton several charging mechanisms were proposed, subsequently considerable increase of the interest towards the

experimentation in electrostatics was observed. [19-21] However, the complexity of the subject still remains to date. The subsequent studies in this concept came from Benjamin Franklin who made the distinction between positive and negative charges in 1740 and Faraday who analyzed the frictional electricity of steam and water against other materials. [18, 22-24] Later on, substantial experimental and theoretical electrostatic studies were carried out by Coulomb, Maxwell, Faraday, Volta, Tesla, Kelvin, Rutherford and Bohr, and the results of all these early stage studies were supported by Maxwell's Treatise. [25]

1.1.2 Examples of Contact Electrification

Contact electrification and dispersal of static charge has a considerable importance in today's technology when considering the manufacturing electronic devices, fabrics and applications of polymeric films in many different fields (auto industry, space applications, textile *etc.*). In other words, contact electrification or triboelectrification process occurs for insulating materials has a dramatic practical importance. Consequently, the wide range of polymer use and its tribocharging due to contact or friction makes the better understanding of this phenomenon necessary. As a result, the subject has caught academic and industrial interest to a great extent nowadays. As it is indicated by Baytekin *et al.* the increasing demand for polymers, that is 454 billion $ for now and 567 billion $ for 2017, and the use of polymers in electronic device components, also in terms of the size of chips that is getting smaller and smaller makes the triborcharging of polymers and charge dissipation becomes a much more important issue. [26] On the other hand, tribocharging has considerable negative side effects whereas its useful applications are present in technological

devices. Since it is hard to get rid of electrostatic discharge (ESD) despite it can be generated easily there are numerous problems are observed in industry, for instance in the fabrication of synthetic films or fibers as they cling on the machinery parts due to the charging that cause the working of the production line stop. [27] As it is pointed out, common hazardous way of tribocharging experienced in industrial processes of fiber spinning, tanker explosions due to the ignition of explosive vapors or defects in the fabrication in photographic films. Yet, the helpful use of tribocharging in applications are widespread, such as xerography, electrostatic spraying or electrostatic separation in the recycling industry and so on. [5, 28-30]

In terms of the examples of contact electrification (i.e. triboelectrification) there are so many areas from electronics to pharmaceutics. Thus, a few of them are covered here.

- Undesirable explosions: When the charge is built-up on the surface of material as a result of contact electrification, it causes sparks that can lead to serious explosions in the presence of any flammable material in the environment. In particular, these kind of explosions are very crucial for granular systems, such as pneumatic conveying and fluidized bed processes. [31-33] Large surface to volume ratio of these highly dispersed particles leads to increase in the area of contact and accumulation of significant amount of charge that cause the combustion during the charge dissipation to the air containing oxygen. [34, 35]
- Xerography (Electrophotography): Whole electrophotographic devices' (e.g. laser printing, photocopying) working principle relies on the contact charging. The toner particles are charged by rubbing them against metal beads that leads

to the attraction of toner particles to corona-charged drum. As a result of patterning, the process is completed. [36, 37]

- Separation of mixed granules: In industrial applications, triboelectrification is utilized as a charging technique in order to sort the mixed granular insulators. The devices used for this purpose are called triboelectric separators. [38-40]
- Space industry: The importance of contact charging is apparent in space applications because many dust storms are known to occur in Moon and Mars, which are much greater than those on Earth that leads to significant amount of charging among the dust particles. Consequently, the electric fields resulting of charged particles which adhere to the astronauts' spacesuits and spaceships can cause serious problems in electronic and mechanical equipments. [41-45]
- Pharmaceuticals: In the production of pharmaceutical chemicals, the powder form is used in the process and contact charging arises during the flow of particles. Due to the electrostatic charge that occurs during the process, problems in the uniformity of blending (i.e. segregation, agglomeration) and non-homogenous dosages are observed. [46-49] Moreover, in pharmaceutical devices using for dispersion purposes, such as dry powder inhalers (DIP) triboelectrification can cause negative effects on the way of introducing particles into the body. [50]
- Electronics: In the electronic devices, with the result that contact charging excess amount of charge is built-up on the components, then ESD occurs which causes serious damages on the electronic parts. Therefore, controlling and preferably eliminating the contact charging is a need for manufacturing of electronic devices. As it is stated in Intel Packaging Data Book, approximately

12000 V of static electricity can be generated by just walking on the vinyl floor which is much greater than the charge that is enough to cause a damage a standard Schottky TTL component. [51]

1.1.3 The Mechanism Behind Contact Electrification

There have been significant efforts to understand the mechanism of contact electrification even though the phenomenon itself is known for decades. In particular, understanding the mechanism behind the contact electrification for insulators (e.g. polymers) is much more complex than for metals. The main reason for this is because the gap between the filled valence band and the unfilled conduction band is much greater than the possible thermal energy in insulators that hinders the electron transfer. [3] On the other hand, contact electrification between two metals that is based on the difference in work functions is considered to be more straightforward than insulators. In metals, there are partially filled electronic states containing vacant conduction states and occupied valence states that are infinitesimally higher in energy than the vacant conduction states. The highest occupied energy state of the valence band is defined by the Fermi level or work function (i.e. the energy needed so that an electron can be removed from the surface). Hence, the contact electrification mechanism of metal surfaces relies on the electron transfer from the material having lower work function (i.e. larger Fermi level) to the material having larger work function (i.e. lower Fermi level). [3, 52] As a result, present difference between the Fermi levels of metals facilitates the electron transfer during the contact of metal surfaces. Possible tribocharging mechanisms via transfer of an electron and transfer of an ion for materials that are made of metal and insulator are depicted in Figure 1.

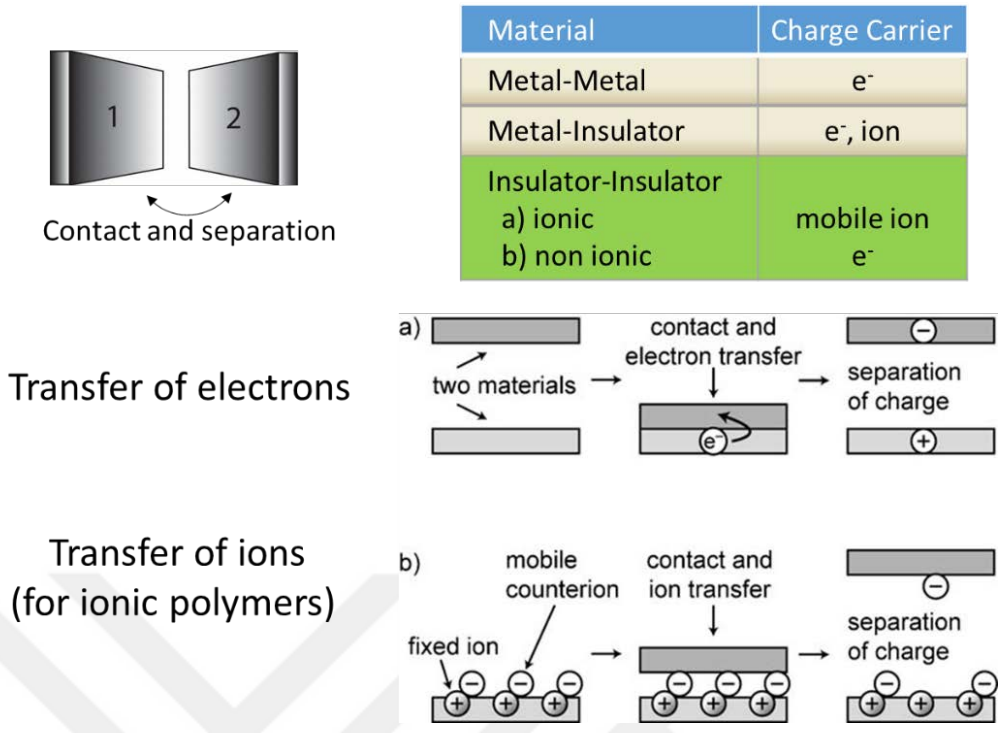

Figure 1. Possible mechanisms of charge transfer, a) transfer of an electron, b) transfer of an ion. (Copyright © 2008 Wiley. Reproduced with permission from ref [65]).

- Electron exchange: The gap separating unfilled conduction band and filled valance band is much larger than the available thermal energy in insulators. Hence, an electron cannot be moved into the valence band as it is filled and it cannot be moved into the conduction band because much higher energy is needed. [3] As a result, electron transfer seems thermodynamically not favorable for insulators. However, there are defects or so-called “trap” states located in the band gap are which partially resided by electrons that are not in their lowest energy state (i.e. not in the stable state). Hence, the magnitude of charge transfer and the resulting sign on the contacted materials depend on the density of these states and the ability of transfer between the states which are at different energy-level.

The existence of trapped electrons which are described as non-equilibrium electrons are remarked by Truscott and Lowell. [53] Later, by the thermoluminescence and phosphorescence analysis they observed that the trapped electrons may persist in high energy level for a long time. [54-56] Thus, the conductivity that provides contact charging in insulators is the result of the existence of these trapped electrons. In order to enlighten the reason for why the trap states containing non-equilibrium electrons appear it has been suggested that the chemical and conformational defects leads to the occurence of these states. [57-59] Another proposed explanation is that the interaction of material surfaces during the contact forms these states. [60, 61] It is pointed out by Seanor that the observed behavior as a consequence of traps may be because of the disorders present in the polymer structure that can be due to the impurities left over from the manufacturing process. [24] Furthermore, as it is stated by Mort *et al.* even present oxygen in the environment can play a significant role for the electronic transfer and contact electrification in terms of low conductivity polymers. Also, adsorbed molecules or the products formed as a result of the interaction between atmospheric molecules and the polymer surface can change the way of electron transfer, subsequently contact electrification. [6, 10, 11, 62, 63] Therefore, the nature of the process for the electron transfer in polymers remains elusive and the parameters that affect the charging are various.

- Ion exchange: There are polymeric systems whereby ion transfer leads to the conductivity and electrification. This mechanism is related with the polymers containing ions, such as polyelectrolytes and ionomers. It leads to the ionizing

with the help of present structural groups that are capable of ionization. The mechanism works in such a way that when two materials that have loosely bound ions and counter ions (i.e. strongly bound) in different polarities the loosely bound ions transfer to the other surface, leaving the host surface with a net charge of the strongly bounded ions. As Diaz and Guay indicate that ionic transfer for the materials containing ionomers is based on correlations between the sign of the charge transferred and the sign of the mobile ion species on the surface the beads taking place in the charge transfer. [64] Hence, ion transfer is proposed as the mechanism for contact charging if salts with mobile ions are present in the polymer.

- Material or Mass transfer: During the contact charging between polymers provides mass transfer at the same time. It is suggested by Baytekin *et al.* that 'mosaic' patterns of charging occur because of the material transfer driven by bond breaking which leads to the heterogeneous alterations on the polymer surface. They revealed the charge mosaics by Kelvin Force Microscopy (KFM) that presents information about the surface charge and confirmed the presence of material transfer with X-ray Photoelectron Spectroscopy (XPS). [66] Thus, during the material transfer between the contacted polymer surfaces bond-breaking and bond-forming take place simultaneously where the atomic-scale changes on the surfaces occur. As it is indicated by Salaneck *et al.* the non-destructive XPS technique makes it possible to detect the material fragments on the polymer surface after the material transfer occurs during the contact. [67]

In addition, by using XPS technique Piperno *et al.* showed that the ability of surfaces to adsorb ions differs in addition to material transfer during the contact of two materials. [68] Consequently, about contact charging it can be said that it is not directly based on only the material transfer, but also on the changes of surface properties. Furthermore, it is considered that for the bond-breaking and bond-forming processes both electronic and ionic transfer mechanisms are involved.

- Mechanochemical transfer: In addition to material transfer during the contact electrification of polymers, also radicals are produced as a result of rupturing in chemical chains. These free radicals which are formed because of mechanical stress is called 'mechanoradicals.' If the bond-breaking is homolytic a pair of radicals is formed whereas if it is heterolytic scission then a negative or positive ion pair is formed. [51] Thus, the electrons released by mechanoradicals or ions released by heterolytic bond cleavage are transferred between the contacted surfaces resulting with the net charging of polymers.

It is considered that there is no single mechanism that reveals triboelectrification (or contact electrification as a special case). Nonetheless, all mechanisms revised above play a part and it is supported by various spectroscopic experiments that the contact which creates stress on the polymer surface produces electrons, ions, and radicals. [69-73] Our research is based on the electrification in polymers, the mechanism behind the contact electrification will be discussed for insulators in the following subsections.

1.1.4 Triboelectric Energy Harvesting Based on Contact Electrification

In this part, polymer-based triboelectric (or electrostatic) generators will be discussed. Since our experimental results are focused on the tricoelectrification of Polypropylene (PP), investigation of the practical or technological use of polymers is important. When today's worldwide problem related with the energy supply is considered, energy harvesting draws intense attention. In this respect, mechanical energy, owing to its abundant availability, is an ideal source that can be benefit from in order to tailor to our needs for energy supply.

When electrostatic generators are taken into account, contact electrification is the base for working of these mechanical devices. On the other hand, materials that have ability of strong triboelectrification effect are less conductive or insulators (e.g. polymers), hence they can retain the charge for an extended period of time. [74] The working principle that tribogenerators rely on is that the contact-induced electrification whereby the materials with different tribo-polarity become electrically charged through contact-separation or relative sliding against each other. When two different materials brought into contact, charging via electron, ion, radicals or material transfer occurs. The most popular tribogenerators are the Van de Graaff and Wimshurst generator, which were invented 1929 and ~1880, respectively. [26, 74, 75] These machines use the accumulated static charges generated by triboelectrification and generates high electric fields to accelerate particles. In addition to mechanical energy harvesting, the other application of tribogenerators is their use of as a self-powered active sensors because they do not need any external source of power to drive. [74, 76] Besides, harvesting energy for nanosystems has been developed nowadays, then

triboelectric nanogenerator (TENG) is commercialized that is considered to be an outbreak in academy and technology. Subsequently, there are many research going on by chemists and materials scientists to increase energy density in TENGs through altering the materials or their morphological properties. [77-81] The mechanism of the TENG can be explained as a combination of electrostatic induction with the conjunction of triboelectrification. As it can be seen in the following schematic representation the fabrication of the implantable TENG (iTENG) is based on the design of a fully packaged structure.

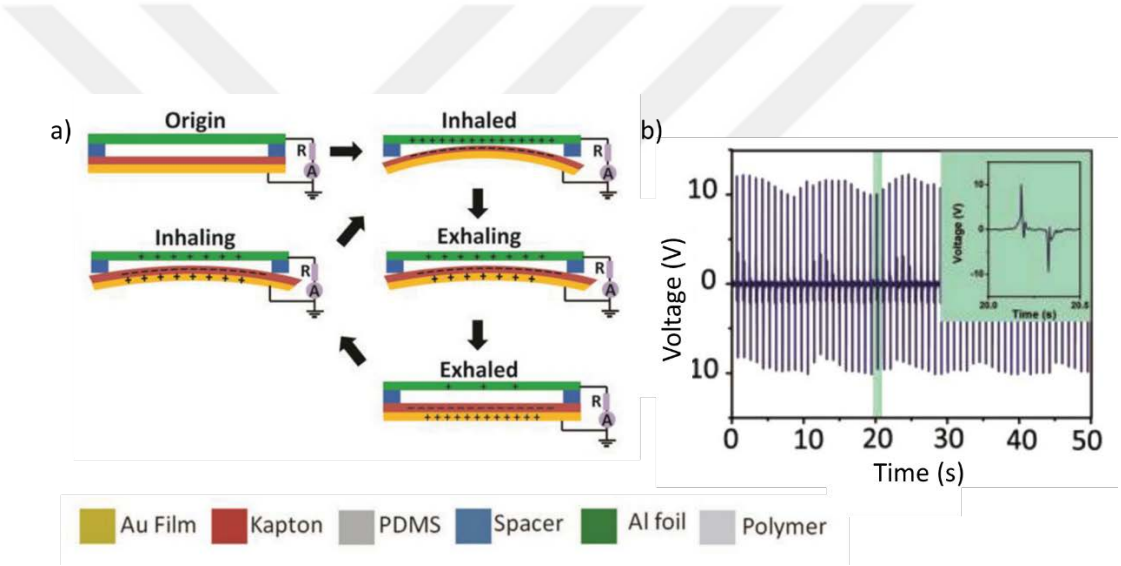

Figure 2. a) Working principle of iTENG, b) Typical voltage output of the iTENG. (Copyright © 2014 Wiley. Reproduced with permission from ref [82]).

It is obvious that channeling the available, however wasted mechanical energy into the power source in order to meet the need of energy supply problem is significantly important. Despite there are various useful technological applications of converting mechanical energy to electricity by contact of insulators, we observed that it is also possible to produce electricity without any contact, but by just applying mechanical stress to a polymer film. The novelty of our study is in the investigation of

practical energy harvesting and to gain a control on the electrification by altering the physical parameters of the material (i.e. degree of crystallinity, roughness). The experimental details and results will be provided in the following sections.

1.2 The Effect of Physical Properties of Materials in Tribocharging

Physical properties of polymers play a crucial role on mechanical strength of polymers when the industrial applications are taken into account. Recent studies showed that these properties can also have high effect on the generation of charge and thus on electrification of polymers. For example, change in elastic properties can determine the charging behavior of two contacting polymeric materials. [14] However, the relation between the polymer structure, which has a big influence on the determination of physical properties, and the triboelectrical properties has not been studied in detail and remains still unclear. In this study we modified the structure of PP and investigated the relation between its physical properties and its tribocharging behavior by using various spectroscopic and microscopic techniques. We think that the outcomes of this study will be one of the milestones for the fundamental research in tribology and hopefully our results will be considerably useful to solve industrial problems arising from tribocharging.

1.2.1 Polymer Crystallinity

In the macromolecular polymer structure, the polymer chains can be highly ordered (crystalline regions) or can be in random coil orientation (amorphous regions). The crystallinity degree is determined by the volume percentage of crystalline regions corresponding to the total volume in the polymeric structure. Moreover, the degree of

crystallinity can change from polymer to polymer, even for the same polymer it can alter because of different treatments of the polymer or due to the differences in the production of polymers. To illustrate, the differences in crystallinity for the same polymer may arise from factors, such as melting and cooling rate, pulling speed or stress applied during pulling of fibers that influence regularity of the polymeric chains during the fabrication process. [83-85] Therefore, depending on the process conditions different % crystallinity can be obtained. In Figure 3 the distribution of crystalline and amorphous regions is depicted schematically.

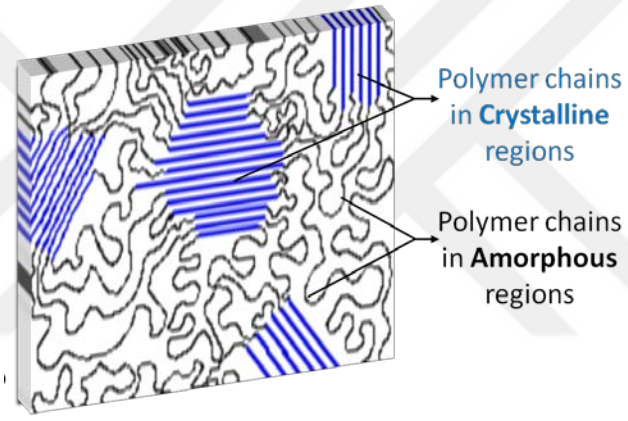

Figure 3. In a semi-crystalline polymer, the distribution of mixed amorphous and crystalline regions.

The well-ordered crystalline regions are also called ‘crystallites’ in which the polymer chain segments are oriented regularly with respect to each other, see Figure 3. [83, 86] Between these well-ordered crystallites there are irregular regions, which have random-coil orientations having amorphous character. The degree of crystallinity plays a significant role in the determination of polymers’ physical and mechanical properties, such as its melting temperature (T_m), glass transition temperature (T_g), hardness/softness, ductility, modulus, mechanical strength and so on. Thus, even two

polymers have the same chemical formula, if their crystallinity degree differs, their physical, mechanical, optical, thermal, electrical properties may be different. Hence, crystallinity becomes highly important when different areas, applications or purposes are considered in the use of polymers. For the determination of the degree of crystallinity, Differential Scanning Calorimetry (DSC), X-ray Diffractometer (XRD), Raman Spectroscopy were used in our study (see Characterization Techniques in Chapter 2). In this thesis, our main approach is that to combine structure and physical properties of PP with its mechanical and tribological behavior. Hence, we investigated the effect of polymer crystallinity on its mechanical and electrical features so that the results can be used for both scientific and industrial purposes.

1.2.2 The Relation Between Crystallinity of Polymers and their Triboelectrical Aspects

It was demonstrated in previous studies that the oxidation and morphology of materials' surfaces are the important parameters that cause alterations in their contact electrification. As it is indicated by Li *et al.* surface roughness can considerably change materials' electronic properties, then it controls the extent of contact between two surfaces. [51, 87, 88] In addition to this indication, it is stated that there is a correlation between surface roughness and charging by Coste *et al.* and Ohara *et al.* [89, 90] On the other hand, no clear link has been established between crystallinity and electrification. In our experiments, charge increased as the degree of crystallinity decreased. Although the alterations in physiochemical properties of a material surface in terms of the charge transfer has been investigated in many studies, the effect of crystallinity in contact electrification could not draw attention. However, the results of

our research show that physical properties of polymers, especially crystallinity, has a significant role as it controls the surface roughness and the extent of contact electrification.

In this thesis, crystallinity of PP samples treated with different experimental techniques (i.e. microwave radiation and mechanical stress) were analyzed. After the investigation of changes in crystallinity for PP samples through the treatments, triboelectrical properties of these samples were analyzed. As different degree of crystallinity leads to the changes in a way of charge transfer, considerable alterations in triboelectrical aspects of the samples were observed. Besides, the reason for different behavior of the samples which have different degree of crystallinity in the contact and non-contact charging needs to be understood. Then, the results which will be obtained from the experiments in this field can be used in various applications of polymers in which static electrification has a notable importance.

1.3 Polypropylene

Polypropylene (PP) is a thermoplastic polymer, which is formed by the polymerization of propylene monomers into the long PP chains. The chemical formula of PP is $(C_3H_6)_n$ and its structure can be designated as in Figure 4.

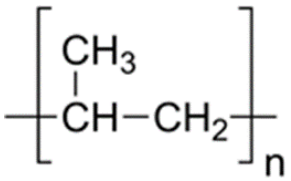

Figure 4. Structure of polypropylene.

In 1954, with the successive work of K. Ziegler and G. Natta the first PP was produced by the polymerization of propylene monomers. Later, in 1957 the most widely used form of commercial PP was produced by Montecatini through the linkage of monomers with the help of Ziegler-Natta catalysts (i.e. Al and Ti based catalysts) that leads to the crystallizable chains. [83, 91, 92] The orientation of the methyl groups (CH_3) during the linking of monomer molecules brings the concept of tacticity into the consideration. If all the methyl groups are on the same side across the backbone chain, it is called isotactic PP (see Figure 5). If the pendant methyl groups are attached to the backbone chain in an alternating manner, it is called syndiotactic PP (see Figure 6). A PP structure, where the methyl groups are positioned in a random manner on the polymer backbone chain, is referred to atactic PP (see Figure 7).

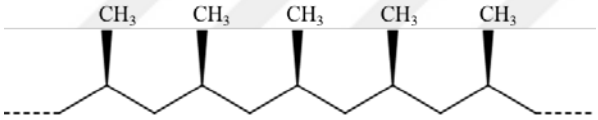

Figure 5. Structure of isotactic PP.

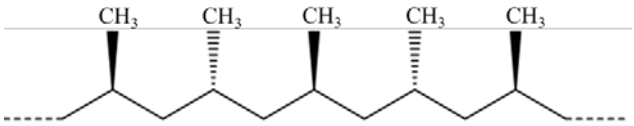

Figure 6. Structure of syndiotactic PP.

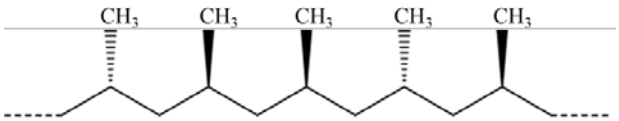

Figure 7. Structure of atactic PP.

When the isotactic PP is considered the methyl groups would be expected to inhibit the packing of the chains. However, these pendant groups (CH_3) impose a helical twist on the backbone of the polymer, then crystallization can occur. The helical structures can pack to form crystal. On the contrary, the atactic PP does not form a helical structure and crystallization is hindered. As a consequence, atactic PP is a soft, flexible solid and is used as an additive to lubrication oils, whereas the isotactic PP is rigid and used for fabrication of hot water pipes in plumbing applications. [93]

In a wide-range industrial use of PP, it is reported that the most commercial form is isotactic PP that has the required properties for a useful plastic material, as isotactic PP is crystallizable, while atactic PP is noncrystallizable. [91] Thus, the relative orientation of the pendant groups against each other is significant in terms of the PP's ability to form crystals which is important in the determination of physical and mechanical properties.

1.3.1 Structure of Polypropylene

PP is a linear hydrocarbon polymer that at first glance approximately resembles polyethylene (PE) which makes PP and PE share many similar properties including electrical behavior. [91] However, the existence of pendant methyl group varies the properties of PP in many ways from PE. For instance, it makes PP chains stiffer and its melting temperature higher even though there is reduction of symmetry in the polymeric chain. In addition, because of pendant methyl groups the tensile strength and modulus of PP are higher compared to PE. On the other hand, the physical, thermal, and mechanical properties of PP can vary by its tacticity, % crystallinity, molecular weight and its distribution. [91] The important parameter for our study is

the percent crystallinity, which is originated through the amount of crystalline and amorphous regions formed by the polymer chains, has significant impact on the physical properties of PP.

The linearity of molecular chains in PP gives an ability to form ordered crystal structure in a way that the chains are packed regularly. However, in some regions the chains may be entangled leading to forming of branches that makes the structure not perfectly regular. Therefore, PP is defined as a semi-crystalline polymer consisting of crystalline and amorphous segments.

In the determination of percent crystallinity and crystal structure, thermal history on the polymer is important that the working principle of thermo-analytical devices is based on (see Characterization by Analytical Techniques section in Chapter 2). As the crystallinity increases density, hardness, modulus, barrier properties, wear and abrasion resistance of the polymer increase, too. On the other hand, when the crystallinity decreases better transparency (advantage for packaging), capability of good thermoforming and good processibility are obtained. [91]

1.3.2 Basic Properties of Polypropylene

Polypropylene is a viscoelastic material, like other thermoplastics. In other words, it exhibits both viscous material's property (i.e. resistant to shear flow and strains in a linear way according to time when stress is applied) and elastic material's property (i.e. quickly returns its original state when the stress is released). Hence, the viscoelastic behavior of PP is described with a strain rate dependence on time that makes the mechanical properties of PP time and stress related. [91, 94]

1.3.2.1 Density

The density of polypropylene is between 0.895 and 0.92 g/cm^3 and typical density of isotactic polypropylene (i-PP) is 0.9 g/cm^3 which makes i-PP the lightest viscoelastic material among the widely used thermoplastics. This feature of i-PP provides the manufacturers with the advantage of constructing many items easily. [91]

1.3.2.2 Mechanical Properties

The mechanical strength of PP is closely related with its degree of crystallinity. As the crystalline phase of semi-crystalline PP maintains mechanical strength, it has high tensile strength, hardness, and stiffness which are the main interest of product design engineers. Albeit, increase in molecular weight causes decrease in its tensile strength, hardness, and stiffness while that leads to the raise in impact strength of PP. [91, 95]

1.3.2.3 Electrical Properties

PP is a good electrical insulator whereby it is a nonpolar hydrocarbon. As it was stated before in Structure of Polypropylene section, PP is in a good similarity with PE in terms of electrical aspects. To clarify, the dielectric strength (i.e. a measure of dielectric breakdown resistance under an applied voltage) of PP is 28 MV/m whereas it is 27 MV/m for low-density PE (LDPE) and 22 MV/m for high-density PE (HDPE). Additionally, the volume resistivity (i.e. electrical resistance when an electrical potential is applied) of PP is 10^{17} Ω cm while it is 10^{16} Ω cm for LDPE and 10^{17} Ω cm for HDPE. [96] In general, PP exhibits low dielectric constant and significantly high electrical resistivity and a good material for electrical insulation.

1.3.2.4 Thermal Properties

In the use and processibility of polymers, their response to the temperature changes is important as their physical, chemical, and electrical properties are very sensitive to temperature. The mechanical properties of PP is mainly determined by its crystallinity and glass transition temperature (ie. the temperature at which the material changes from a glassy hard state to a soft state).The second-order glass transition temperature of PP is -10 ^{0}C (predicted). The actual value can be found in the range of 0-20 ^{0}C that depends on the rate of heating. Further, its crystalline melting point is in between 160-170 ^{0}C and recrystallization temperature is found in the range of 115-135 ^{0}C with the slow cooling rate of the melt. [91] Different morphological forms of PP shows different melting behaviors. For example, beta form of PP which has a hexagonal unit cell melts at 152-155 ^{o}C, and monoclinic alpha phase melts at higher, 165-168 ^{o}C. These two forms of PP have their characteristic XRD signals.

1.3.3 Applications and Importance of Polypropylene

PP has a high-volume usage in industry due to its excellence in physical, thermal, and mechanical properties. First of all, it is a low-cost engineering plastic. Its resistance to higher temperatures and high stiffness at low density are the key characteristics of PP. Secondly, it offers good chemical and fatigue resistance, good hardness, good external stress cracking resistance and ease of machining, together with good processibility that makes PP highly important and requested among the commonly used commodity materials. Its high flexibility, low density, and resistance to corrosion make PP the material of choice for many applications. [91, 97]

Some of the main applications of PP are the household items (bottles, bottle caps, buckets, bowls, luggage *etc.*), packaging (films, blister packaging, strapping tapes, thin-walled packaging for disposable food trays *etc.*), automotive industry (wheel arch liner, steering wheel covers, radiator expansion tanks, brake fluid reservoirs fittings, bumpers *etc.*), pipes and fittings (hot wire reservoirs, domestic waste water pipes, heat exchangers, solid rods *etc.*), domestic appliances (microwave oven cabinet, refrigerator components, dishwasher and washing machine parts *etc.*), fibres (filament yarns, artificial sport surfaces, woven carpet backing, monofilaments for rope *etc.*), furniture (stackable chairs *etc.*) and so on. [91]

It was reported that "the total worldwide demand for PP has currently reached an amount of approximately 47 million tons (prediction for 2008)" and this number has reached 55.1 million tons in 2013 remaining increase in the worldwide market by 5.8 % per annum until 2021 according to the Market Study: Polypropylene (© 2016 Ceresana). [98]

1.4 Techniques used in the Characterization of Polypropylene

In our research, various spectroscopic and microscopic techniques were used in order to analyze the polymer (i.e. PP films) surface in terms of physical and chemical properties, also to investigate the triboelectrification behavior electrical mesaurements were carried out via our home-made tapping device and oscilloscope. Main characterization techniques that we have used in this study are X-ray Diffractometer (XRD), Raman, Differential Scanning Calorimetry (DSC), Polarized Optical Microscope (POM) in order to analyze the crystalline property of PP and Kelvin Probe Force Microscopy (KPFM) to investigate the surface distribution of electrical

potential, also X-ray Photoelectron Spectroscopy (XPS) for the analysis of surface chemistry. The detailed information about the instruments and their usage purposes will be presented in Chapter 2, under Characterization Techniques.

1.5 Motivation and Goals of the Thesis

Static electrification and dissipation of the generated charge is of great importance when considering the applications of polymers in a wide-range of fields (e.g. from electronics to textile industry). In order to fabricate new technological devices by taking an advantage of tribocharging and to find exact solutions to the problems related with static electrification occurring in the practical use of polymers, in the first step there is a need to investigate the physical and chemical properties of polymers multi-dimensionally. Therefore, the relations of these properties with their triboelectrical behavior needs to be understood by using modern analytical characterization techniques.

In this thesis, our main goal is to reveal the effect of crystallinity for PP on its static electrification. The reason for why we selected PP is that its hydrophobic nature tends to relatively slow charge decay that facilitates the measurement of generated charge on film surface. [99] Crystallinity is one of the major parameters that determine the physical properties of polymers, therefore, it plays a crucial role in polymer science and technology.

1) This study makes a difference as it proves the fact that changing the degree of crystallinity and the physical properties of the polymer (e.g. mechanical strength, surface roughness, etc.), it is possible to obtain different triboelectrical behavior that gives an opportunity to gain a control on the

polymer's triboelectrical charging. As a result, it would be possible to reduce the static electrification of a commercially available material by a single change in its physical property through the application of mechanical stress which leads to outstanding alteration in the crystallinity and surface roughness of a material.

2) We motivated also to show that it is possible to generate electricity from a polymer just by applying mechanical force to the polymer film. As a consequence, the results will serve the valuable information for the fabrication of more efficient tribo-electric generators.
3) Another goal to conduct this research is to verify if the formation of a mosaic of nanoscopic patches of positive and negative charges can also exist on large scale after the application of mechanical stress onto polymer film.
4) It was aimed to deeply understand the mechanism behind the static electrification of a polypropylene so that it would be possible to monitor and control its triboelectric charging which will be very helpful in the practical use of polymers in both industrial, scientific and technological essence.

To sum up, the lack of knowledge in literature in terms of understanding the mechanism and the relation between crystallinity of a polymer and its tribocharging property has led and motivate us for conducting this research.

Chapter 2

Experimental

2.1 Materials

The specimens that were used throughout our research were commercial isotactic polypropylene, i-PP, (see also the characterization results from XRD, Raman, and DSC in Chapter 3). For the tensile tests, standard-sized dog-bone shaped PP samples which were obtained from Colorito item no: Colkapka were prepared by the die cutting machine (Model: MULTI-DIE CUTTING, Serial Number: MDC2015058) so that the specimens (whose gage length, L_o = 40 mm, total length, L = 114.6 mm, width, W = 6 mm, thickness = 0.0476 mm) could suit the technical specific standards. Thus, the obtained samples follow “Type A” standards (i.e. Generic Safety Standards) which are described as UNI EN ISO 12100-1 and UNI EN ISO 12100-2.

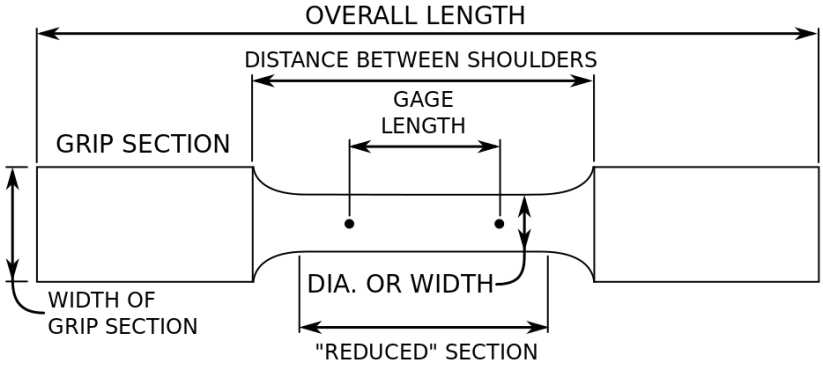

Figure 8. Dog-bone shaped tensile test specimen for polymers. Source: Wikipedia.

2.2 Experimental Procedure

In the experimental procedure, in order to differentiate % crystallinity of untreated PP films two procedures were applied. First treatment was microwave irradiation and the second treatment was application of mechanical test or tensile stress.

2.2.1 Microwave Radiation

In this part of the experiment, samples in the same standard shape were positioned as equally far from the center of the rotating table in a kitchen microwave oven (Samsung, Model: MS23F301EAW). It is important for the samples to be located perfectly symmetrical against each other (i.e. in equal distance to the center of the table and to each other) because they have to be treated in just the same scale. Otherwise, deviations in the results may be observed due to different amount of exposure to the microwave radiation. There were different watt and radiation time options available in the microwave oven. Then, we alternated both watt (100 W, 300 W, 450 W, 600 W, 700 W, 800 W) and radiation time parameters (5 min, 10 min, 15 min, 30 min) in order to analyze the change in crystallinity degrees. After each microwave treatment process the samples were left in the oven for approximately 40 min to relax and reach to the room temperature so that the polymeric chains could have enough time to re-arrange.

2.2.2 Mechanical Treatments

In the mechanical treatment of the samples, Instron mechanical tester (Model: 5969MTS) was used. The strain rate (mm/min), shape and dimensions of the PP films were loaded to the BlueHill 3 software system of the machine, and then strain-stress

curves of the specimens were obtained. The tensile tests were applied to the untreated and microwave treated PP samples during our non-contact electrification experiments as we observed that introducing mechanical stress generates charging on the film polymer samples. Moreover, the extension rate was the parameter that we changed in order to observe differences in the electrification of the specimens.

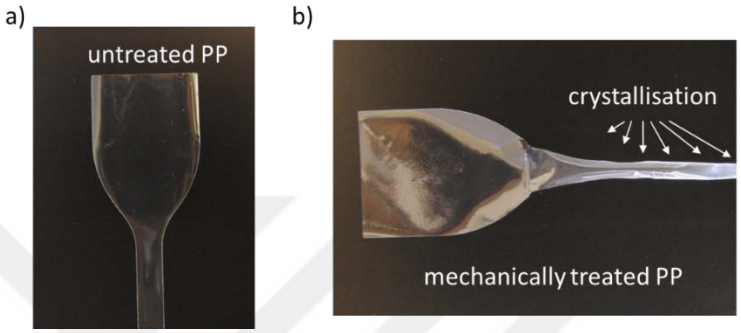

Figure 9. a) Untreated PP film, b) Crystallization occurring on PP film is indicated by whitening of the highly stretched areas that occur after application of tensile stress (L_{final} = 325 mm).

2.3 Characterization Techniques

In the characterization of PP samples that were treated by the methods presented in the previous section, various mechanical, microscopic, spectroscopic and analytical techniques were conducted. The listed characterization techniques were used in order to analyze the mechanical properties, crystallinity, the surface potential, and surface chemistry of PP before and after treatments.

2.3.1 Mechanical Characterization

The mechanical properties of untreated and treated PP samples were characterized via the mechanical tester. After performing repetitive tensile tests, the

stress versus strain curves of PP were obtained in order to determine the mechanical strength, modulus, and ductility of the specimens. The results will be presented in Results and Discussions part.

2.3.2 Characterization by Microscopic Techniques

2.3.2.1 Polarized Optical Microscope (POM)

Polarized optical microscope (POM) is based on illumination of the sample with polarized light. It offers a benefit for blocking of directly transmitted light with the help of a polarizer oriented at 90^0 to the illumination. Further, it is possible to change the intensity of transmitted light just by changing the degree of polarizer orientation. As it is explained in "Quantummadesimple" (Web) by the scientific supervision of Bobroff *et al.* a typical POM is composed of a detector, lenses and polarizing filters. A first filter selects a polarization, which means a single orientation among all waves composing light. A second polarizing filter selects a single orientation once again. When the two filters are perpendicular, no wave can go through anymore. A sample is positioned along the light beam whose orientation leads to the variations in transmitted light intensity. If it is birefringent, it will split the light by polarization into two rays with different delays. The second filter allows through only the waves whose polarization was affected by the sample. Then, the sample becomes visible. Hence, with this working principle POM allows to determine the direction of molecular order for certain samples. Also, through the detection of polarized light led by the submicroscopic molecular arrangements makes the analysis of sample morphology possible. [100, 101]

In our study, we used POM (Carl Zeiss) in order to observe the changes in the crystalline domains of PP before and after microwave and mechanical treatments.

2.3.2.2 Atomic Force Microscopy (AFM)

After the invention of Scanning Tunneling Microscope (STM) that presents imaging of individual surface atoms for electrically conductive materials with considerably high resolution, the studies for inventing other scanning probe microscopes that are able to mechanically scan by a sharp tip over the sample surface was accelerated. Consequently, in 1980s Atomic Force Microscopy (AFM) was developed by Binnig *et al.* in order to analyze both conductive and insulating surfaces on the nanometer-scale. [102, 103] The working principle of AFM is based on that a sharp tip is positioned on a cantilever spring so that the deflection of cantilever can be sensed throughout the feedback system which controls and monitors the deflection and the interaction force. In the end of the process, display system converts the collected data into an image. [102]

There are different modes of AFM for variety of practical purposes. In contact-mode AFM, the tip is mechanically contacted with the sample surface and force is applied. Then, short-range interatomic forces (e.g. ionic repulsion forces) between the tip and sample are measured. In noncontact-mode AFM, the tip is moved away from the sample by 10-100 nm and the cantilever oscillates above the surface of the sample. In this mode, the tip and sample interaction is in the attractive or van der Waals regime. The force is measured by comparing the frequency and/or amplitude of the cantilever oscillation relative to the driving signal. In tapping-mode AFM, which is also noncontact, the image is formed by the amplitude signal from the oscillation of

cantilever near its resonance frequency. [104] The noncontact mode of AFM can used for soft, fragile surfaces and biological samples.

AFM is a highly sensitive microscopic technique allowing a variety of surfaces to be characterized and imaged at atomic level. Further, it differs from other microscopes, such as optical or electron microscope, since it does not generate image by focusing light or electrons onto a surface. It is based on the sensing of force arising between tip and sample surface. Moreover, AFM technique requires neither a vacuum environment nor any special sample preparation, it can be used under ambient conditions that makes it very advantageous tool. [105]

As AFM offers the analysis of surface structure precisely by providing high-resolution topography image at atomic scale, we used tapping mode AFM (Asylum, Model: MFP-30 and Nanosurf: Flex-Axiom with C3000 controller) for the investigation of surface morphology. In our experiments we dealt with polymer crystallinity that also might cause alterations in the structure of sample surface. Since roughness is significant in the static electrification and it can also be affected by the degree of crystallinity, we analyzed the sample surface in terms of roughness via AFM.

2.3.2.3 Kelvin-Probe Force Microscopy (KPFM or KFM)

Kelvin-Probe Force Microscopy (KPFM or KFM) is a scanning probe microscopy technique introduced by Nonenmacher et al. in 1991. [106] Its working principle is based on the measurement of contact potential difference between probe and sample surface, hence it gains laterally resolved work function images. [106, 107] Since it is used for profiling the surface potential distribution with nanometer resolution, we used KPFM (Asylum, Model: MFP-30) in order to obtain the surface

potential mapping for PP samples which leads to observation of whether charging on the surface after the treatments has been occurred or not and to profile the charge distribution on the polymer's surface.

2.3.3 Characterization by Analytical Techniques

2.3.3.1 X-ray Diffraction (XRD)

X-ray Diffraction (XRD) method is used for the detection of average spacings between atomic layers, for the determination of crystal or grain orientation, also it is used in the measurement of size and shape of the crystalline domains, above all XRD is very important technique to find the crystal structure of an unknown material. Its operation mode is basically relies on the Bragg's law ($n\lambda = 2dSin\theta$), that is incident beam of X-rays interfere with one another when they leave the crystal due to the atomic planes of a crystal which is called X-ray diffraction. [108, 109]

As X-ray diffraction is considered to be the main technique for the determination of crystalline polymers structure, we used XRD (X'Pert PRO) for the qualitative analysis of crystallinity in PP through the diffraction patterns of well aligned polymer crystallites.

2.3.3.2 Differential Scanning Calorimetry (DSC)

Differential Scanning Calorimetry (DSC) is widely used thermo-analytical technique that measures the difference in the amount of heat required in order to increase the temperature of a sample and reference. It is very useful technique for the characterization of thermal transitions of polymeric materials. The device includes two platinum holders where the sample (5-10 mg) in a sealed small aluminum pan and

reference (empty aluminum pan) are located. The differential heat flow to the sample and reference is monitored by the thermocouples. Then, with the help of differential power that keeps both the sample and reference pans at equal temperatures throughout the programmed heating cycle which is recorded as a function of temperature. [110]

Thermal history, melting temperature (T_m), glass transition temperature (T_g) where the polymer chains start to become mobile during heating, crystallization temperature (T_c) where the ordering and the production of crystalline regions occur during the cooling, crystallinity, rate of crystallization, can be obtained by DSC. [110, 111] The degree of crystallinity depends on the heating and cooling rate and it can be calculated by the following equation:

$$\% \text{ Crystallinity} = (\Delta H_{sample} / \Delta H_{100\ \%\ crystalline}) \times 100 \qquad [110]$$

where ΔH is the heat of fusion (J/g) of the sample and $\Delta H_{100\ \%\ crystalline}$ is the heat of fusion for the 100 % crystalline analogue (148 J/g in the case of polypropylene [112, 113]). Hence, because of its applicability to polymers and offering the determination of percent crystallinity, we used DSC (TA Instruments, Model: Q2000) to investigate the changes in crystallinity for PP samples quantitatively.

2.3.4 Characterization by Spectroscopic Techniques

2.3.4.1 Raman Spectroscopy

Raman spectroscopy is a spectroscopic technique that is used for the observation of vibrational, rotational, and other low-frequency modes in a system. It accounts the scattering molecule as a total number of atoms undergoing simple

harmonic vibrations. Raman effect can be simply described as the inelastic scattering (or Raman scattering) of light coming from a laser in visible, near infrared, or near ultraviolet range.

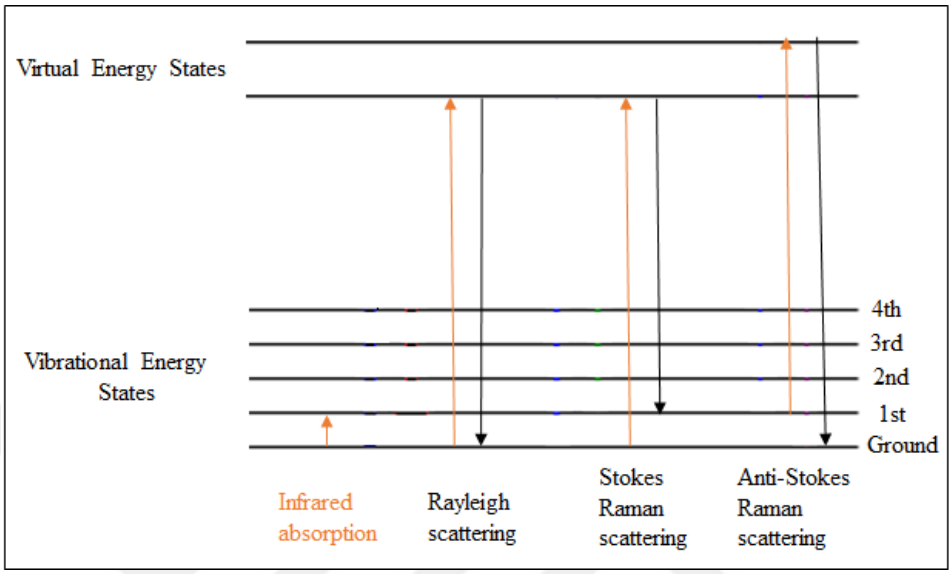

Figure 10. Energy-level diagram indicating the states in Raman spectrum.

The laser light interacts with molecular vibrations, excitations or phonons in the given system that causes shifts (up or down) in the energy of the laser photons. Hence, the shifts in energy bring the information about the vibrational modes in the system. [114, 115]

Raman spectroscopy is commonly used in order to identify the molecules by looking at their fingerprint peaks obtained in a Raman spectrum. Moreover, we used Raman spectroscopy (Witec, Model: Alpha300S + Raman Module) as the specific Raman peaks give information about the crystallinity of PP. [116] In the instrument that we used, power and wavelength of the laser are 40 milliwatt and 532 nm, respectively. Also, it provides high spectral resolution which is 0.1 cm^{-1}/pixel and the spatial resolution specified as 200 nm.

2.3.4.2 X-ray Photoelectron Spectroscopy (XPS)

X-ray Photoelectron Spectroscopy (XPS) is widely used characterization technique that allows the surface analysis as it offers outstanding chemical selectivity. In the sense of chemical structure of surface it provides quantitative and qualitative information.

In XPS, the sample is radiated with high-energy X-ray in order to emit photoelectrons from the core levels of the sample. Then, the kinetic energy of these emitted photoelectrons is measured via an electron spectrometer (or electron energy analyzer). The collected data is converted into intensity versus binding energy for selected specific elements. [117, 118]

In our study, we used XPS (Thermo, Model: K-Alpha – Monochromated high performance XPS spectrometer) in order to analyze the surface in terms of its chemical properties before and after treatments on PP films as the surface chemistry plays a considerable role in the contact electrification and tribocharging.

2.3.5 Electrical Measurements

For the identification of triboelectrical properties of PP samples, we designed a mechanical tapping device as it can be shown in Figure 11. The device allows the contact of two surfaces in different frequencies and resolutions (peak/1s and peak/50ms) through the oscilloscope (see Figure 12) which is connected to metal electrodes that are attached to the tapping machine.

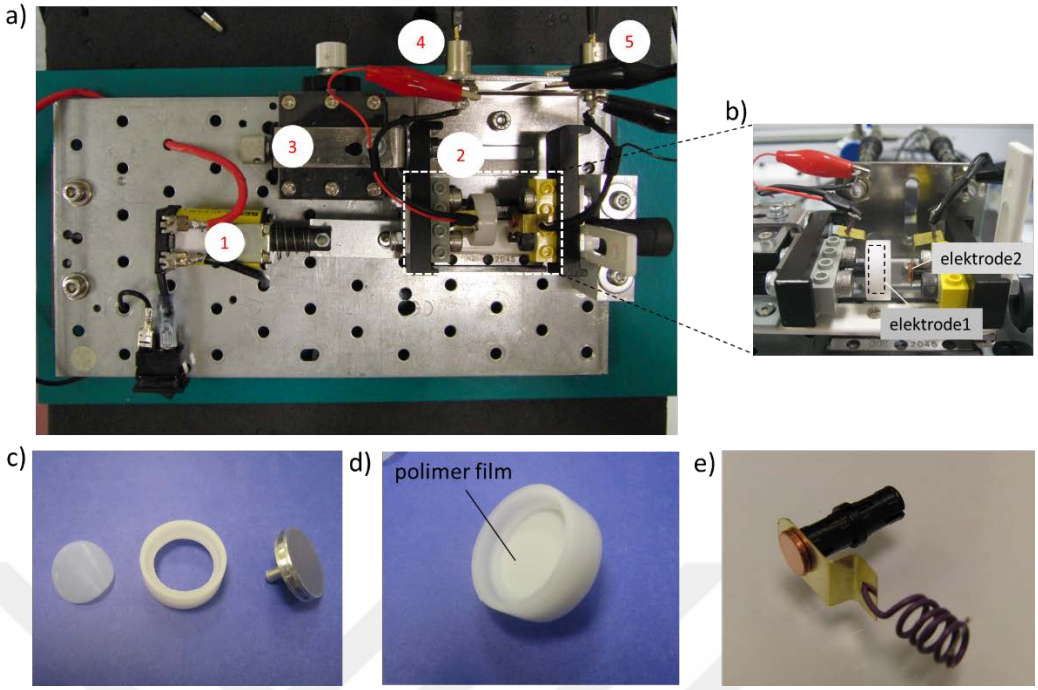

Figure 11. a) Mechanical tapping device developed in our laboratory; 1) solenoid linear motor, 2) sample and electrode compartment, 3) XY positioner stage, 4) Oscilloscope channel-1 connected to polymer containing metal electrode, 5) Oscilloscope channel-2 connected to Cu electrode, b) electrodes, (i.e. SEM metal stubs), c) components of the sample holder for polymer film (PTFE is illustrated as an example), d) Fixed electrode on which polymer sample is put, e) copper electrode on a linear X stage used in the metal-polymer contact electrification experiments.

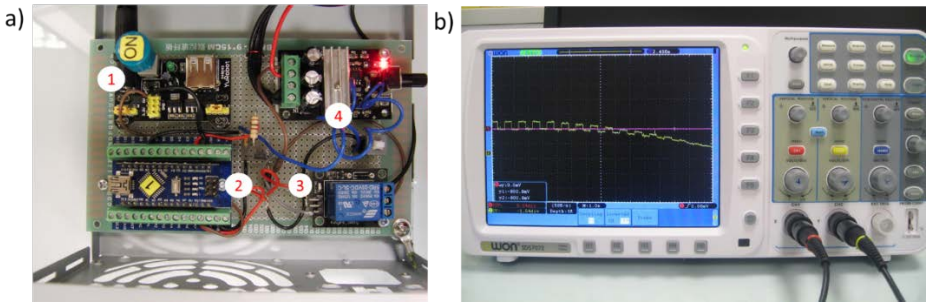

Figure 12. a) Electronic control unit for the tapping device 1) power supply of the microprocessor, 2) Arduino-nano microprocessor, 3) On-Off switch to control power supply of solenoid, 4) power supply for solenoid. b) Oscilloscope used in electrical measurements for metal-polymer contact electrification experiments.

The oscilloscope was used to monitor the change of an electrical potential in volts (V) over time. It allows observation of constantly varying signal voltages by converting the data into a 2D plot of one or more signals as a function of time. For our experiments, typical obtained plot for the contact electrification can be seen in Figure 13.

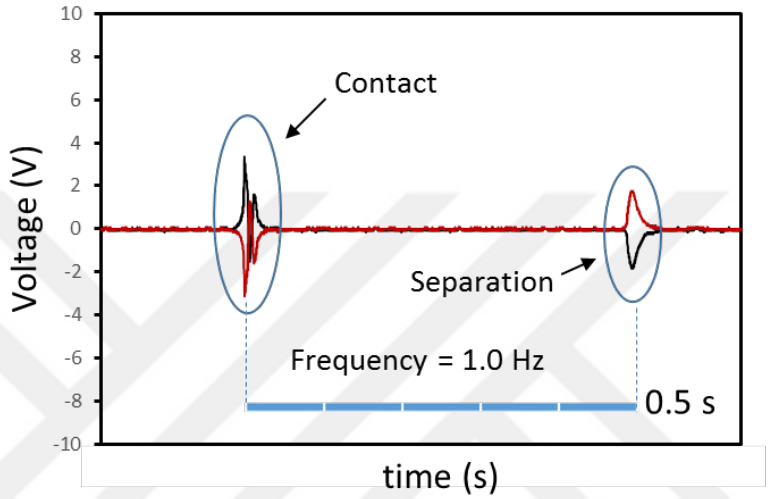

Figure 13. Typical 2D voltage (V) versus time (s) plot obtained through contact electrification experiments.

In this part of the contact electrification experiment, untreated and treated PP samples (after microwave radiation and mechanical stress) were analyzed, that is each specimen was contacted to the Copper (Cu) surface whose radius is 6 mm with different tapping frequencies (1 Hz, 3 Hz, 5 Hz, and 10 Hz). After the contact of polymer and metal surfaces, the extent of voltage (V) for the electrically charged PP samples was recorded. We used digital oscilloscope (Owon SDS7072 70 MHz, 2+1 Channel, 1 GS/s) with P4100 Series probes (100:1/100 MHz, Input voltage 2KV DC + AC pk, P4100 series High voltage probes), low-noise current preamplifier (SR570 Current Preamplifier) to take our data.

In addition to the contact electrification, for the measurement of non-contact electrification of PP brass-made Faraday cage was used so that we could collect the charges generated during the tensile stress and the amount of charge (Q) was determined quantitatively in nanocoulomb (nC) via Keithley electrometer that is connected to the Faraday cage.

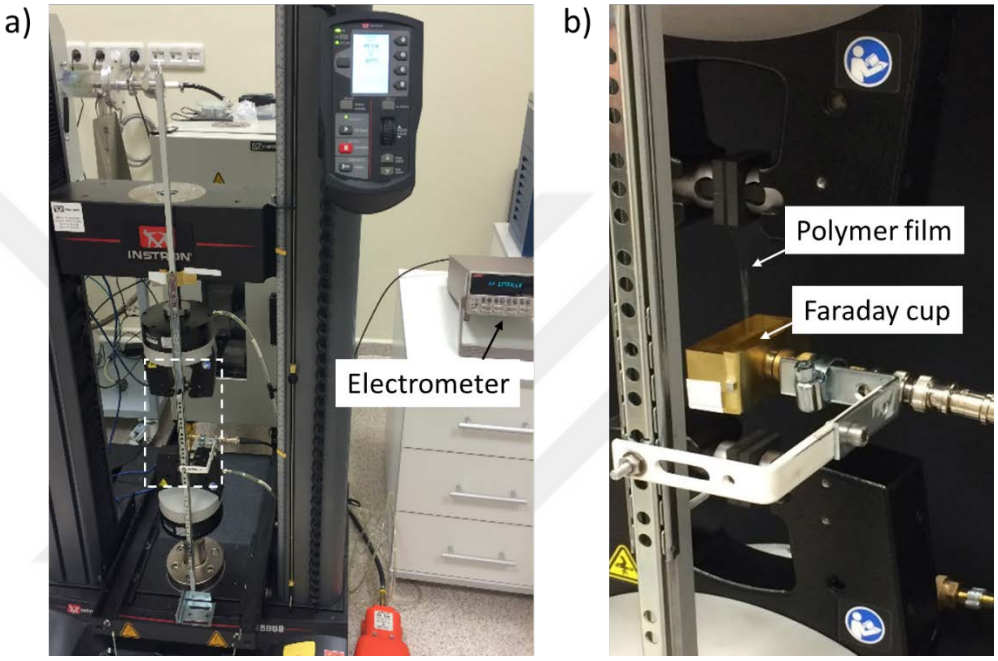

Figure 14. a) The whole representation of non-contact electrification measurement with Keithley 6514 electrometer, Faraday cage, and the mechanical tester, b) Faraday cage around PP film positioned between the grips.

Chapter 3

Results and Discussions

3.1 Determination of Degree of Crystallinity of PP

As we investigate the relation between degree of crystallinity and triboelectrical properties of PP, before going through the electrical measurement we analyzed the changes in crystallinity of PP after the microwave and mechanical treatments which were elucidated in the Experimental part.

3.1.1 Preliminary Examination by POM

First of all, untreated and treated PP samples were analyzed under the polarized light since POM offers the visualization of crystalline domains in outline. Hence, it makes possible to investigate the differentiations in crystalline structure of PP in first approximation.

Despite the POM images with 20x and 50x magnifications roughly show the differentiation of crystalline structure of PP owing to the microwave radiation and mechanical stress, it can be seen more obviously in the 100x magnified POM images how the crystalline domains are significantly affected from the treatments.

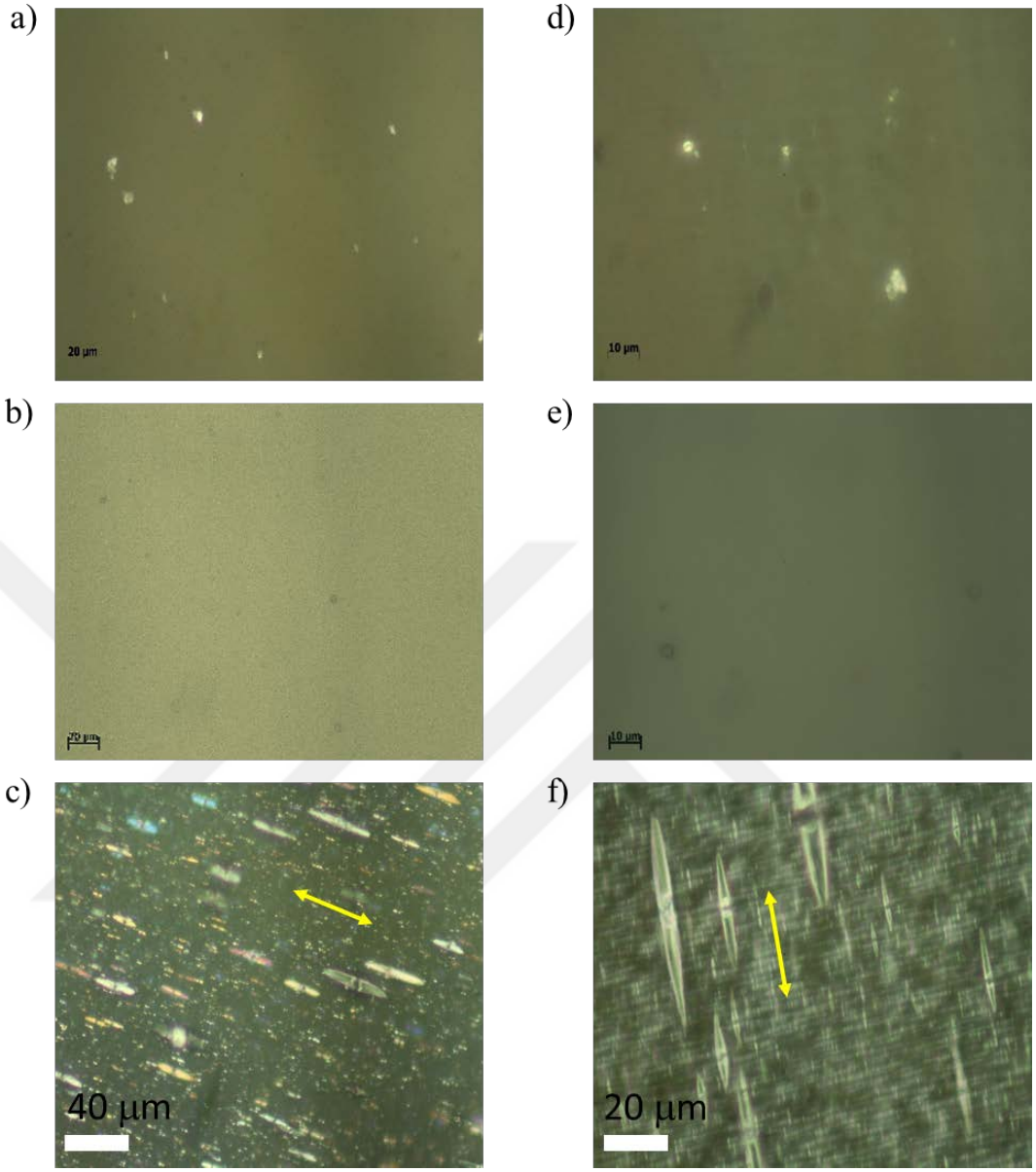

Figure 15. a) The 50x magnified POM image of untreated PP, b) The 50x magnified POM image of 600 W-10 min microwave radiated PP, c) The 50x magnified POM image of mechanically treated PP with 40mm/min extension rate, d) The 100x magnified POM image of untreated PP, e) The 100x magnified POM image of 600 W-10 min microwave radiated PP, f) The 100x magnified POM image of mechanically treated PP with 40mm/min extension rate. Arrows in c) and f) indicate the direction of stretching of the sample.

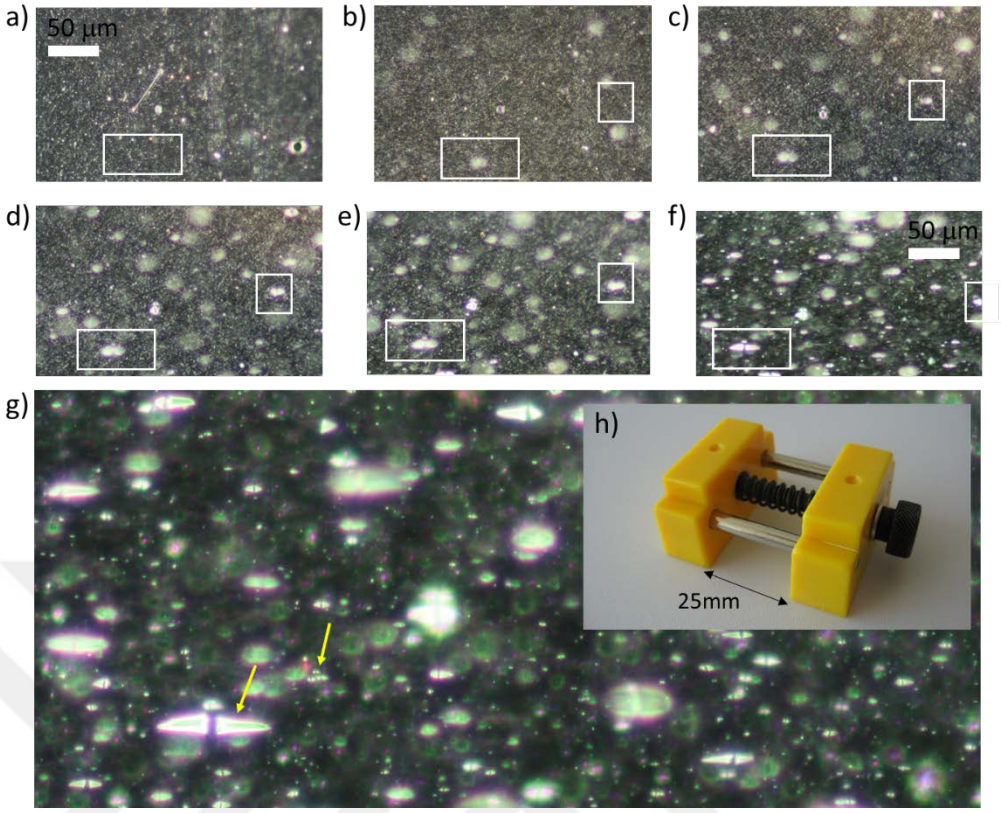

Figure 16. PP film under mechanical stress increasing from (a) to (g) and the representation of the change in crystalline structure of PP, and h) the device used in the application of mechanical stress.

The observation of the sharp line-shape crystal structures in PP film after the application of mechanical stress was demonstrated via POM and it will be verified by the AFM topography images of the specimen. The stress-induced crystallinity was indicated by POM images which illustrate that the main impact belongs to the application of mechanical stress in terms of the structural changes in PP crystallites. After the tensile test with 40 mm/min extension rate of PP films, tenuous small crystalline domains in untreated samples become clearly visible needle-shape crystalline structures, even many of them are seen as broken from the middle or near middle. This illustration of the alteration in crystal structure of PP with the applied

stress onto the film samples is outstandingly important as it presents the visual proof of the differentiation via microscopic technique. Since the crystallites are not in the same level, that is some of them are far away from the surface while some of them are closer to the film surface, it was hard to focus on the large area under POM due to the height differences. On the other hand, we carried out the microwave radiation as an instant way of treatment to cause changes in the crystalline and morphological properties of PP. However, it can be said that microwave treatment has not any drastic effect as much as the mechanical treatment in terms of the crystalline structure of PP by considering the POM images.

3.1.2 Qualitative Analysis

After the visual characterization of untreated and treated PP samples' crystalline regions via polarized optical microscope, we analyzed the degree of crystallinity throughout the X-ray diffraction method and Raman spectroscopy.

3.1.2.1 XRD Results

In order to observe differences in the crystallinity of PP samples, analytical measurement was performed via XRD technique. As the X-ray diffracts due to the crystal regions, it gives information about the relative percent crystallinity of the polymer and the changes in the crystallographic planes.

Table 1. Diffraction peaks of the i-PP samples [119-121]

2θ (°)	Crystalline plane (hkl)	i-PP phase
14.1	(110)	α
16.1	(300)	β
16.8	(040)	α
18.5	(130)	α
21.2	(111)	β
21.8	(301)	α
25.5	(060)	α

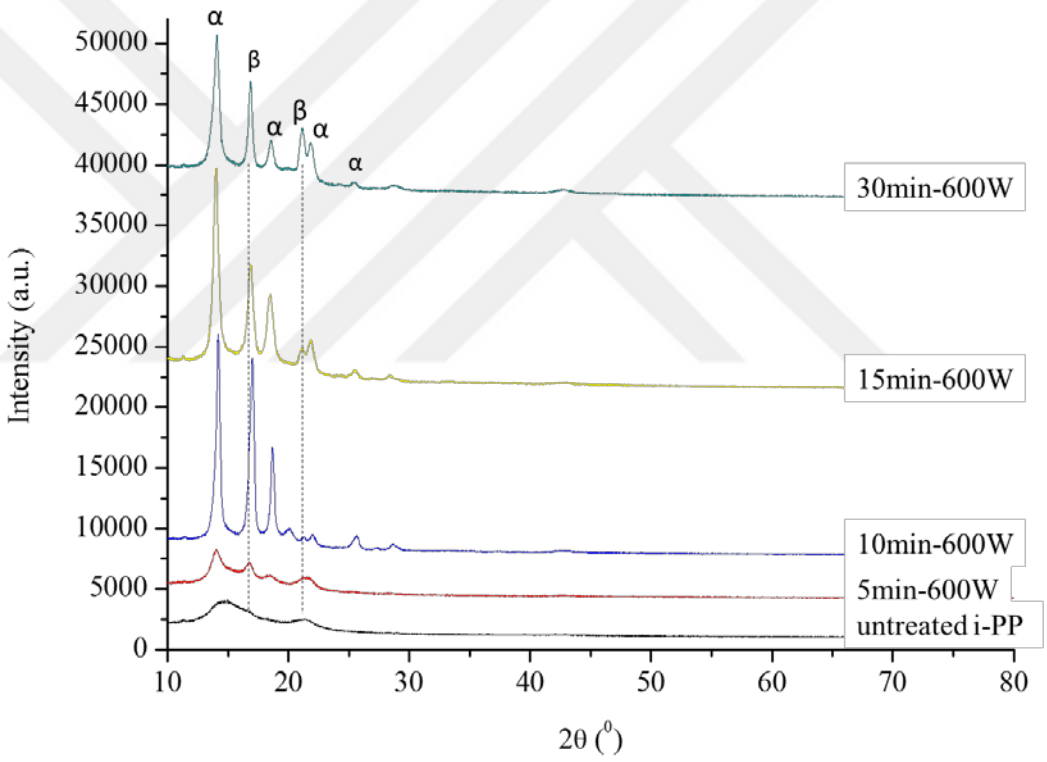

Figure 17. X-ray diffractograms of untreated and 600W-microwave treated PP samples with respect to the different period of time for radiation exposure.

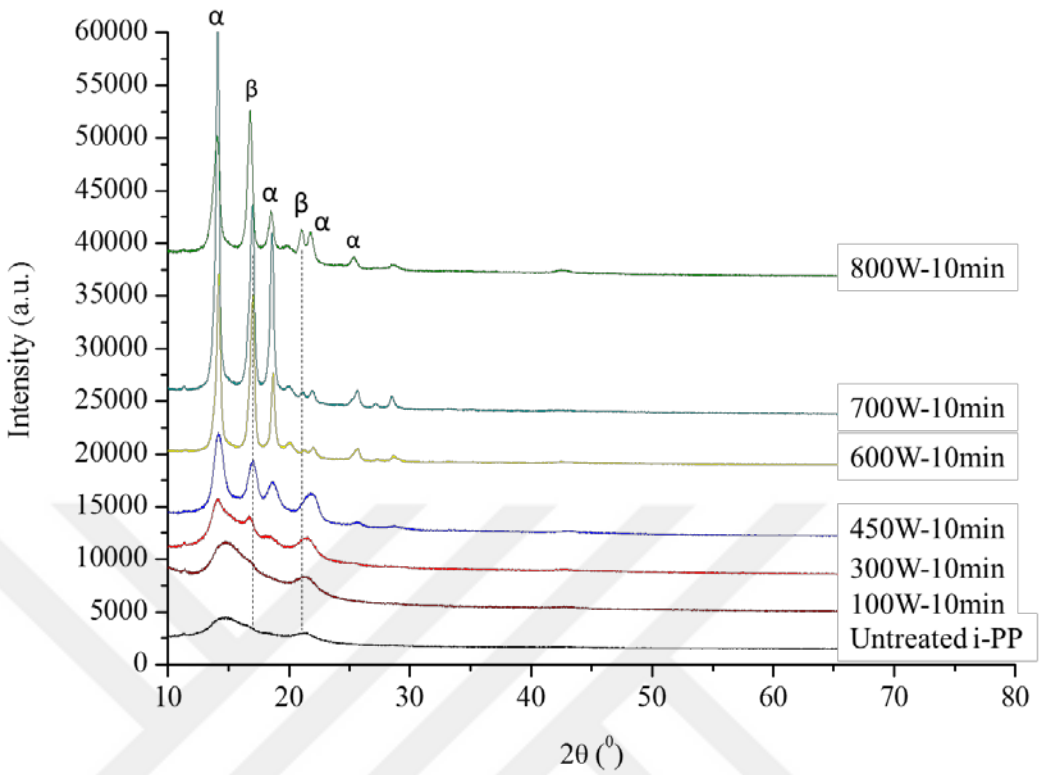

Figure 18. X-ray diffractograms signals of untreated and 10min-microwave treated PP samples with respect to the different power of radiation.

As X-ray diffractions determine the crystallinity, it can be said that exposure of bare PP samples to the microwave radiation leads the significant alterations in the crystallographic orientation of the specimens that can be seen in Figure 17 and Figure 18. It was observed that after the microwave treatment new crystalline planes appear and broad signals in the X-ray diffraction of untreated PP are getting sharper that means crystallinity increases in the duration of microwave radiation. Moreover, when the exposure time and the power of the radiation increases the sharpness of the signals meanwhile the crystallinity of PP increases. However, when the POM images of 600W-10 min microwave radiated PP sample are compared with its X-ray diffraction,

which consists of sharp signals, it can be said that the POM images present elusive indication for microwave treatment unlike mechanical treatment.

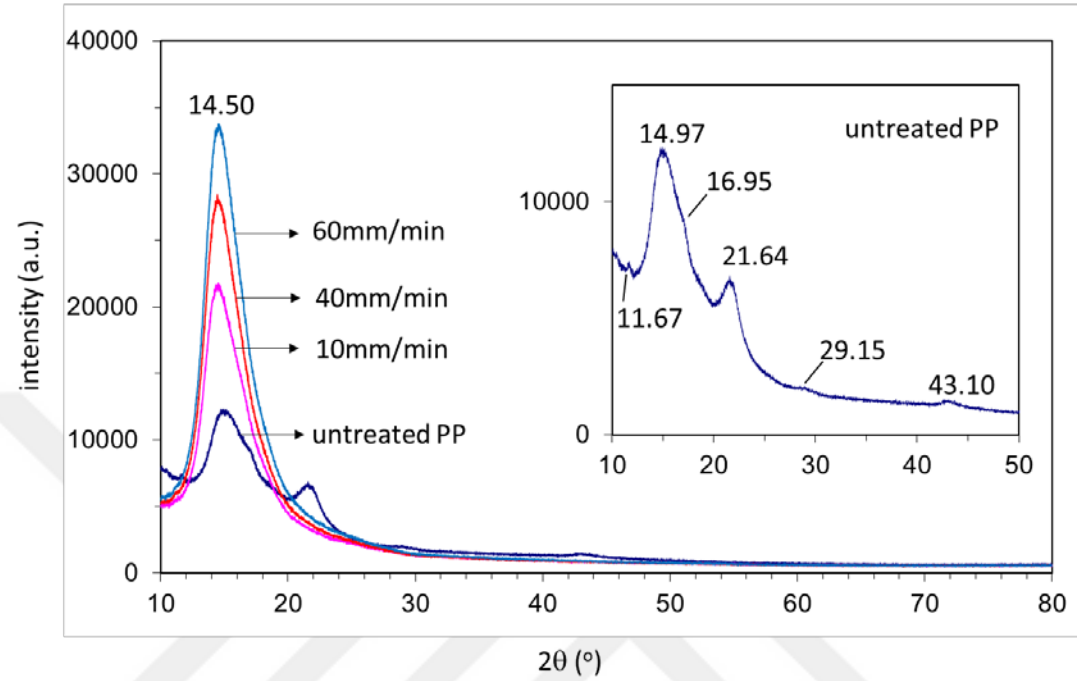

Figure 19. X-ray diffraction diffractograms of untreated PP and mechanically treated PP with different extension rates.

After the application of mechanical stress on PP films, X-ray diffractograms of the samples were analyzed and it was observed that the alterations occur in the X-ray diffraction signals of PP in a different way than the obtained X-ray diffractions after the microwave treatment. As it is shown in Figure 19, the area under the crystalline peaks differs throughout the treatment. It was stated before that the decrease in the broadness of XRD signals leads to the increase in % crystallinity. However, not only the sharpness of the signals, but also the area under crystalline XRD peaks determines the % crystallinity as crystallinity equals to (crystalline area) / (total area). [122] Therefore, the crystalline and total area were calculated in X-ray diffractograms and the ratio between them was obtained. Consequently, the percent crystallinities for

untreated, mechanically treated and 600 W-10 min microwave radiated PP samples were found according to the equation % crystallinity = (crystalline area) / (total area) x 100.

% Crystallinity for untreated PP = 30394 / 117584 = 26 %

% Crystallinity for 10 mm/min stretched PP = 68306 / 115520 = 59 %

% Crystallinity for 40 mm/min stretched PP = 87469 / 143544 = 61 %

% Crystallinity for 60 mm/min stretched PP = 107716 / 168584 = 64 %

% Crystallinity for 600 W-10 min microwave treated PP = 25751 / 45820 = 56 %

It was observed that during the mechanical stress and microwave radiation the degree of crystallinity significantly increased from 26 % (for untreated PP). However, in order to change the degree of crystallinity, application of mechanical stress is more effective than microwave treatment as the percent crystallinity for 600 W- 10 min microwave treated PP was obtained as 56 % while it was determined as 59 %, 61 %, and 64 % for 10 mm/min, 40 mm/min, and 60 mm/min extension rates, respectively. Hence, differing extension rate did not cause a drastic change in % crystallinity.

In addition, the crystallite size of untreated and treated PP samples can be determined by using the Scherrer equation:

$T = \frac{K\lambda}{\beta \mathrm{Cos}\theta}$ where T is the peak width which is inversely proportional to crystallite size (β), K is the Scherrer constant that depends on the crystal shape, λ is the wavelength of X-ray, and θ is the position of the peak (half of the plotted 2θ value). [122] According to this equation, untreated PP has the smallest crystallite size as its peak width is larger (i.e. broad) whereas the peak width is getting smaller through the

microwave and mechanical treatments and the stretched PP specimen has the greatest crystallite size due to its smallest peak width as a result of stretching.

3.1.2.2 Raman Results

In order to determine the extent of crystalline regions in semi-crystalline PP consisting of crystalline and amorphous regions heterogeneously, a complementary qualitative analysis was carried out by using Raman spectroscopy. As it is indicated by Nielsen *et al.* the relative intensities of Raman bands at ~808 cm^{-1} and ~841 cm^{-1} estimate the crystallinity of i-PP since the 808 cm^{-1} band is assigned to helical chains within crystals while the 841 cm^{-1} indicates the amorphous regions that corresponds to shorter chains in helical conformation. [116] Therefore, by utilizing Raman spectroscopy the observation of the changes in these two specific peaks of PP corresponding to the crystalline and non-crystalline regions in the sample will lead to the qualitative determination of differences occurred in degree of crystallinity for untreated and treated samples.

a)

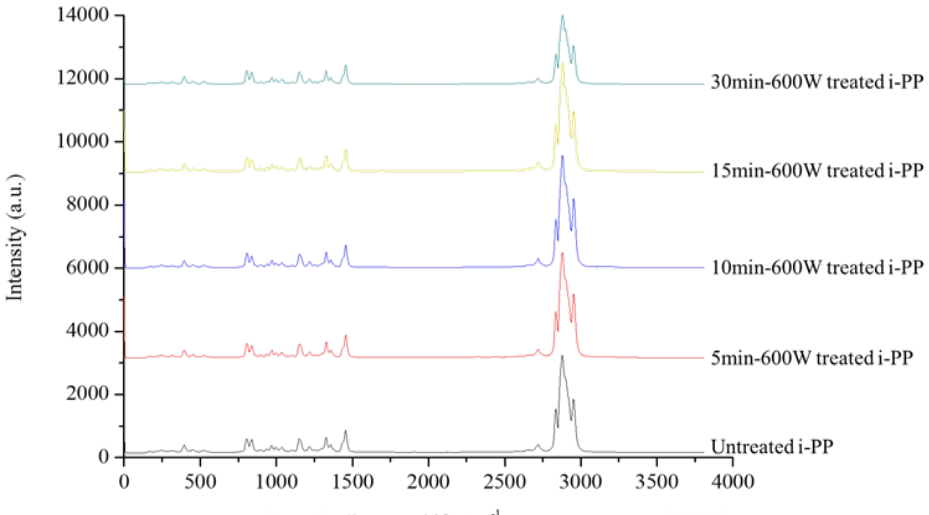

b)

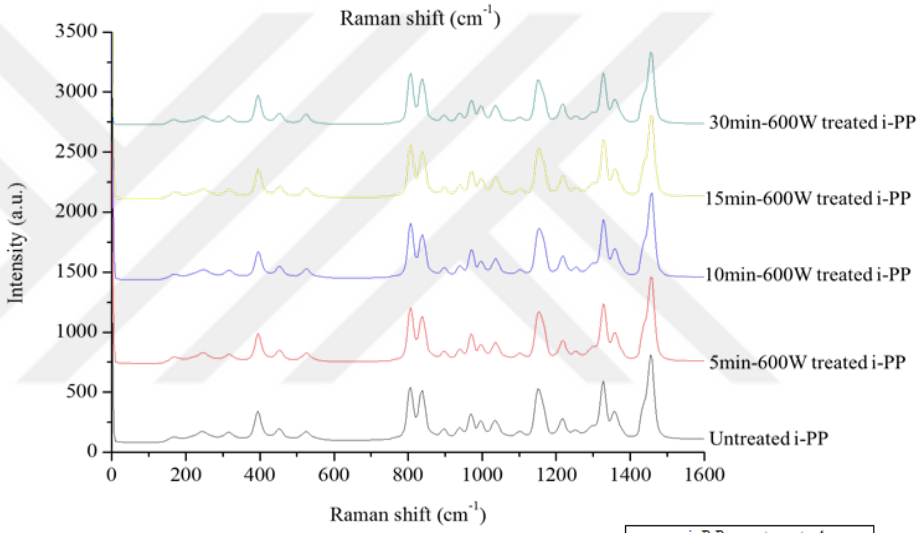

c)

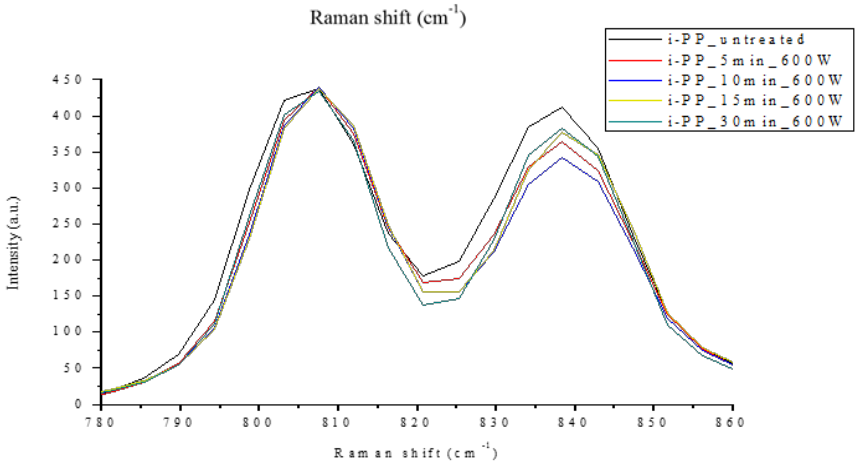

Figure 20. Raman spectra of untreated and 600W-microwave treated PP samples with respect to the different period of radiation exposure time a) in the Raman spectrum range 0-4000 cm^{-1} b) 0-1600 cm^{-1} and c) the normalized Raman spectra according to the peak at 808 cm^{-1} in the range of 780-860 cm^{-1}.

a)

b)

c)

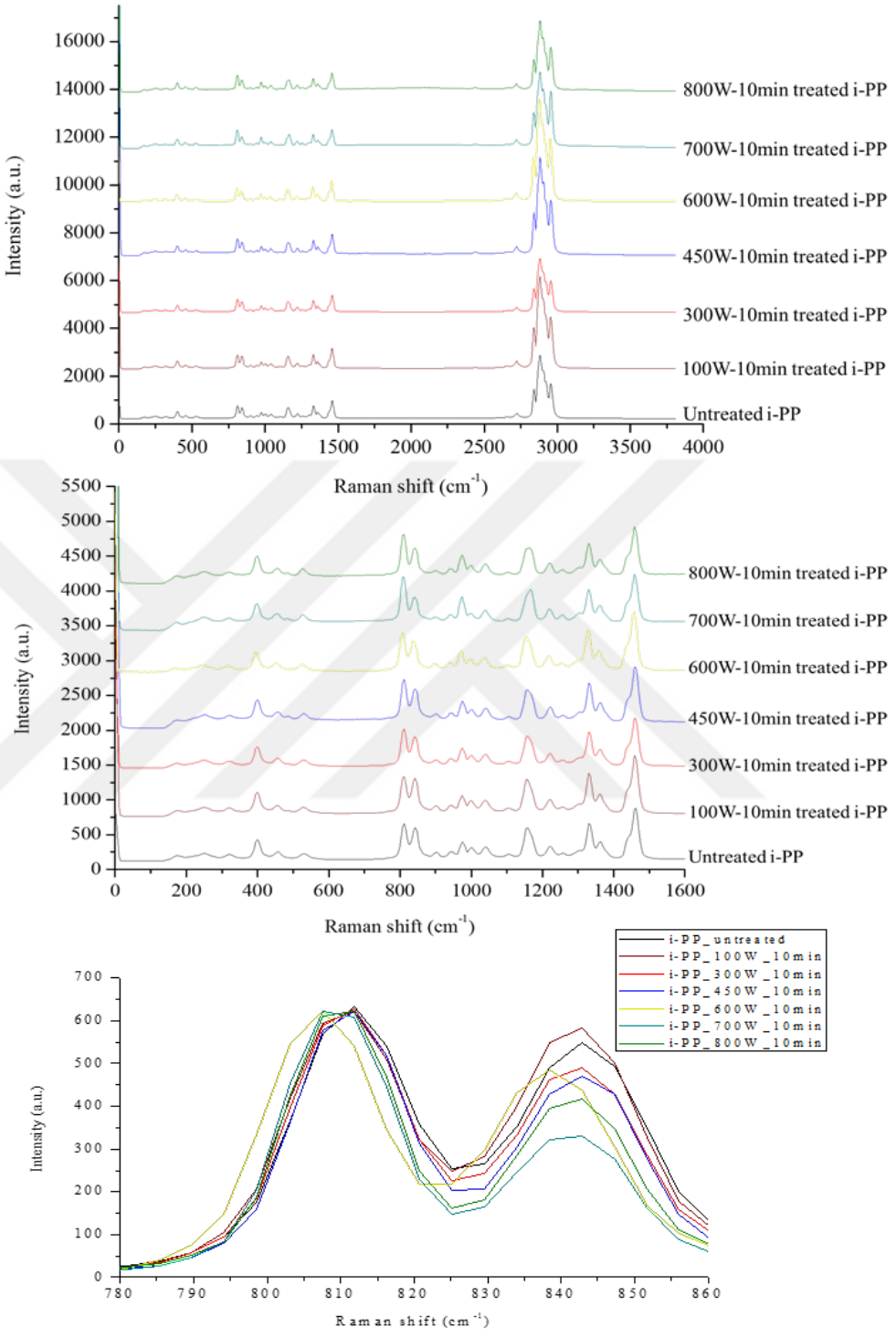

Figure 21. Raman spectra of untreated and 10min-microwave treated PP samples with respect to the different power of radiation a) in the Raman spectrum range 0-4000 cm^{-1} b) 0-1600 cm^{-1} and c) the normalized Raman spectra according to the peak at 808 cm^{-1} in the range of 780-860 cm^{-1}.

In Figure 20b and Figure 21b, the characteristic peaks of PP were analyzed more detailed in a narrow range of Raman spectrum (0-1600 cm^{-1}). Furthermore, in Figure 20c and Figure 21c the relative intensities of two Raman bands assigned for crystalline (808 cm^{-1}) and non-crystalline regions (841 cm^{-1}) were compared. It was observed that the ratio between crystalline and amorphous peaks is smaller for the untreated PP sample whereas the difference between these two specific peaks is getting larger after the microwave radiation.

In addition, when Figure 20 and Figure 21 are taken into account it is seen that the power of microwave radiation is slightly more effective in the raising of the ratio between crystalline and non-crystalline peaks rather than the duration of exposure. Yet, both period of time and the power of microwave radiation have considerable impact on the % crystallinity. Moreover, as it can be seen in Figure 21 when the sample is exposed to microwave radiation with different intenseness small signal shift occurs that leads to the change in the crystalline phases of PP. On the other hand, it was observed that both power of microwave radiation and the duration of radiation exposure influence the degree of crystallinity in a proportional manner.

In the second step, the mechanically treated PP was analyzed via Raman spectroscopy. Since it was determined by XRD in the first part of the experiment that 10 mm/min or 40 mm/min extension rate does not cause any significant alteration in terms of percent crystallinity, in the following experiments we studied the samples which were strained 40 millimeter per minute. Then, by using Raman spectroscopy we analyzed different parts of the mechanically treated PP sample in order to observe whether there are differences in the % crystallinity across the specimen or not. Since the elongation of PP with 40 mm/min results in L_o = 370 mm after the applied tensile

stress, single spectra from different fractions across the PP film were taken by choosing one end as a reference point (L_o = 0).

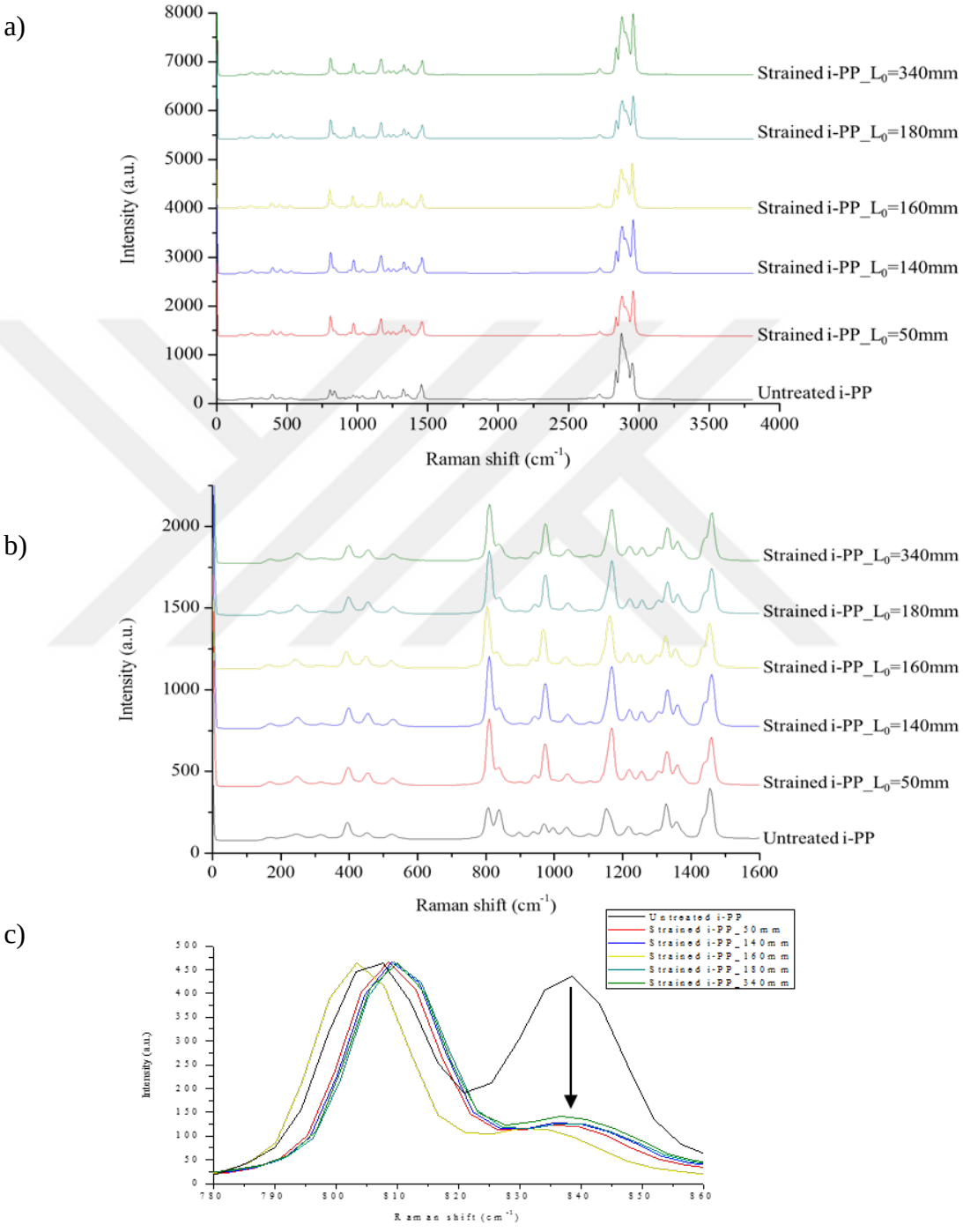

Figure 22. Raman spectra of mechanically treated PP from different points across the sample a) in the spectrum range 0-4000 cm^{-1}, b) 0-1600 cm^{-1}, and c) the normalized Raman spectra according to the peak at 808 cm^{-1} in the range of 780-860 cm^{-1}.

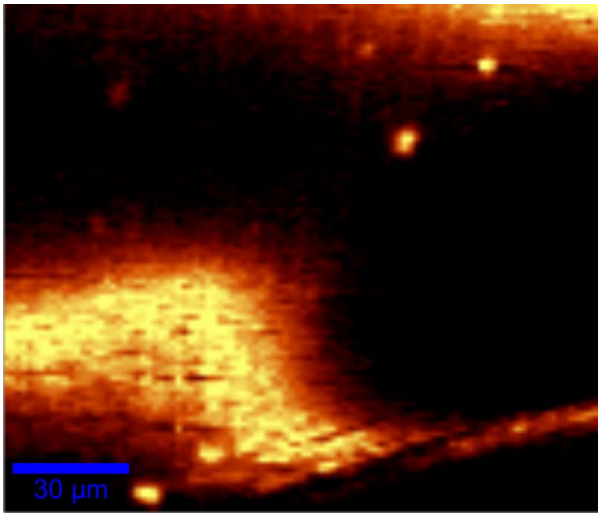

Figure 23. Raman scan image of crystalline regions in mechanically treated PP.

The Raman spectra of mechanically treated PP specimen shows that there are some signal shifts and the difference between the specific peaks assigned for crystalline (808 cm^{-1}), whose mapping is presented in Figure 23, and non-crystalline segments (841 cm^{-1}) of PP is getting hugely larger during the mechanical treatment. Therefore, an important change in the crystallinity occurs with the application of tensile stress to the film PP sample. When the results are compared with the microwave radiation it can be said that the applied stress has much more significant impact on the polymer's percent crystallinity.

3.1.3 Quantitative Analysis

After the qualitative investigation of crystallinity, DSC was used in order to obtain numeric results for the % crystallinity of untreated and treated PP samples.

3.1.3.1 DSC Results

In order to verify the analytical outcomes obtained from XRD and the spectroscopic results from Raman spectroscopy a thermo-analytical measurements were utilized via DSC for the calculation of degree of crystallinity.

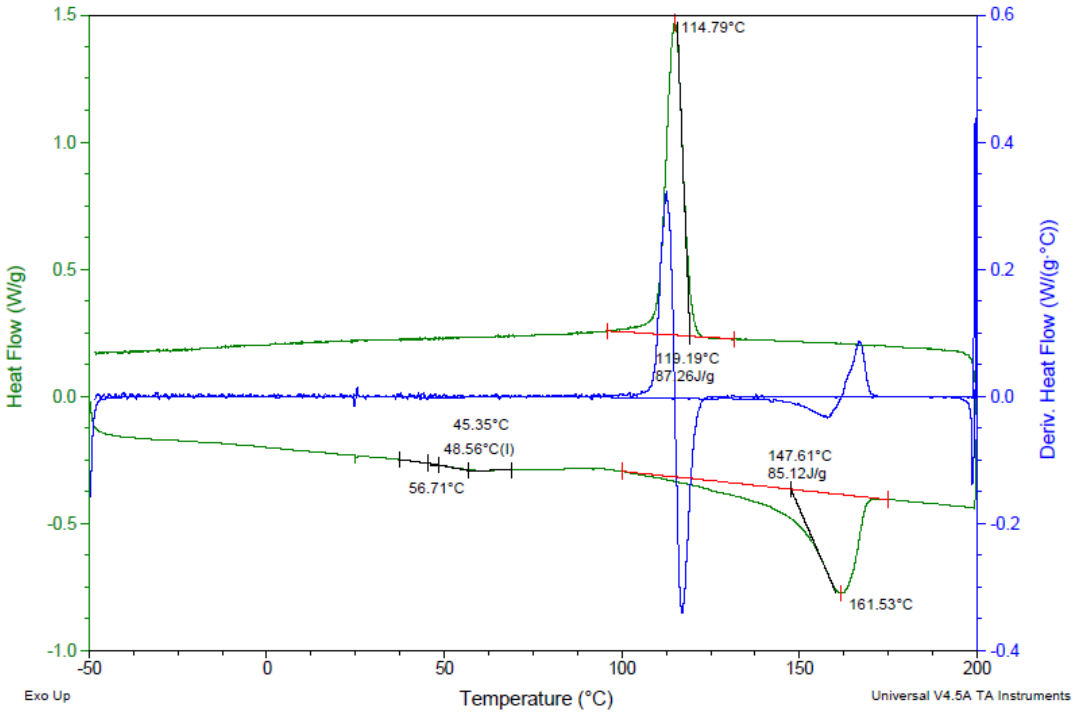

Figure 24. DSC curve of untreated PP (8.9 mg) with 10 ^{0}C/min in a cyclic method.

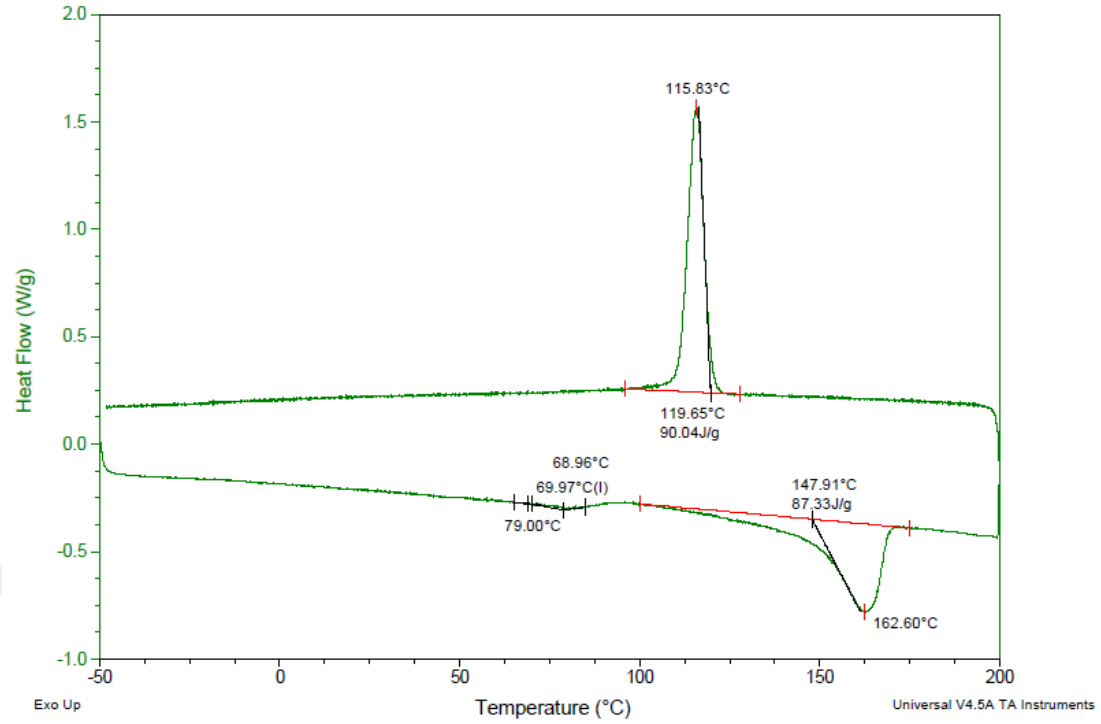

Figure 25. DSC curve of 600 W-10 min microwave radiated PP (9.0 mg) with 10 ^{0}C/min in a cyclic method.

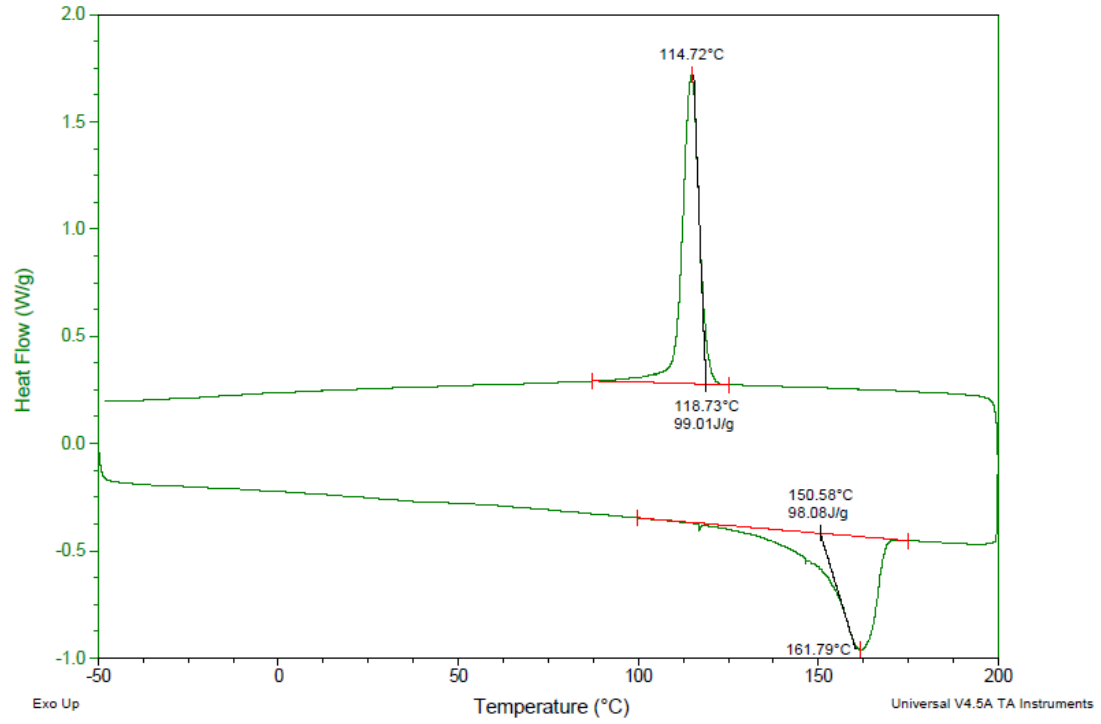

Figure 26. DSC curve of 40 mm/min mechanically strained PP (9.0 mg) with 10 ^{0}C/min in a cyclic method.

As it was stated before in the Characterization by Analytical Techniques section (Chapter 2), the device includes two platinum holders where the sample (5-10 mg) in a sealed small aluminum pan and reference (empty aluminum pan) are included. The differential heat flow (W/g) is measured as a function of temperature change (^{0}C) during the heating and cooling process. Then, the % crystallinity is obtained by the determination of heat of fusion or melting enthalpy (ΔH_m) that is the area under the melting peak, which was observed at ~161 ^{0}C (T_m) for the PP samples.

The degree of crystallinity depends on the heating and cooling rate, therefore for each sample the rate kept constant at 10 ^{0}C/min and in the calculation of ΔH_m the temperature range was taken between 100 ^{0}C and 175 ^{0}C in the obtained DSC curves, then the comparison was proceeded between untreated and treated PP samples relatively. The percent crystallinity can be calculated based on the following equation:

$$\% \text{ Crystallinity} = (\Delta H_{sample} / \Delta H_{100\ \% \text{ crystalline}}) \times 100 \quad [110]$$

where ΔH is the heat of fusion (J/g) of the sample and $\Delta H_{100\% \text{ crystalline}}$ is the heat of fusion for the 100% crystalline analogue (148 J/g in the case of polypropylene [112, 113]). Hence, the obtained DSC results suggest that:

For untreated PP,

$$\% \text{ Crystallinity} = \frac{\Delta H \text{ (sample)}}{\Delta H \text{ (100\% crystalline)}} \times 100$$

$$= \frac{85.12 \text{ J/g}}{148 \text{ J/g}} \times 100$$

$$= 57.51 \%$$

For microwave radiated PP,

$$\% \text{ Crystallinity} = \frac{\Delta H \text{ (sample)}}{\Delta H \text{ (100\% crystalline)}} \times 100$$

$$= \frac{87.33 \text{ J/g}}{148 \text{ J/g}} \times 100$$

$$= 59.01 \%$$

For mechanically treated PP, $$\% \text{ Crystallinity} = \frac{\Delta H \text{ (sample)}}{\Delta H \text{ (100\% crystalline)}} \times 100$$

$$= \frac{98.08 \text{ J/g}}{148 \text{ J/g}} \times 100$$

$$= 66.27 \%$$

As a result of the thermo-analytical measurements by DSC, the microwave radiation (600 W-10 min) and mechanical treatment with 40 mm/min extension rate led to the increment in the degree of crystallinity of PP. Furthermore, the increase in the degree of crystallinity is much more significant for the mechanically treated samples than the microwave treated samples since after the microwave radiation crystallinity raised from 57.51 % to 59.01 % whereas for the mechanically treated samples it was increased to 66.27 %. Although the DSC results support the suggestion of XRD analysis (i.e. lowest degree of crystallinity belongs to the untreated PP, highest degree of crystallinity belongs to the mechanically treated one, and the microwave radiated PP is in between), unlike the XRD results the % crystallinity was found not high as much as expected. The reason for this is because the sample is exposed to heating and cooling procedures during the DSC measurement that creates a thermal history on the sample. Therefore, the potential structural changes due to the applied thermal energy in DSC may cause deviations from the outcomes of XRD analysis for the % crystallinity.

3.2 Results of Mechanical Tests

The applied mechanical stress on PP film samples leads to the considerable alterations in mechanical properties (tensile strength, modulus etc.) of the specimens in addition to changes in % crystallinity. Hence, in this part of the experiment the

mechanical strength of PP is analyzed so that we can draw a comprehensive picture for the scientific and industrial applications of triboelectricity.

The tensile stress was applied to the PP films till the specimens reached 100 % elongation according to their original length, then the mechanical strength of the samples, which were treated differently, was analyzed. The extension rate was adjusted to 10 mm/min so that the experiment could be stopped exactly at the time when 1.0 (mm/mm) tensile strain was reached.

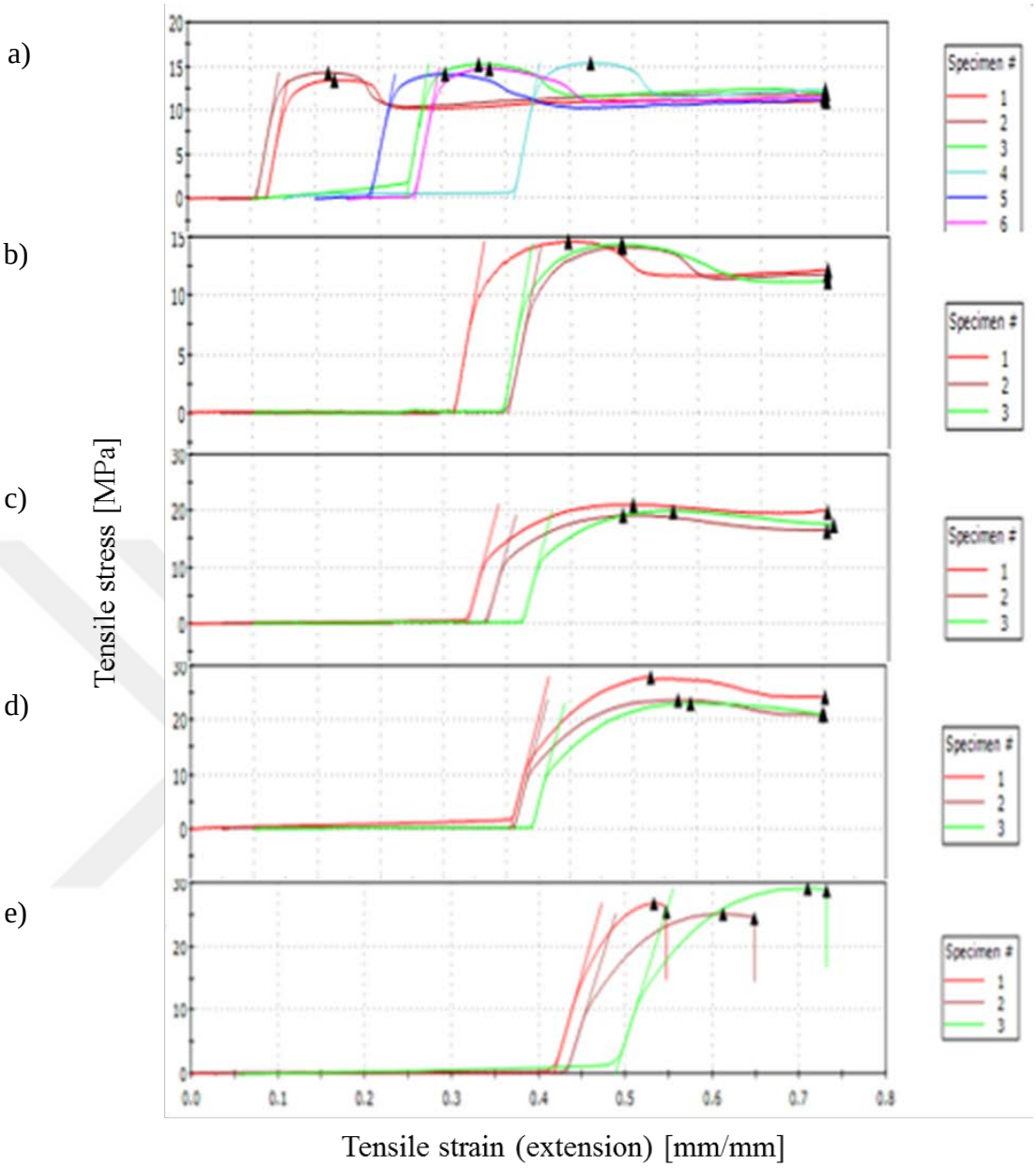

Figure 27. The tensile test of a) untreated, b) 600 W-5 min microwave treated, c) 600 W-10 min microwave treated, d) 600 W-15 min microwave treated, e) 600 W-30 min microwave treated PP samples with 10 mm/min extension rate.

In the sense of mechanical properties, the yield strength, modulus, and ductility were considered for untreated and microwave treated PP samples.

- Yield strength (σ_y): The stress a material can withstand without permanent deformation. [97]
- Modulus (E): It defines the stress-strain relation and can be expressed as the tangent of the stress versus strain curve.

  $E = \frac{\sigma}{\varepsilon}$ where σ refers to stress and ε refers to strain. [97]
- Ductility: The measure of the degree of plastic deformation under tensile stress by the time fracture occurs. It can be assessed quantitatively as percent elongation (% EL).

  $$\% \text{ EL} = \frac{l(\text{final}) - l(\text{initial})}{l(\text{initial})} \text{ x } 100 \quad [97]$$

As a result of the applied tensile tests it was observed that throughout the microwave treatment the average tensile stress at yield point (σ_y) that corresponds to the average yield strength gradually increased from 14.54 MPa to 26.97 MPa after 30-min microwave radiation. The average value of modulus raised from 395.40 MPa to 451 MPa during the microwave radiation although the modulus value for 5-min microwave radiated PP is slightly smaller than the untreated one; however, it is not important when the typical tensile test results are considered since ±15 deviations are commonly experienced in this highly sensitive instrument. Furthermore, the ductility which is determined by the percent elongation significantly decreased that can be observed in Figure 27 as the 30-min microwave radiated PP specimens could not even elongate 100 %, they broke before 1.0 mm/mm tensile strain was reached. The decrease in % EL made the PP specimens more brittle after the exposure to microwave radiation. Thus, the change in the mechanical strength is drastic when the period of time for radiation exposure is differentiated.

Table 2. Average values of Tensile Stress at Yield Point and Modulus for untreated and microwave treated PP samples.

	Tensile stress at Yield (Slope threshold 0.2 %) [MPa]	Modulus (E) [MPa]
Untreated PP	15	395 ± 15
600W_5min mw	16	381 ± 15
600W_10min mw	21	390 ± 15
600W_15min mw	25	449 ± 15
600W_30min mw	27	452 ± 15

To sum up, the yield strength, modulus, and brittleness of the PP specimens are increased by raising % crystallinity that makes the polymer films more brittle and glassy.

3.3 Physical Investigation of Polypropylene Surface

The investigation of whether polymer surface is affected throughout the experiment due to the microwave radiation and the applied mechanical stress was proceeded by obtaining topography images from Atomic Force Microscopy.

3.3.1 AFM Results

In order to analyze the possible physical alterations on the PP film surface due to the treatments AFM was carried out as a surface characterization technique at nano-scale. It is indicated by Li *et al.* surface roughness can change materials' electronic properties, then it controls the extent of contact between two surfaces. [87] Therefore, the magnitude of contact electrification is affected by the surface roughness.

In this part, AFM (Nanosurf) was utilized to obtain topography images that can be considered as a preliminary examination before going through the investigation of electrical potential via KFM.

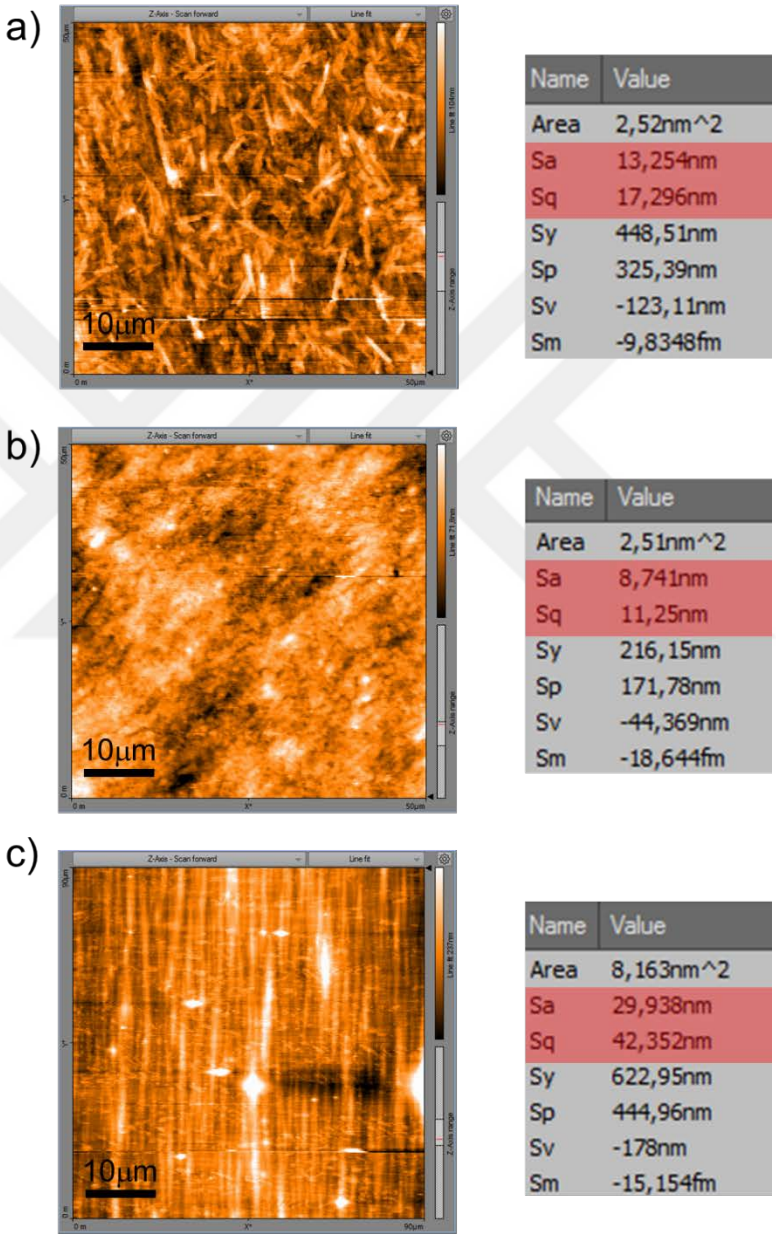

Figure 28. AFM height profile images with the surface roughness values (Sa and Sq) for a) untreated PP, b) 600 W-10 min microwave radiated PP, c) mechanically strained PP (extension rate is 40 mm/min).

In order to determine the surface roughness Sa and Sq values are considered where Sa refers to the average roughness and Sq indicates the root mean square roughness which are evaluated over the complete 3D surface respectively. Then, the height profile images containing Sa and Sq values yield that the surface roughness of PP decreases after treating the samples with microwave irradiation (600 Watt 10 minutes). Presumably, microwave absorption by the polymer causes an increase in the mobility of the polymer chains and heating of the polymer close to Tg resulted in fusion of crystal domains at the surface and hence surface roughness decreases. On the contrary, mechanical treatment causes a high increase in the surface roughness. Surface deformations on the polymer is clear from the Figure 28c upon stretching the PP film at room temperature, much below Tg.

Surface topography image of the stretched PP sample is in a good agreement with its POM images as the line-shape crystalline structures could be observed via both optical and mechano-optical imaging techniques. These line-shaped features has heights up to a few micrometer and their length changes from sub-micron to tents of micrometer. In addition to these changes, 1-2 micrometer wide vertical lines (Figure 15f and Figure 28c) that are perpendicular to stretching direction are formed upon mechanical stretching, evident by either surface imaging techniques.

3.4 Chemical Investigation of Polypropylene Surface

The effects of the treatments on the surface chemistry were analyzed via a comprehensive surface-sensitive spectroscopic technique, XPS.

3.4.1 XPS Results

XPS is a useful spectroscopic technique that presents an opportunity to analyze the surface qualitatively and quantitatively in terms of the elemental composition. Hence, we used XPS to specifically obtain the atomic percent ratio of oxygen (O) to carbon (C) in order to observe if any oxidation takes place on the material's surface due to the treatments. Since the tensile stress and electrification experiments were carried out in an ambient environment, the samples in concern were exposed to the oxygen present in the air. Thus, we investigated that whether the adsorbed oxygen by the polymer surface, consequently the possible surface oxidation plays a role in the static electrification of PP.

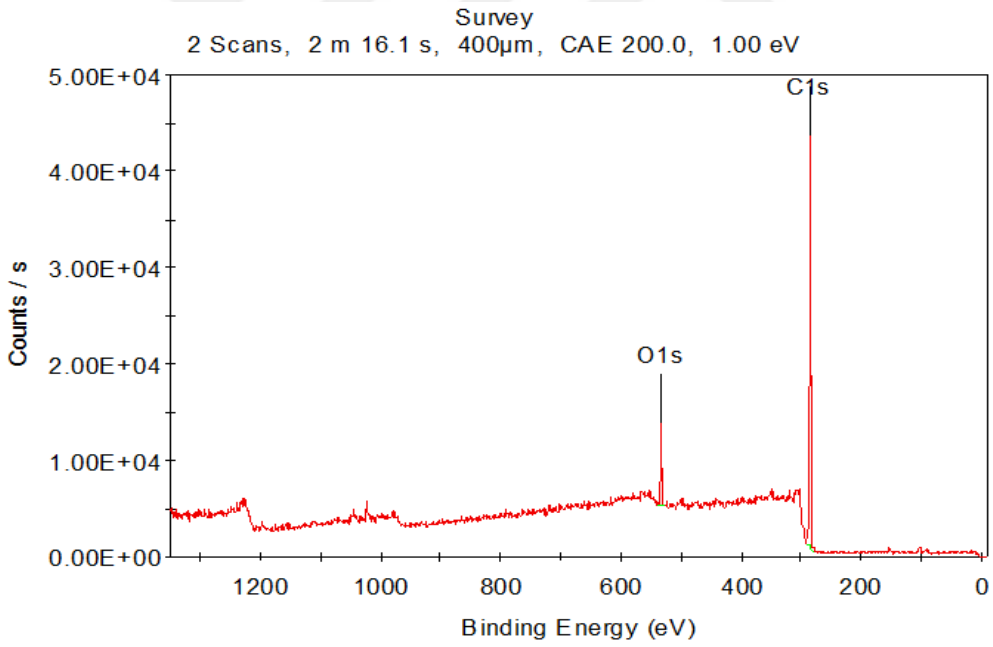

Figure 29. XPS survey scan of the untreated PP films.

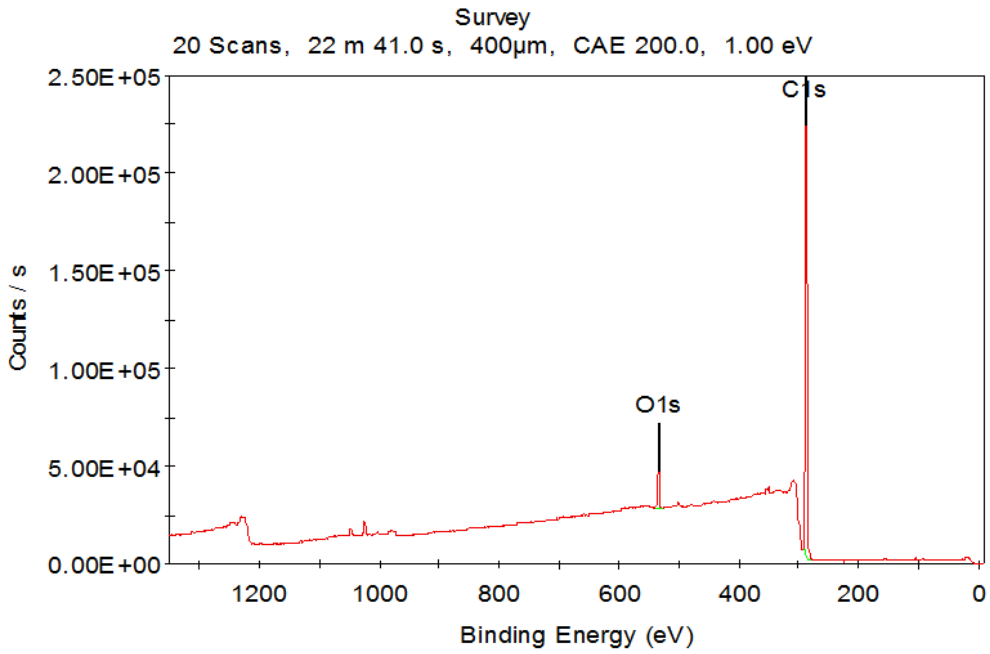

Figure 30. XPS survey scan of the mechanically stretched (with 40 mm/min) PP films.

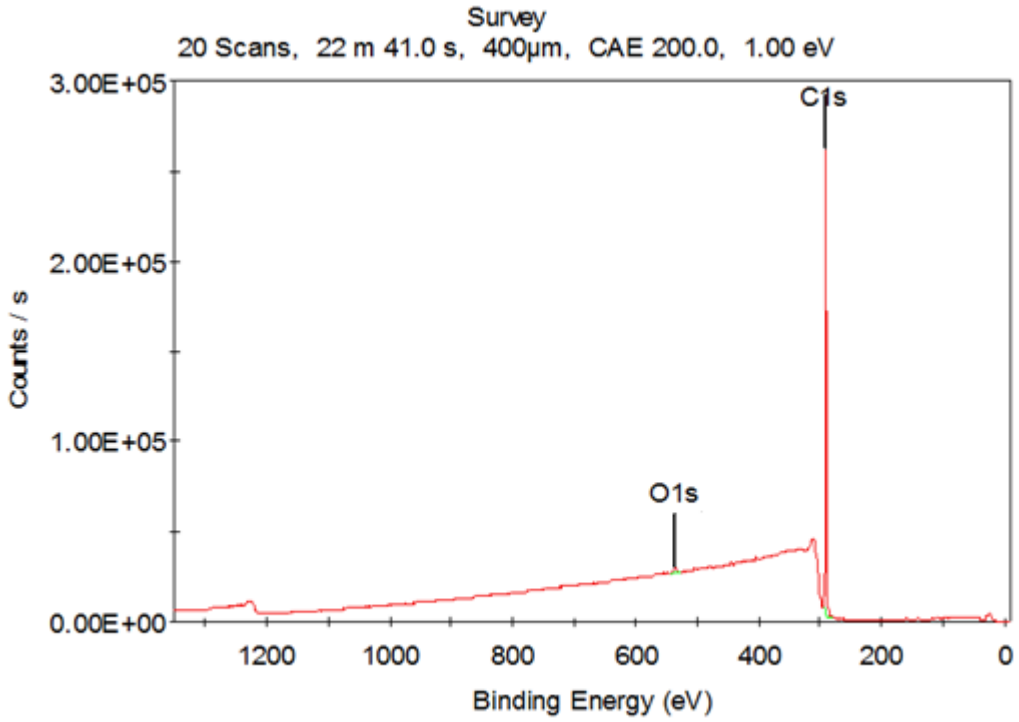

Figure 31. XPS survey scan of the 30 min-600 W microwave radiated PP films.

Table 3. The atomic % ratio of oxygen (O) to carbon (C) obtained from XPS.

0/C ratio	Point#1	Point#2	Point#3	Average
PP_untreated	0.112	0.098	0.086	0.099
PP_stretched	0.038	0.030	0.048	0.039
PP_mw (5min_600W)	0.012	0.013	0.006	0.010
PP_mw (30min_600W)	0.013	0.008	0.015	0.012
PP_mw (10min_100W)	0.012	0.006	0.004	0.007
PP_mw (10min_800W)	0.010	0.006	0.012	0.009

As the XPS survey scans indicate that after the treatments there is no oxidation taking place on the PP film surfaces. In contrast, it was determined that there is a decrease in the oxygen presence on the treated samples' surfaces. As the atomic % of oxygen was observed significantly higher in untreated PP samples than the treated ones, we tried to eliminate the possibility of water adsorption on bare PP surface. Therefore, we initially performed 600 W-10 min microwave radiation on a PP sample, then carried out the mechanical treatment and vice versa, i.e. we applied the mechanical stress first, then treated samples with 600 W-10min microwave radiation. However, the result did not change. It was verified that the water adsorption is not the reason for the higher atomic % of oxygen for untreated PP or lower in microwave treated PP samples. The possible explanation for the decrease in the O/C ratio is that as a consequence of microwave and mechanical treatments some cavities on the surface might occur during the re-organization of the polymeric chains meanwhile the movement of crystalline domains taking place, hence the oxygen molecules that are on some moieties, e.g. COOH, on the surface are moved into these cavities and embedded there. Therefore, the surface became oxygen deficient. Another highly possible reason is that due to the bond cleavage during the tensile stress oxygen may associate with the carbon present in the sample structure so that they can make C-O

containing compounds. As a result, the bare oxygen level decreases after the treatments. Besides, it was observed that the microwave treatment causes more drastic decline in the O/C ratio rather than the mechanical stress that makes the utilization of microwave radiation significant in the chemical identity of material's surface.

3.5 Electrical Investigation of Polypropylene Surface

After studying the crystallinity, physical, mechanical, and chemical properties of PP samples, electrical measurements were conducted.

3.5.1 KFM Results

KFM was utilized in order to examine the polymer's surface charge distribution after the degree of crystallinity and surface roughness was changed with the application of mechanical stress.

Before examining the surface potential the height profile image was taken from a specific area on the PP film surface, then the potential map was derived for that area corresponding to the obtained height profile.

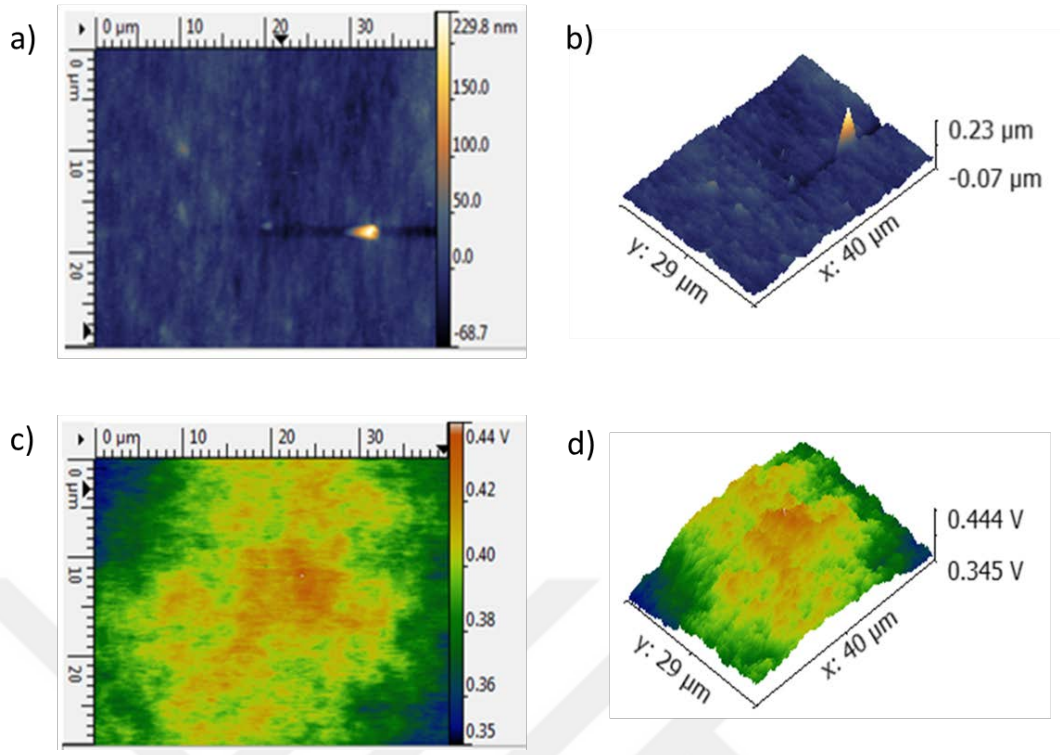

Figure 32. 2D (a) and 3D (b) height profile of untreated PP, 2D (c) and 3D (d) potential map of untreated PP.

AFM measurement of untreated and discharged PP sample shows that the sample has some irregularities in topography and some large structures on it, see Figure 32c and Figure 32d. KPFM measurement of the same area shows that the sample bears very little overall positive charge on it, see Figure 32c and Figure 32d. However, the potential window is only 90 mV from the most positive to the most negative potential value on the untreated PP sample surface. This result indicates that even a discharged sample can accumulate a small charge on it within time due to e.g. thermal effects and possible relaxation processes in the polymer, water deposition (since the measurements were done at the ambient conditions).

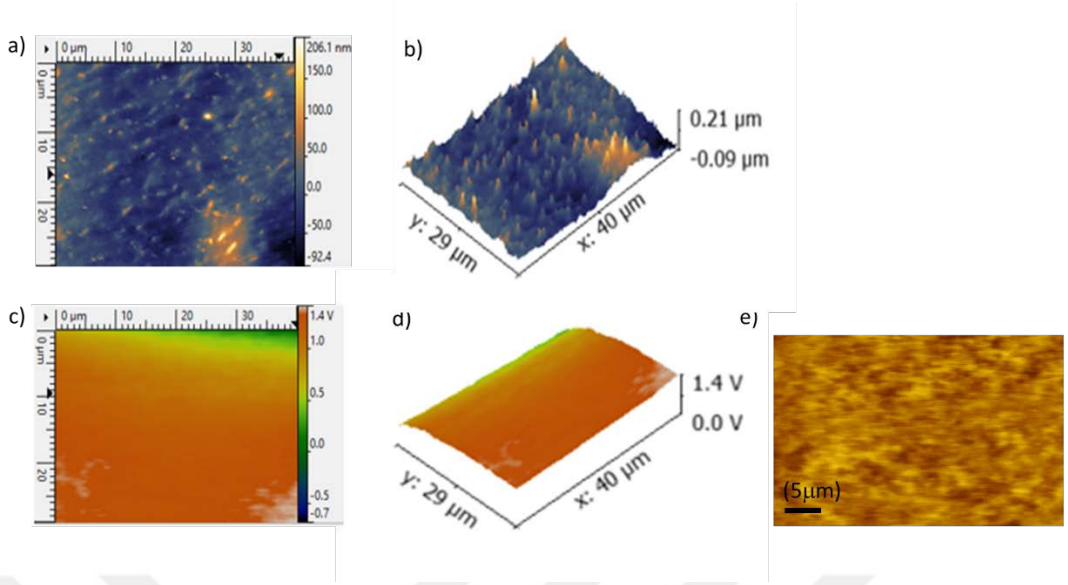

Figure 33. 2D (a) and 3D (b) height profile of 40 mm/min-mechanically strained PP, 2D (c, e) and 3D (d) potential map of 40 mm/min-mechanically strained PP.

Unlike untreated PP sample, KPFM measurement on the mechanically treated PP surface gives a large potential window of 2.1 V from the most positive to the most negative potential. Mechanical stretching causes a significant increase in the electrical potential of the polymer's surface compared to the bare untreated polymer sample. The potential maps show that mechanically treated samples bears a highly positive charge over the surface, though there are some, but relatively small negatively charged regions (Figure 33). As far as we know, this result is observed for the first time and it is an outstanding example of non-contact triboelectrification. Here, mechanical stress is applied to a polymer film and an electrical potential on the sample was generated. We also did macro-scale experiments and measurements where triboelectricity is produced from mechanical action, discussed in Non-Contact Electrification Results. Moreover, as a result of potential mappings of untreated and treated PP by KFM it was verified that the surface of the samples are not uniformly charged. When the mechanically

treated PP is considered it is clearly seen that nanoscale mosaics containing both positive and negative charges are developed by the surface.

3.6 Metal-Polymer (PP) Contact Electrification Results

The contact electrification was performed by the tapping of copper (Cu) to the polymeric surface of PP. After this metal-polymer contact the voltage was recorded via digital oscilloscope (Owon SDS7072 70 MHz, 2+1 Channel, 1 GS/s) with P4100 Series probes (100:1/100 MHz, Input voltage 2KV DC + AC pk, P4100 series High voltage probes), low-noise current preamplifier (SR570 Current Preamplifier). The classic, basic method of measuring a static charge is to place the charge on a capacitive system connected to an electrometer. If the collective capacitance of the system plus electrometer is C and the voltage, the reading of the electrometer, is V, the charge q equals to, according to the following equation,

$$q = CV \qquad [123]$$

The temperature and % humidity play a significant role in the static electrification as temperature affects the mobility of surface and air molecules and humidity affects the adsorption of water molecules generating a layer on the material's surface that alters the dissipation of charge. [27, 51] Therefore, for each electrical measurement the temperature and relative humidity (RH) were recorded and these values were tried to be kept approximately same in order to avoid the possible deviations for charge recording.

The typical schematic representation of the obtained 2D plots for the contact electrification was illustrated in the Experimental part under the Electrical

Measurement (see Figure 13). To clarify, the first peak appears at the moment of contact and the second relatively small peak appears at the moment of separation.

The mechanism of contact electrification relies on tapping of metal electrode to the base electrode which is coated with PP film in our system. Then, the contact of PP and metal (Cu) takes place, consequently the triboelectrification of PP is determined with the voltage versus time plots obtained from oscilloscope.

3.6.1 Mechanism of Metal-Polymer Contact Electrification

Since polymers are insulating materials, it is not possible to extract the electricity from PP without a base electrode. After the first contact, subsequently the charge generation on the polymer surface takes place. Then, the convergent induction (I_c) peak is observed when the polymer on the base electrode is getting closer to the metal electrode again. Later, the divergent induction (I_d) peak appears when the polymer is getting far away from the metal electrode during the separation.

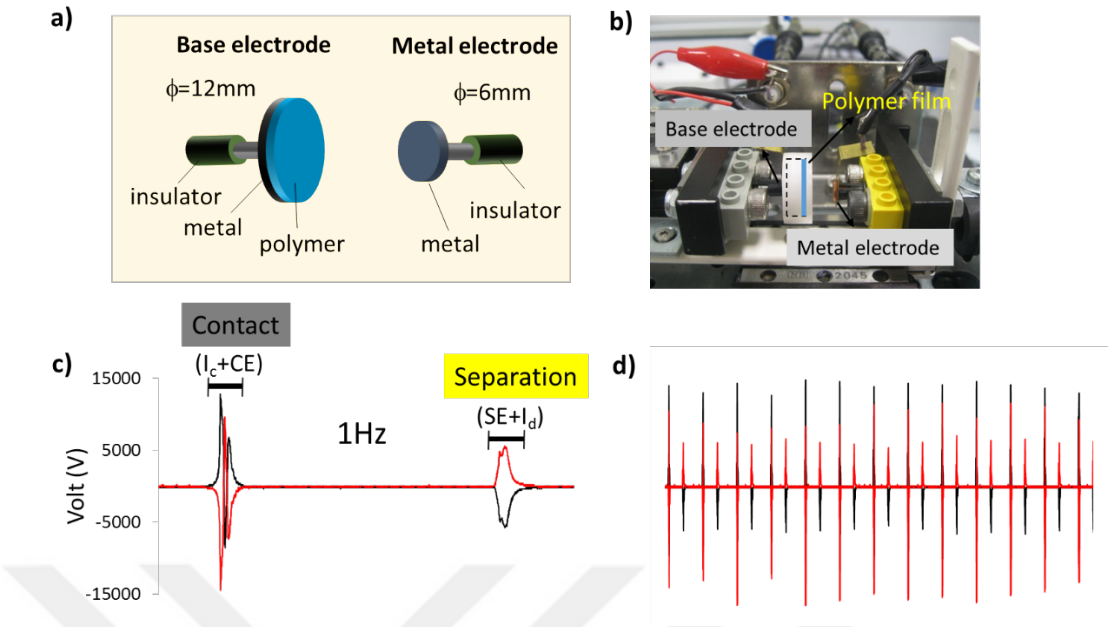

Figure 34. a) The illustration of base electrode which is Cu SEM stub (in 12 mm diameter) coated with the polymer film (PP) and the metal electrode which is Cu in 6mm diameter, b) The schematic representation of the mechanical tapping device, c) The contact electrification (CE) peak with the convergent induction (I_c) and the separation electrification (SE) peak with the divergent induction (I_d) at 1 Hz tapping frequency, d) The overall contact and separation peaks in 1 Hz tapping frequency obtaining 1 data in 2 s.

In the literature, one channel measurement is commonly used to take the electrification data from charge. [82] Therefore, they could not observe CE and SE signals in both positive and negative side simultaneously. However, by using two channels connected to the oscilloscope we enabled to observe the CE and SE signals in detail. Consequently, in our study we revealed that during the contact the pair of (+) and (–) electrification signals are produced. This observation leads to the fact that in the contact electrification both (+) and (–) charges are generated. The separation electrification (SE) and CE mechanisms on the base electrode (PP on it) and metal electrode (Cu) are demonstrated in Figure 35.

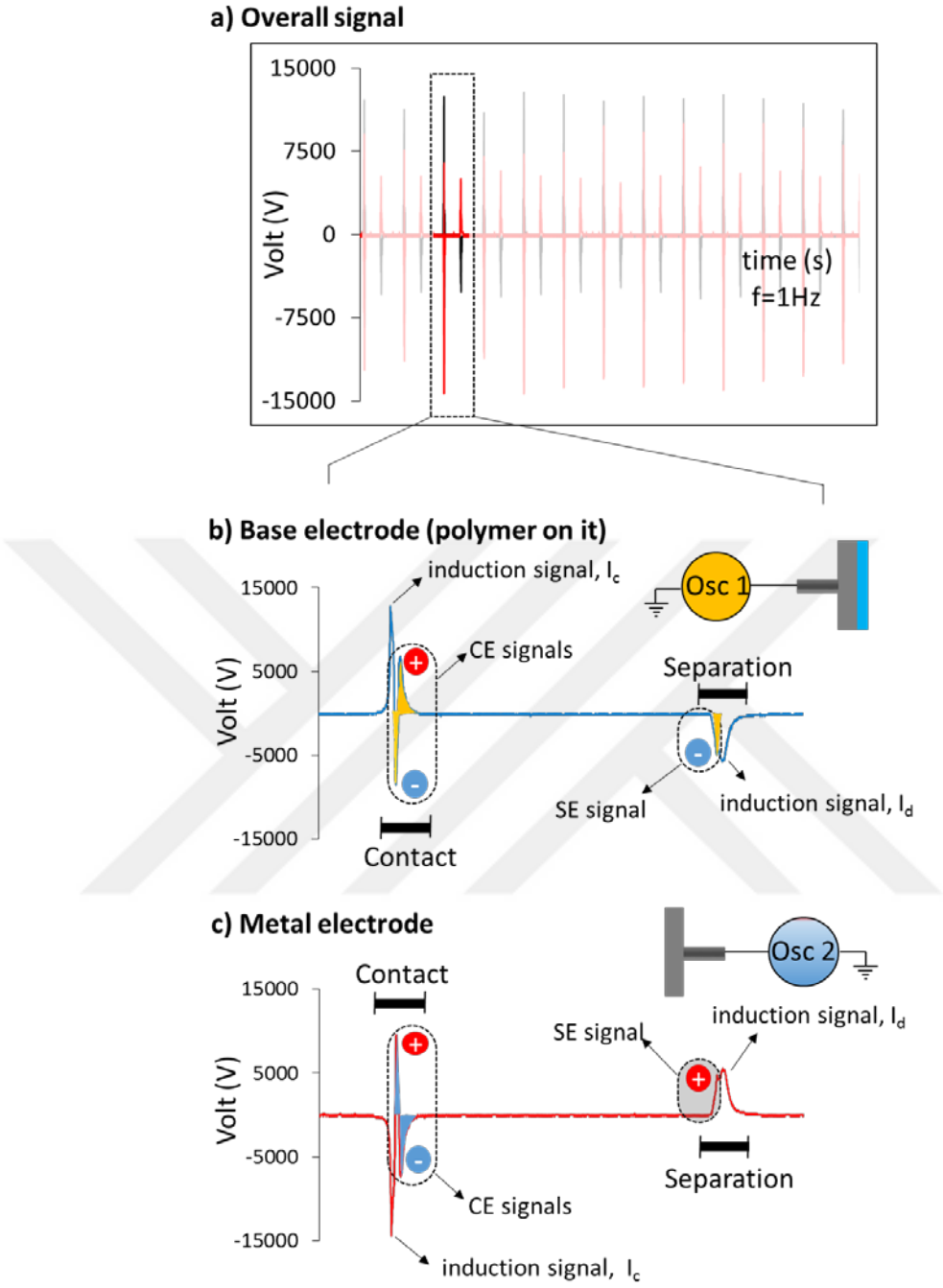

Figure 35. The representation of a) overall contact and separation peaks obtained from two different channels, oscilloscope 1 (Osc 1) and oscilloscope 2 (Osc 2), b) the CE and SE mechanisms on the base electrode (PP on it) which is connected to Osc 1, c) the CE and SE mechanisms on the Cu metal electrode which is connected Osc 2. (Adapted from Umar Gishiwa Musa's M.S. thesis: "Mechanism of Triboelectricity: A Novel Perspective for Studying Contact Electrification Based on Metal-Polymer and Polymer-Polymer Interactions")

Figure 35 shows that during the contact of Cu metal electrode and PP which is on the base electrode's surface both (+) and (–) CE signals are produced that indicates the existence of charge mosaic after the contact. In addition, due to the charging of two contacted surfaces after the first contact, the positive induction signal for the base electrode and symmetrically the negative induction signal for the metal electrode are noted. Later on, when the separation takes place two signals assigning for SE and induction are identified in our proposed mechanism.

The whole mechanism behind the contact electrification of PP which covers the base electrode's surface and Cu (i.e. metal electrode) is explained in Figure 36 and Figure 37. (Adapted from Umar Gishiwa Musa's M.S. thesis: "Mechanism of Triboelectricity: A Novel Perspective for Studying Contact Electrification Based on Metal-Polymer and Polymer-Polymer Interactions")

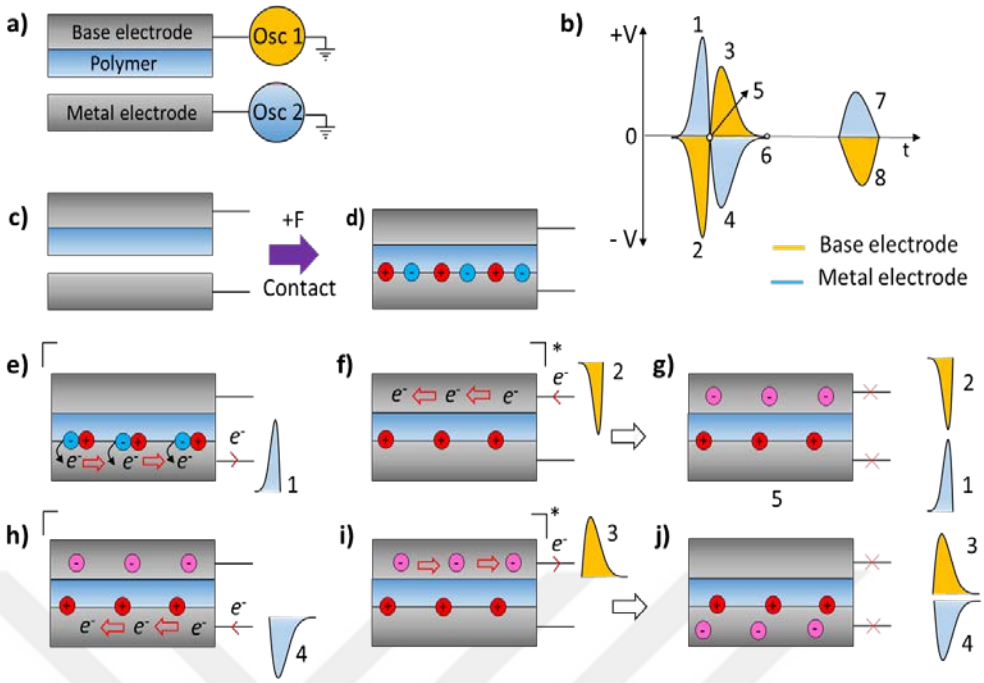

Figure 36. The mechanism during contact a) The base electrode whose surface is covered by PP connected to the first channel, Osc1 which is grounded and the metal electrode connected to the second channel, Osc 2 which is also grounded, b) The voltage versus time plot containing the signals from base and metal electrode, c) PP surface and metal electrode is getting closer indicated by the application of positive force, +F, d) The positive and negative charges are generated during the contact of polymer and metal surface, e) The electrons (negatively charged particles) are not stable, that is they flow towards the ground that makes the metal electrode e^- deficient leading to the generation of positive CE signal (1) from the metal electrode and at the same time (f) takes place, f) The electrons flow from the ground towards the base electrode that makes the base electrode e^- rich resulting in the generation of negative CE signal (2) obtained from the base electrode simultaneously with the generation of signal (1) from the metal electrode, g) The negative charges on the base electrode and the positive charges on the contacted surfaces remain for a very short time, i.e. around nanosecond, and there is no signal observed at this moment which is indicated by point 5 in the plot, h) The electrons in the ground move towards the e^- deficient metal electrode leading to the generation of negative CE signal (4) from the metal electrode and concurrently (i) takes place, i) The remaining electrons in the base electrode flow towards the ground that leads to the generation of positive CE signal (3) from the base electrode simultaneously with the generation of signal (4) from the metal electrode, j) The negative charges on the metal electrode and the positive charges on the contacted surfaces remain for a short time without any signal generation which is indicated by point 6 in the plot.

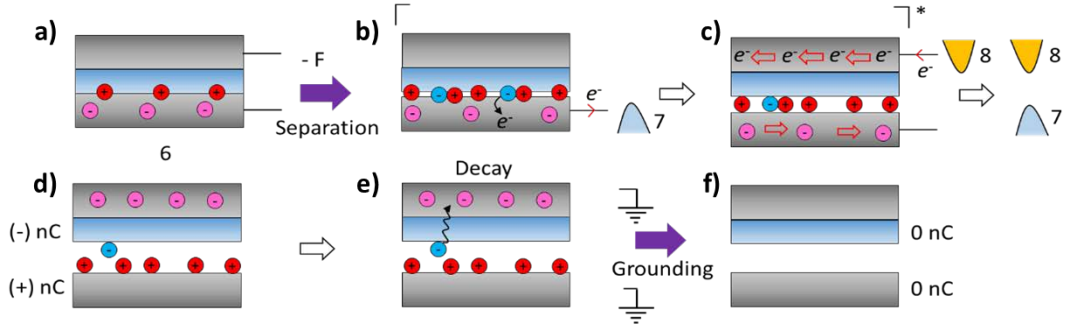

Figure 37. The mechanism during separation a) The negative force, -F, is applied to separate the contacted metal and polymer surface, b) During the separation electrons flow from the contacted surfaces towards the ground throughout the metal electrode that results in the positive SE signal (7) obtained from the metal electrode and at the same time (c) occurs, c) The electrons move from the ground to the base electrode that leads to the generation of negative SE signal (8) from the base electrode simultaneously with the generation of signal (7) from the metal electrode, d) After the separation, due to the bond breaking and subsequently material transfer (+) and (-) charges are recorded on the polymer and metal electrode surface at nC scale, e) When the system is left after the separation, charge decay is observed that yields decrease in the amount of charge on the polymer surface, f) After the grounding both polymer and metal surfaces lose their charges leading to the recording of zero charge.

There is compensation taking place in the electron flow between (e) and (f), also between (h) and (i). As a result, during the contact of polymer and metal surfaces positive and negative CE signals are recorded for both base electrode (PP on it) and metal electrode via Osc1 and Osc 2, respectively. When the separation happens only positive SE for the metal electrode and only negative SE signal for the base electrode is observed.

3.6.2 The Contact Electrification of PP Before and After Treatments

The contact electrification whose mechanism was proposed in the previous section was carried out for untreated and treated PP, then the results were presented in the following voltage versus time plots.

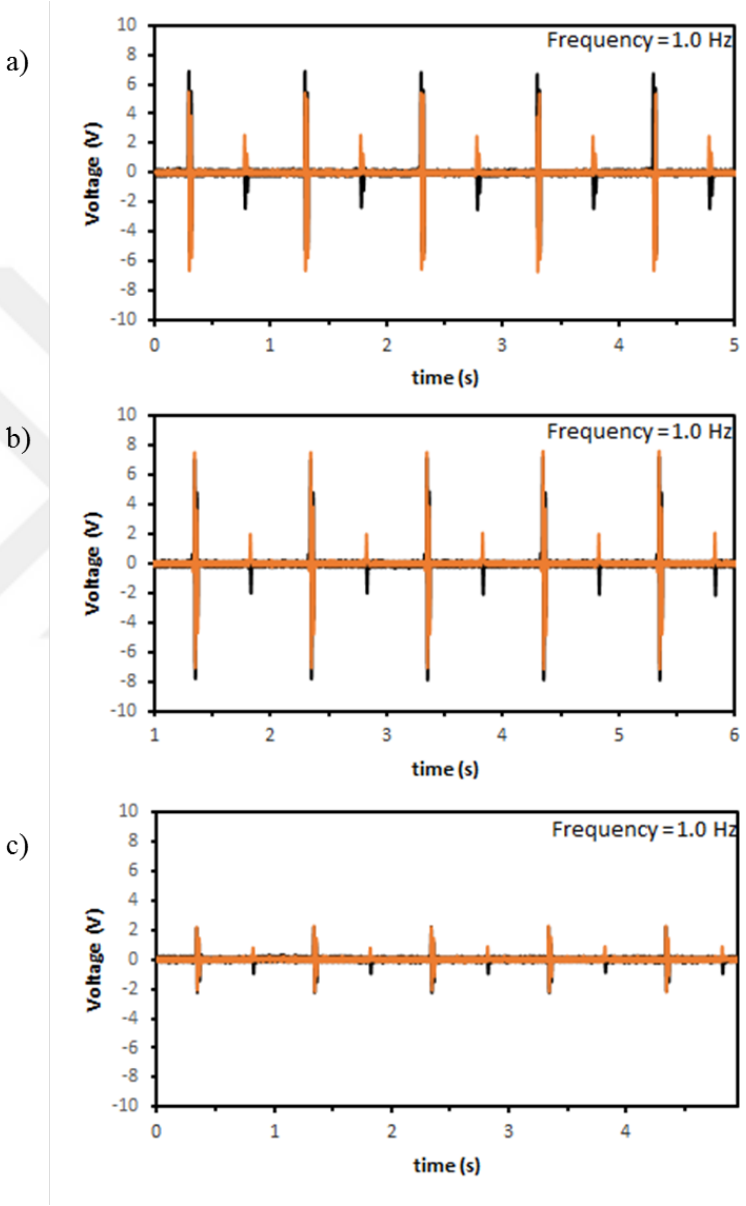

Figure 38. The measurement of static electrification (data/1s) for the constant tapping of Cu electrode with 1.0 Hz frequency onto a) untreated PP, b) 600 W-10 min microwave radiated PP, c) with 40 mm/min extension rate mechanically treated PP (26 ^{0}C, 18.66 % RH).

As it can be seen in Figure 38 the application of mechanical stress to the samples leads to a dramatic decline in their tribocharging tendency, hence smaller CE and SE signals are observed. On the other hand, the microwave radiation causes relatively smaller decrease in tribocharging, and in CE, SE signals of PP compared to the mechanical stress. This is because of the higher degree of crystallinity in addition to high surface roughness for the mechanically treated PP samples.

3.6.2.1 The Effect of Period of Time for Microwave Radiation on Contact Electrification of PP

In the second part of the experiments on contact electrification, the effect of the period of time for the exposure to the microwave radiation was studied. It was observed that by changing the duration of radiation exposure a small decrease occurs in the static electrification of PP. Figure 39 shows that even though the microwave treatment causes notable decrease in the CE and SE signals of untreated PP, there is not any significant change takes place in the intensity of the CE and SE signals due to the application of different period of time for microwave radiation.

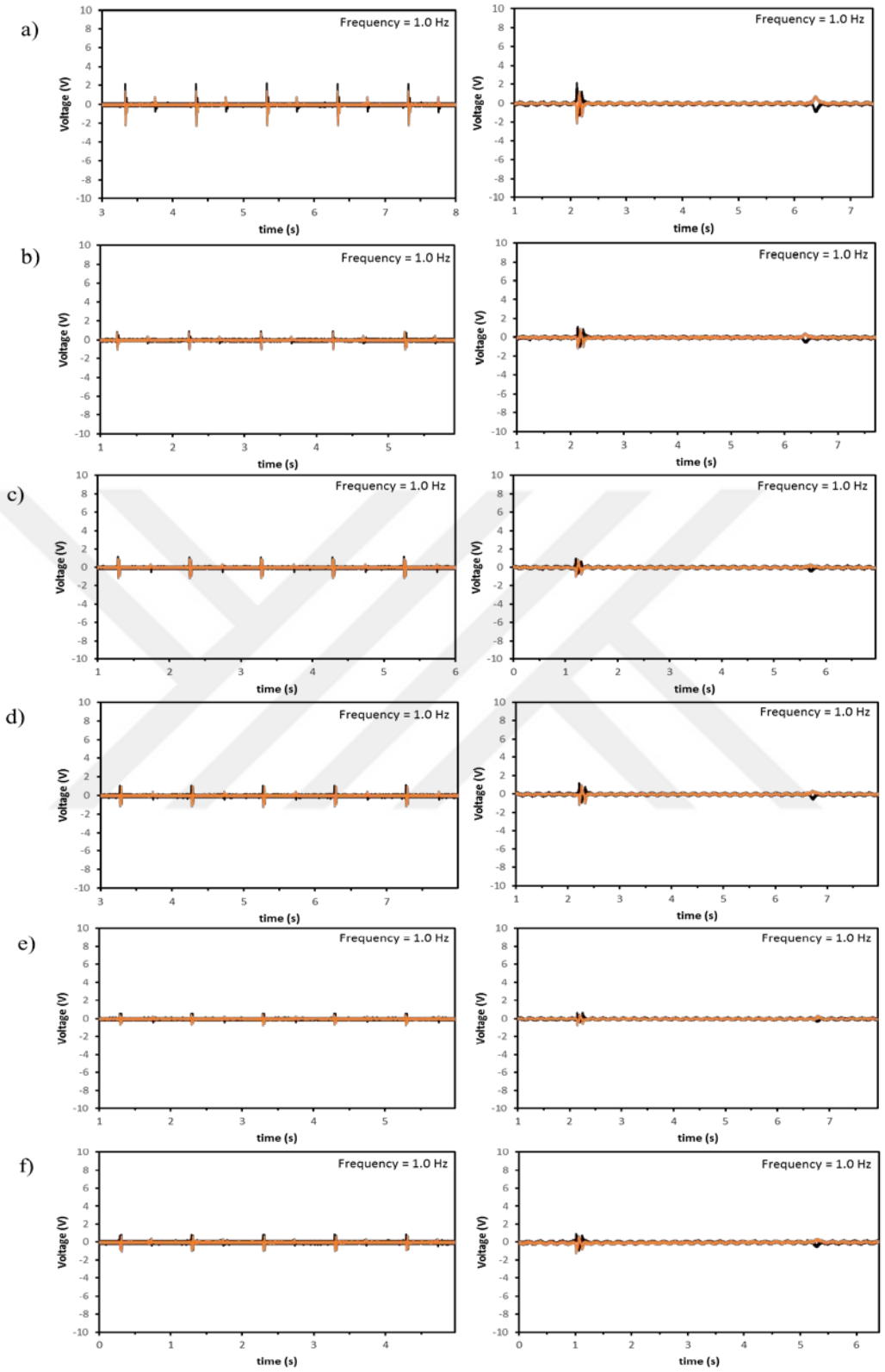

Figure 39. The measurement of static electrification with data/1s (left) and data/50ms (right) for the constant tapping of Cu electrode with 1.0 Hz frequency onto a) untreated PP b) 600 W-1 min microwave radiated PP c) 600 W-2 min microwave radiated PP d) 600 W-5 min microwave radiated PP e) 600 W-15 min microwave radiated PP f) 600 W-30 min microwave radiated PP (26.5 ^{0}C, 17 % RH).

As it can be seen in Figure 39 the voltage for the untreated PP was obtained as ~2V whereas it was ~1V for the 600 W-30 min radiated PP. Hence, tribocharging decreased when the PP was exposed to microwave radiation. However, the change was very small between the microwave treated samples with respect to different radiation times. Thus, the period of time for the microwave exposure did not cause any significant alteration in tribocharging.

3.6.3 The Effect of Tapping Frequency on Contact Electrification

In the last step of the contact electrification, the effect of the tapping frequency on tribocharging of PP was investigated.

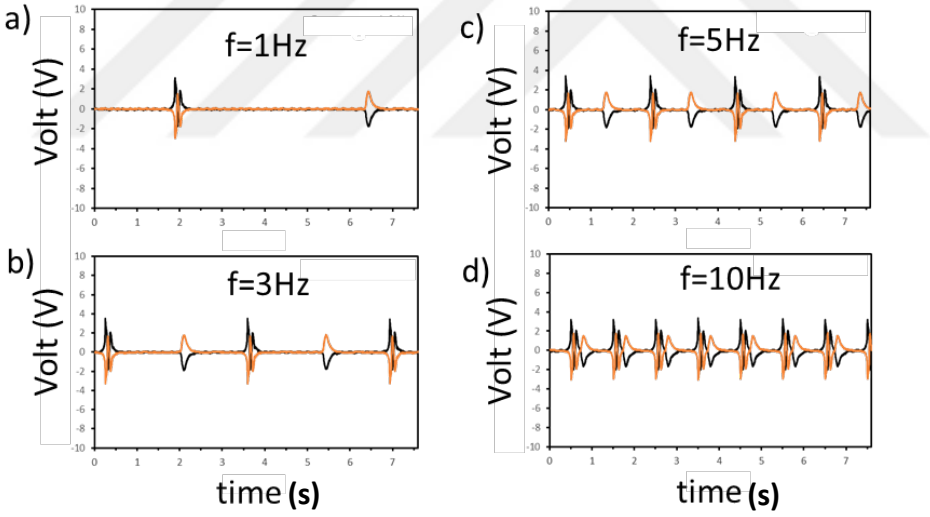

Figure 40. The measurement of static electrification with data/1s (left) and data/50ms (right) for the constant tapping of Cu electrode onto untreated PP with a) 1.0 Hz frequency, b) 3.0 Hz frequency, c) 5.0 Hz frequency, d) 10.0 Hz frequency (25 ^{0}C, 18.05 % RH).

As it is shown in Figure 40, changing the tapping frequency did not considerably change the intensity of tribocharging and the voltage values were

obtained at ~2V for the untreated PP samples. However, the resolution of the peaks in the same time interval was affected by the tapping frequency. When the frequency was increased the separation peak was getting closer to the contact peak, even they were getting intertwine that makes difficult to differentiate the CE and SE signals during the contact and separation.

3.7 Non-Contact Electrification

The effect of triboelectric charging was observed not only in contact of two surfaces, but also it was generated during the performing of tensile stress to the PP films in our study. This observation plays a crucial role for triboelectricity harvesting from mechanical energy in order to meet with the energy supply problem which is today's one of the main concerns.

The experiment was proceeded in a way that during the application of tensile stress onto PP film which was enclosed by a Faraday cage for the inductive charge measurement the generated charge was recorded quantitatively in nanocoulomb (nC) via Keithly Multimeter that was connected to the Faraday cage (See the representation of whole system in Figure 14).

We obtained charging data in two different modes. In the first mode, constant position mode, Faraday cup was held at a fixed position and charging of the polymer film as the film is stretched was obtained. Non-contact charging of the polymer film in Figure 42b was obtained in this way. In the second mode, scan mode, Faraday Cup was moved along the e.g. 30 cm stretched polymer film after the first fixed mode measurements. Non-contact charging of the polymer film in Figure 42c was obtained in this mode of measurement.

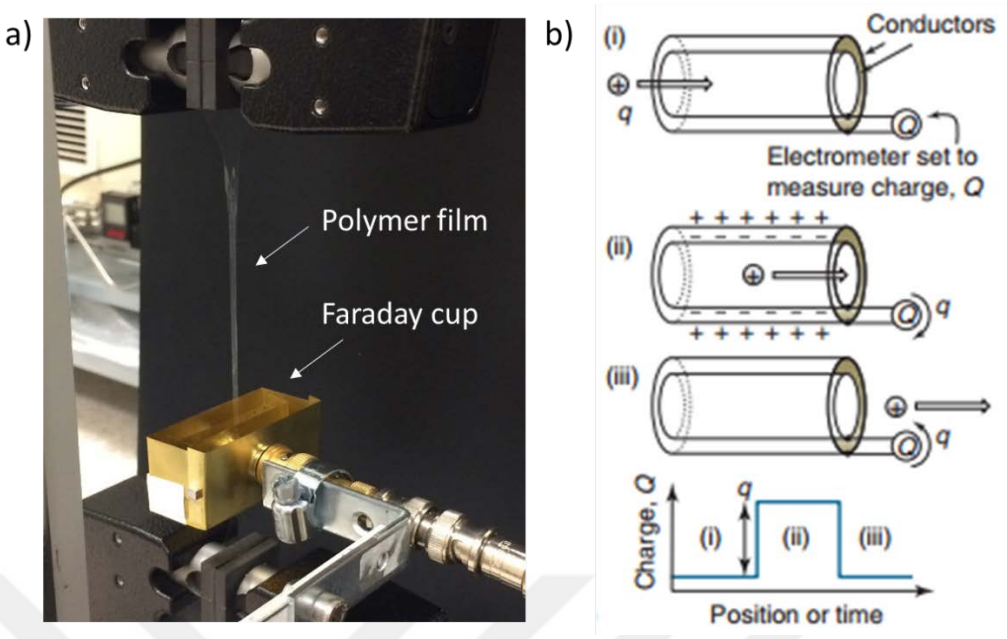

Figure 41. a) Presentation of the brass-made Faraday cage used throughout non-contact electrification experiments, b) Charge, *q*, flows between the inner and middle brass components of the Faraday tube to compensate for the enclosed charge on the material. Measuring the charge on the electrometer as a function of time will indicate the value of *q*. [124]

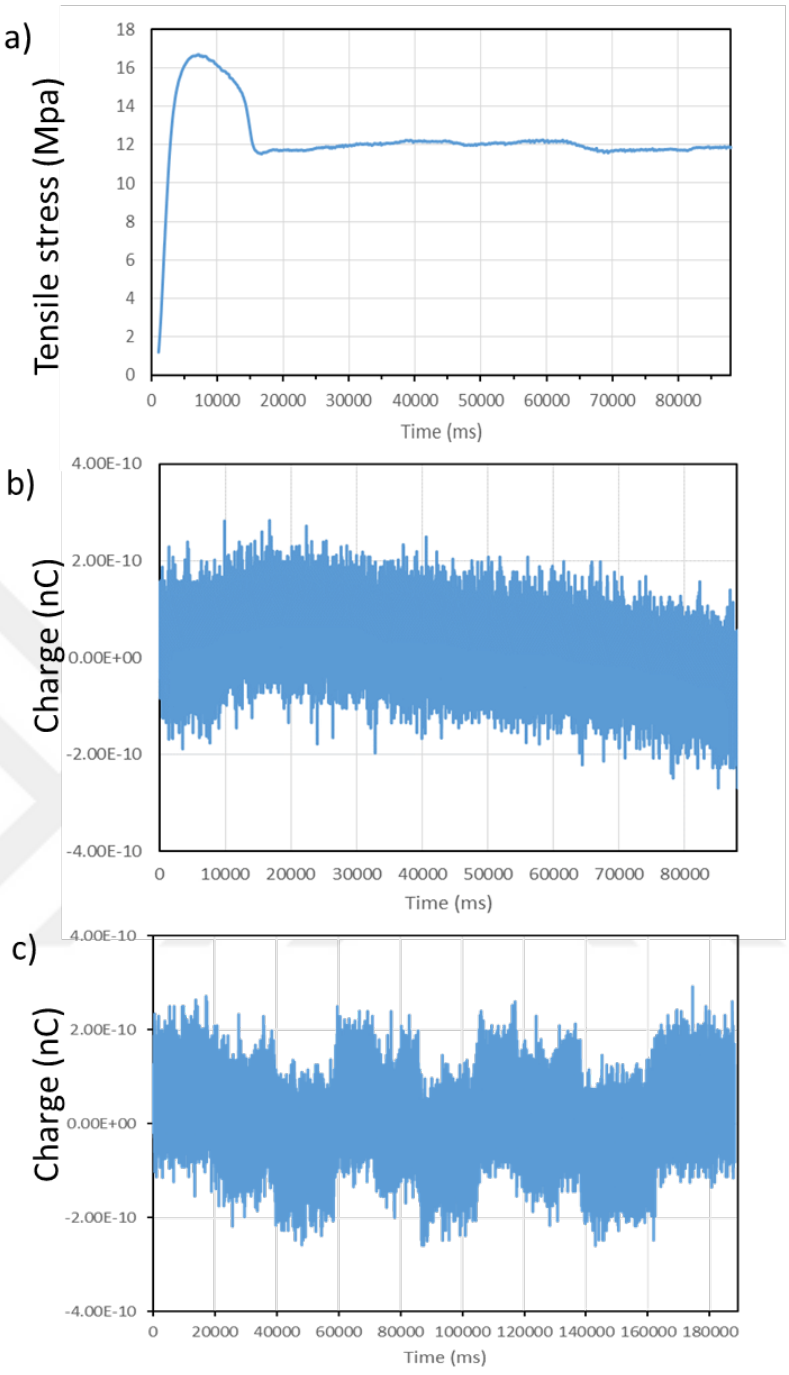

Figure 42. a) The plot of tensile stress versus time from mechanical tester during tensile extension with 40 mm/min extension rate for untreated PP sample, b) The plot of charge versus time from the mid-point of the original untreated PP during tensile extension with 40 mm/min, c) The typical plot of partial charge distribution for the extended PP after tensile extension with 40 mm/min (25 ^{0}C, 22 % RH).

The repeated non-contact triboelectrification experiments yield that there is not any regularity in the way of charging, that is in one measurement the charge accumulation progressed towards positive (+) while in another measurement with the same conditions and the same stress-strain curve the charge accumulation can incline towards negative (-) side.

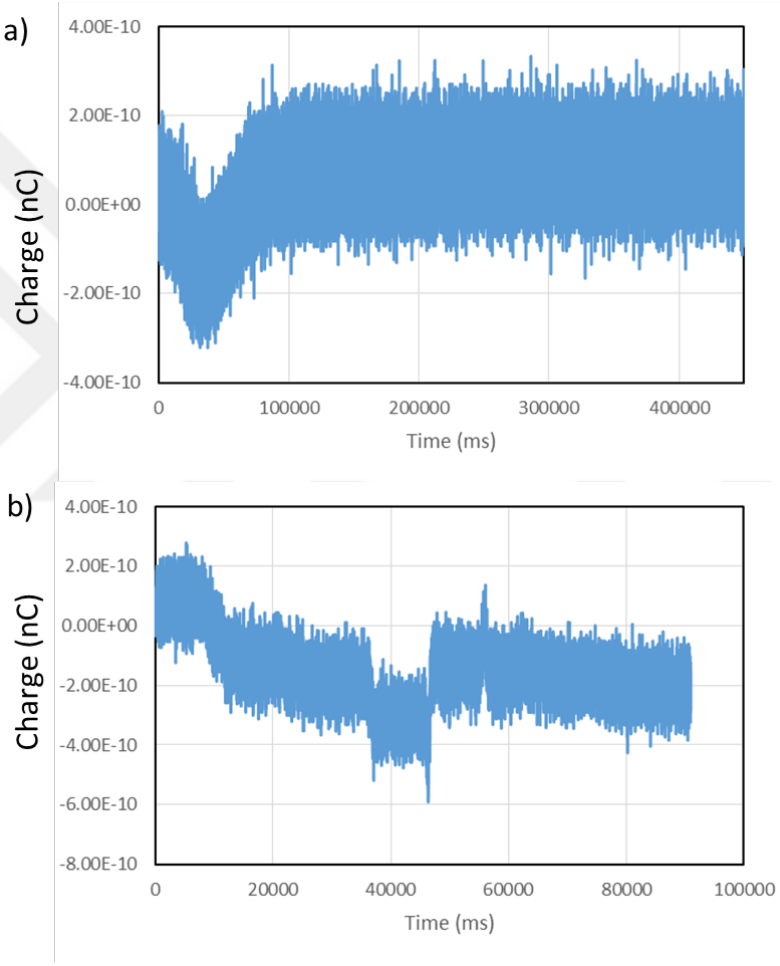

Figure 43. a) The plot of charge versus time from the mid-point of the original untreated PP during tensile extension with 40 mm/min, b) The partial charge distribution of the extended PP after tensile extension with the rate of 40 mm/min (26.1 ^{0}C, 31 % RH).

As it is indicated by Lacks *et al.* tribocharging is unpredictable and usually irreproducible since various parameters play a role, such as experimental conditions (temperature, humidity *etc.*), different mechanisms taking place in bond scissions/formations and so on. [15]

Our current understanding of tribocharging suggests that the differentiations in direction of charge accumulation arise because multiple properties or mechanisms contribute to charging. As the bond dissociation and chemical changes occur simultaneously at different rates the alterations in the way of charging is possible.

3.7.1 The Effect of Microwave Radiation on Non-Contact Electrification of PP

As a second step, the effect of microwave treatment and the relaxation time after the microwave radiation were analyzed. Since the experimental conditions (i.e. temperature and humidity) are important in terms of the precision the measurements were proceeded for both untreated and microwave treated samples at the same conditions so that a reliable comparison could be done. Since the microwave treated sample could not reach the same elongation with untreated one due to its brittle feature, the l_{final} = 325 mm for untreated PP and l_{final} = 160 mm for microwave radiated PP were noted in order to avoid any break.

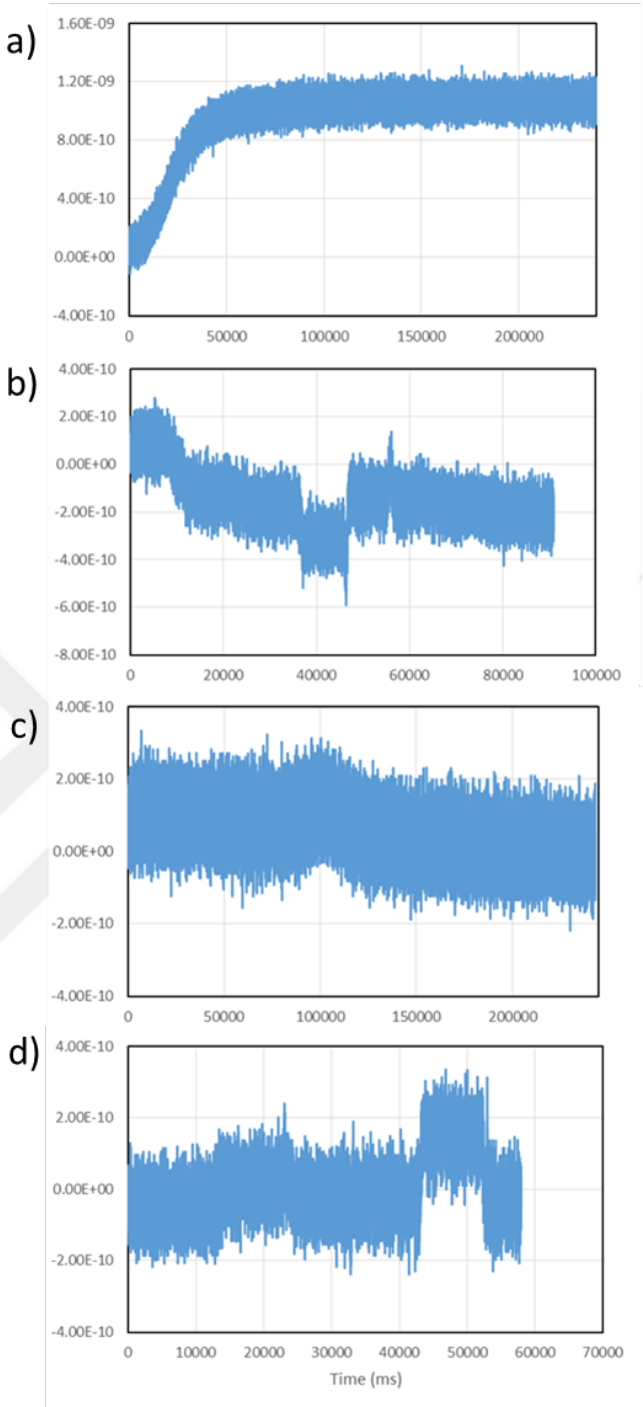

Figure 44. a) The plot of charge versus time during tensile extension with 40 mm/min from the mid-point of the original 600 W-10 min microwave-radiated PP after 40 min relaxing time, b) The partial charge distribution of the extended microwave-treated PP after 40 min relaxing time, c) The plot of charge versus time during tensile extension with 40 mm/min from the mid-point of the original 600 W-10 min microwave-radiated PP after ~4 hrs relaxing time, d) The partial charge distribution of the extended microwave-treated PP after ~4 hrs relaxing time (26.1 ^{0}C, 31 % RH).

As a result, the relaxation time after the microwave radiation plays an important role in the magnitude of tribocharging, thus when the duration of relaxation after the microwave is increased the tribocharging of PP specimen decreases because charge decay occurs after a while. Moreover, when Figure 42b and Figure 44a are compared it is seen that the charge increased from ~0.2 nC to ~1.2 nC after the microwave radiation to bare PP samples. Therefore, the increased degree of crystallinity and surface roughness throughout the microwave radiation results in the higher extent of tribocharging for microwave treated PP rather than the tribocharging of untreated PP specimen.

3.7.2 The Effect of Extension Rate on Non-Contact Electrification of PP

In this part of the non-contact electrification experiment, the effect of extension rate on tribocharging of PP was investigated.

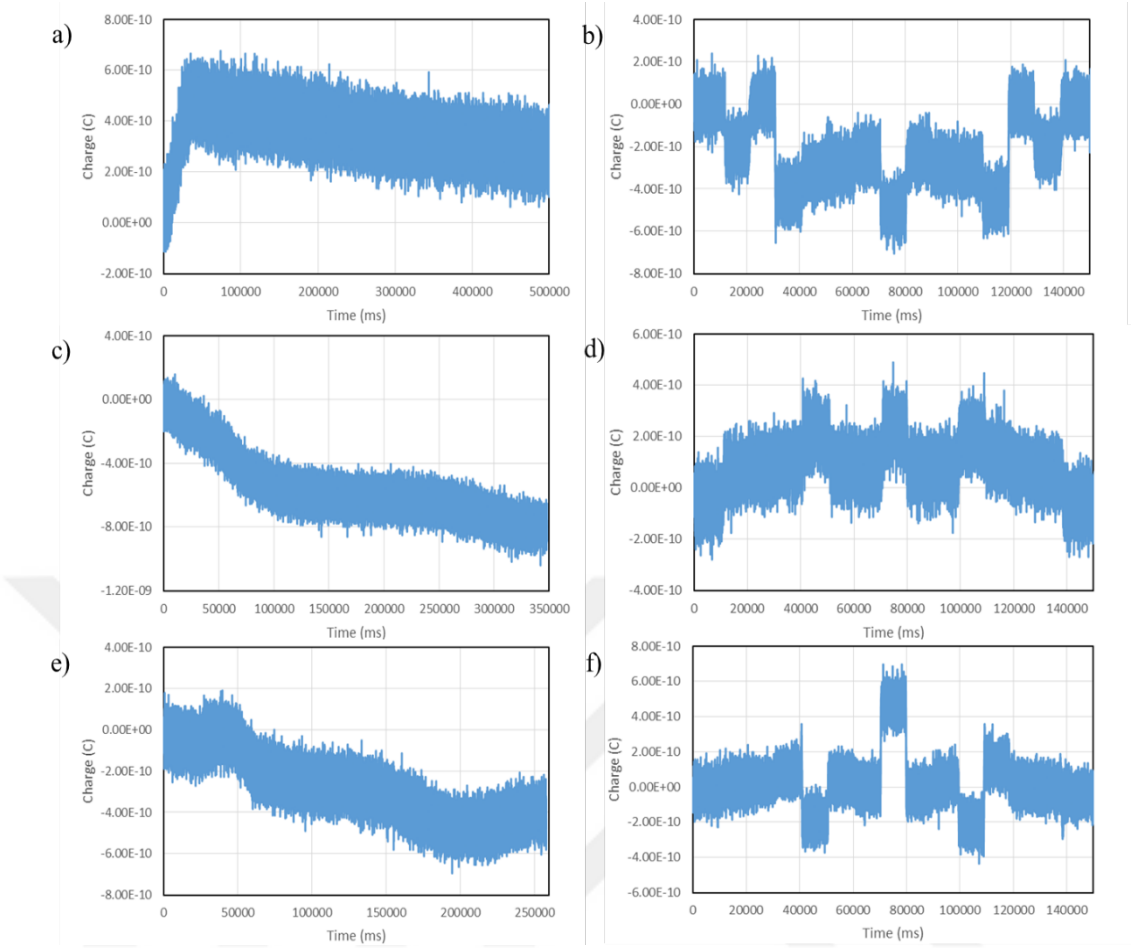

Figure 45. a) The plot of charge versus time from the mid-point of the original untreated PP sample during tensile extension with 40 mm/min, b) The partial charge distribution of the extended PP after tensile extension with 40 mm/min, c) The plot of charge versus time from the mid-point of the original untreated PP sample during tensile extension with 60 mm/min, d) The partial charge distribution of the extended PP after tensile extension with 60 mm/min, e) The plot of charge versus time from the mid-point of the original untreated PP sample during tensile extension with 80 mm/min, f) The partial charge distribution of the extended PP after tensile extension with 80 mm/min (24.5 ^{0}C, 26.0 % RH).

By considering the partial charge distribution plots in Figure 45, the scale of tribocharging is determined as 0.8 nC, 0.6 nC, and 1.0 nC for the specimens extended with 40 mm/min, 60 mm/min, and 80 mm/min extension rate, respectively. Therefore,

the extension rate does not significantly change the extent of tribocharging, but it affects the way of charging as the initial sharp peak is getting disappear when the extension rate increases, also the charging progresses continuously towards the negative side for the samples whose extension rates are high (60 mm/min and 80 mm/min).

3.7.3 The Relation Between Crystallinity and Charge Mosaic in Non-Contact Electrification of PP at the Large Scale

In the final part, the ratio of crystalline and non-crystalline Raman peaks, which were obtained centimeter by centimeter on the mechanically extended PP sample, was traced across the plot of tribocharging. Hence, by this way it was analyzed that whether the changes in tribocharging are parallel with the differentiations in percent crystallinity.

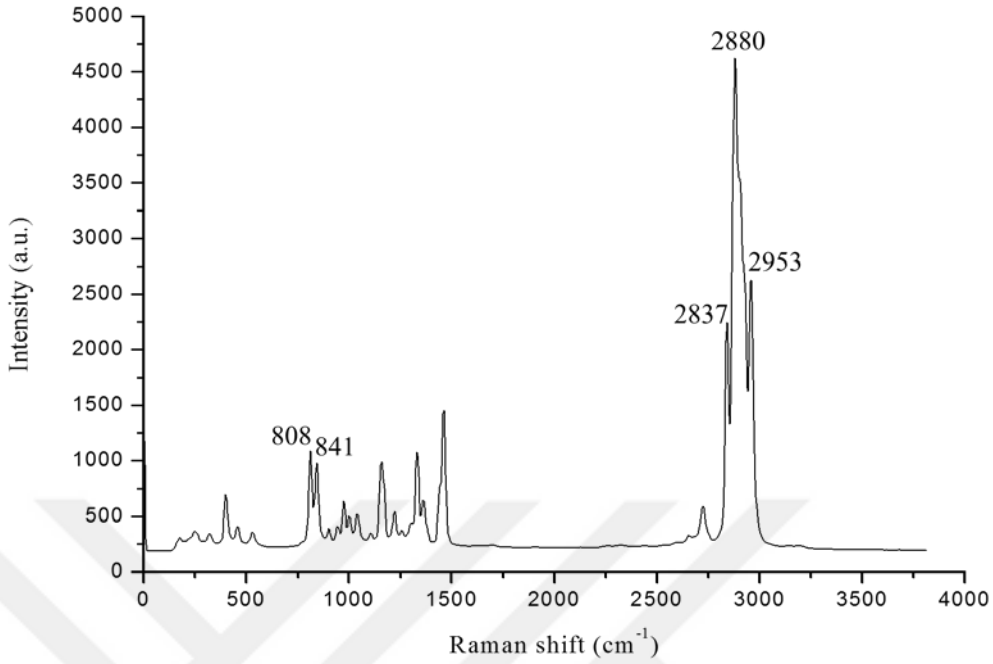

Figure 46. Raman spectrum of untreated PP with the indication of the peaks that are concerned in terms of crystallinity.

Table 4. a) The ratio of intensity of the crystal peak at ~808 cm^{-1} (I_1) to the amorphous peak at ~841 cm^{-1} (I_2), b) The ratio of intensity of the peak at ~2837 cm^{-1} (I_3) to the peak comes around 2880 cm^{-1} (I_4) and the peak at ~2953 cm^{-1} (I_5) to the peak comes at ~2880 cm^{-1} (I_4) that belong to the vibrational assignment of C-H bond in CH_3. [116]

(a)	I_1/I_2
Untreated	1.05
Point#1	1.64
Point#2	1.40
Point#3	1.31
Point#4	1.20
Point#5	1.66
Point#6	1.36
Point#8	1.20
Point#10	1.21
Point#12	1.67
Point#14	1.31
Point#16	1.26
Point#18	1.20
Point#20	1.45
Point#22	1.31
Point#24	1.16
Point#26	1.12
Point#28	1.35
Point#29	1.30
Point#30	1.18
Point#31	1.17
Point#32	1.46
Point#33	1.26
Point#34	1.19

(b)	I_3/I_4	I_5/I_4
Untreated	0.47	0.56
Point#1	0.79	1.03
Point#2	0.84	1.03
Point#3	0.86	1.04
Point#4	0.87	1.03
Point#5	0.82	1.06
Point#6	0.84	1.04
Point#8	0.92	1.02
Point#10	0.92	1.03
Point#12	0.81	1.05
Point#14	0.87	1.03
Point#16	0.89	1.03
Point#18	0.92	1.02
Point#20	0.85	1.03
Point#22	0.87	1.03
Point#24	0.88	1.03
Point#26	0.91	1.03
Point#28	0.81	1.04
Point#29	0.85	1.03
Point#30	0.91	1.02
Point#31	0.91	1.01
Point#32	0.80	1.03
Point#33	0.87	1.02
Point#34	0.90	1.01

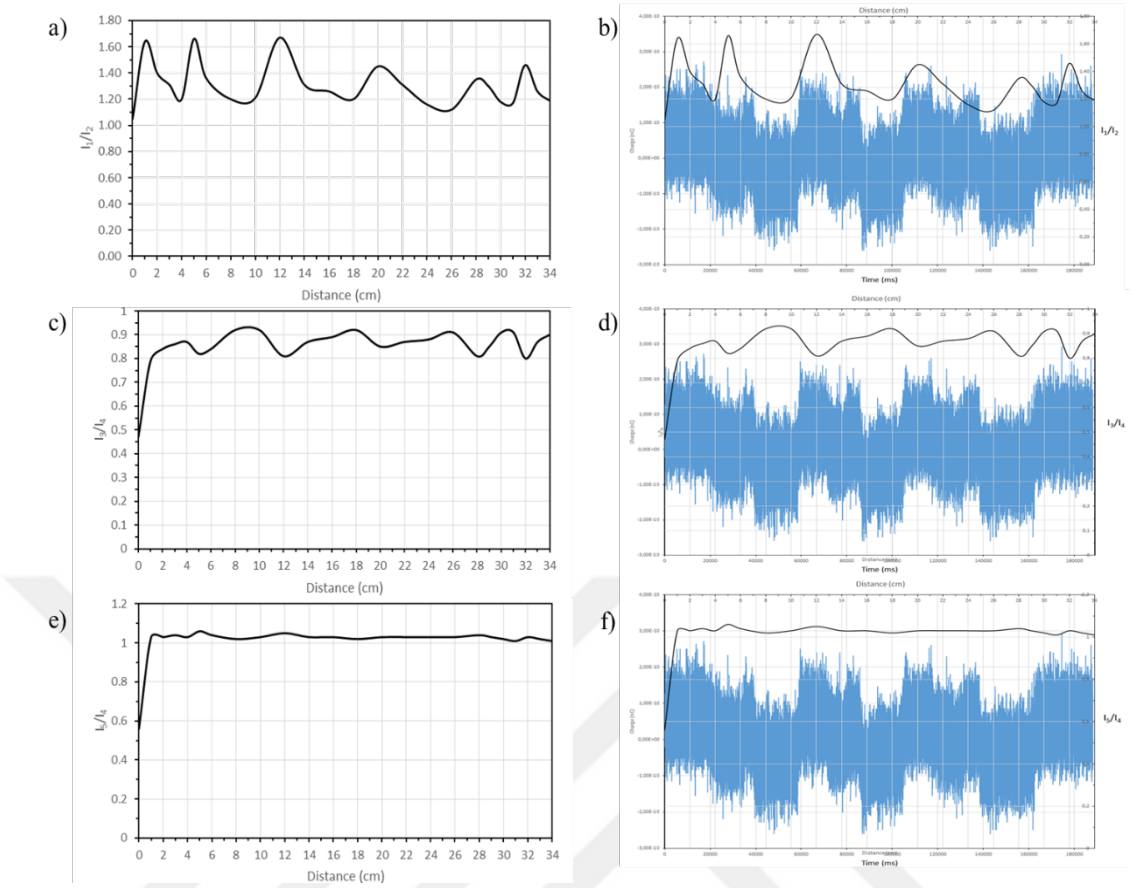

Figure 47. a) The Raman intensity ratio of the peaks at 808 cm^{-1} and 841 cm^{-1} (I_1/I_2) versus distance after the application of mechanical stress to PP film, b) The superimposed plot of the partial charge distribution and I_1/I_2, c) The Raman intensity ratio of the peaks at 2837 cm^{-1} and 2880 cm^{-1} (I_3/I_4) versus distance after the application of mechanical stress to PP film, d) The superimposed plot of the partial charge distribution and I_3/I_4, e) The Raman intensity ratio of the peaks at 2953 cm^{-1} and 2880 cm^{-1} (I_5/I_4) versus distance after the application of mechanical stress to PP film, f) The superimposed plot of the partial charge distribution and I_5/I_4.

It was verified that the charge mosaic on the surface, which was observed in the measurement of partial charge distribution, is in a good agreement with the fluctuations in the degree of crystallinity across the sample while the last three peaks at ~2837 cm^{-1}, ~2880 cm^{-1}, and the peak at ~2953 cm^{-1} that belong to the vibrational

assignment of C-H bond in CH_3 are not that much effective in the determination of crystallinity. On the other hand, it was showed that any relative variation between the peaks assigned for the crystalline (at 808 cm^{-1}) and amorphous regions (at 841 cm^{-1}) in i-PP are significant in terms of triboelectric charging of i-PP.

Chapter 4

Conclusion and Future Perspectives

In this thesis, the relation between the degree of crystallinity, which is a highly important parameter in the determination of polymers' physical properties, and the triboelectrical aspect of polypropylene was investigated. Since PP is widely used low-cost engineering plastic in industry due to its excellence in physical, thermal, and mechanical properties, it was studied in this current work.

As a first step after the performance of different treatment techniques (i.e. microwave radiation and tensile stress) the degree of crystallinity for PP film samples was altered. Then, the changes were determined qualitatively and quantitatively via analytical (XRD, DSC) and spectroscopic technique (Raman spectroscopy).

In the second part, the samples were characterized in terms of their physical (roughness), chemical (O/C), and triboelectrical properties. In this sense, it was observed that the increase in degree of crystallinity leads to an increment in the surface roughness of PP that determines the extent of contact between two surfaces (Cu and PP) during the metal-polymer contact electrification measurement. The potential mappings of the mechanically treated PP films suggest that by introducing mechanical stress the surface potential of the material can be increased. Furthermore, it was proved that the application of a mechanical action either by contact or by the application of tensile stress onto polymer film leads to the formation of a mosaic of nanoscopic patches of positive and negative charges. This mosaic structure was directed by the

coexistence of positive and negative CE, SE signals in the contact electrification of PP and by the partial charge distribution in the non-contact electrification of PP.

The contact and non-contact electrification experiments verified that by controlling the polymer's degree of crystallinity, hence the surface roughness it is possible to control the extent of static electrification which is crucial for both academia and industry.

As a future perspective it is important to analyze different polymers by taking different aspects of the experiments into account, such as studying the non-contact triboelectrification behavior of PP in only elastic region or only plastic region.

To sum up, it was revealed that it is possible to obtain different electrification capacities by varying the polymer's crystalline structure. Hence, we demonstrated the physical and mechanical properties have a considerable effect on the generation of static electricity from polypropylene that makes this study important in the polymer based triboelectrical applications, such as TENGs. As a result, this novel research leads us to a new perspective in tribological studies and triboelectric energy harvesting through mechanical action.

Bibliography

1. Stachowiak, G. and A.W. Batchelor, *Engineering tribology*. 2013: Butterworth-Heinemann.
2. Robb, K., *Thales of Miletus: The Beginnings of Western Science and Philosophy (review).* Journal of the History of Philosophy, 2005. **43**(1): p. 107-108.
3. Lowell, J. and A. Rose-Innes, *Contact electrification.* Advances in Physics, 1980. **29**(6): p. 947-1023.
4. Horn, R.G. and D.T. Smith, *Contact electrification and adhesion between dissimilar materials.* Science, 1992. **256**(5055): p. 362.
5. Homewood, K., *Surface Contamination and Contact Electrification*, in *Treatise on Clean Surface Technology*. 1987, Springer. p. 235-245.
6. Mort, J. and G. Pfister, *Electronic properties of polymers*. 1982: John Wiley & Sons.
7. Harper, W., *Contact and frictional electrification, 1967*. 1943.
8. Lowell, J., *Contact electrification of metals.* Journal of Physics D: Applied Physics, 1975. **8**(1): p. 53.
9. Loeb, L.B., *Static electrification*. 2012: Springer Science & Business Media.
10. Davies, D., *Charge generation on dielectric surfaces.* Journal of Physics D: Applied Physics, 1969. **2**(11): p. 1533.
11. Freund, T., *Tribo-electricity.* Advances in Colloid and Interface Science, 1979. **11**(1): p. 43-66.
12. Horn, R.G., D. Smith, and A. Grabbe, *Contact electrification induced by monolayer modification of a surface and relation to acid-base interactions.* Nature, 1993. **366**: p. 442-443.
13. Baytekin, B., H.T. Baytekin, and B.A. Grzybowski, *What really drives chemical reactions on contact charged surfaces?* Journal of the American Chemical Society, 2012. **134**(17): p. 7223-7226.
14. Baytekin, H.T., B. Baytekin, J.T. Incorvati, B.A. Grzybowski, *Material transfer and polarity reversal in contact charging.* Angewandte Chemie, 2012. **124**(20): p. 4927-4931.
15. Sow, M., R. Widenor, A. Kumar, S.W. Lee, D.J. Lacks, R.M. Sankaran, *Strain-Induced Reversal of Charge Transfer in Contact Electrification.* Angewandte Chemie International Edition, 2012. **51**(11): p. 2695-2697.
16. Meurant, G., *Tribology: a systems approach to the science and technology of friction, lubrication, and wear*. Vol. 1. 2009: Elsevier.
17. Gilbert, W., *Of the attraction exerted by amber, De Magnete, 1600, translated by P. Fleury Mottelay 1892*. 1958, Dover reprint New York.
18. Olenick, R.P., T.M. Apostol, and D.L. Goodstein, *Beyond the mechanical universe: from electricity to modern physics*. 1986: Cambridge University Press.
19. Brewster, D., *The Edinburgh Encyclopedia first American Edition*. 1832, Philadelphia.
20. Pounder, C., *The Quest for a Charging Mechanism to the End of the 19th Century.* Journal of Electrostatics, 1977. **3**(4): p. 389-394.

21. Boyle, R., *Experiments and notes about the mechanical origin and production of electricity*. 1975, London.
22. Faraday, M., *On the forms and states assumed by fluids in contact with vibrating elastic surfaces.* Philos. Trans. R. Soc. London, 1831. **121**(319): p. 1831.
23. Franklin, B. and W.T. Franklin, *Memoirs of the life and writings of Benjamin Franklin*. Vol. 1. 1818: H. Colburn.
24. Seanor, D.A., *Electrical properties of polymers*. 2013: Elsevier.
25. Maxwell, J.C., *A treatise on electricity and magnetism*. Vol. 1. 1892: Clarendon.
26. Baytekin, B., H.T. Baytekin, and B.A. Grzybowski, *Retrieving and converting energy from polymers: deployable technologies and emerging concepts.* Energy & Environmental Science, 2013. **6**(12): p. 3467-3482.
27. Liu, L., W. Oxenham, and A.-F.M. Seyam, *Contact electrification of polymeric surfaces.* Ind J Fiber Text Res, 2013. **38**: p. 265-269.
28. Williams, M., *The dependence of triboelectric charging of polymers on their chemical compositions.* Journal of Macromolecular Science—Reviews in Macromolecular Chemistry, 1976. **14**(2): p. 251-265.
29. Williams, M.W., *Triboelectric charging of insulating polymers–some new perspectives.* AIP Advances, 2012. **2**(1): p. 010701.
30. Apodaca, M.M., P.J. Wesson, J.M. Bishop, M.A. Ratner, B.A. Grzybowski, *Contact electrification between identical materials.* Angewandte Chemie, 2010. **122**(5): p. 958-961.
31. Boland, D. and D. Geldart, *Electrostatic charging in gas fluidised beds.* Powder Technology, 1972. **5**(5): p. 289-297.
32. Liang, S.-C., J.-P. Zhang, and L.-S. Fan, *Electrostatic characteristics of hydrated lime powder during transport.* Industrial & engineering chemistry research, 1996. **35**(8): p. 2748-2755.
33. Al-Adel, M.F., D.A. Saville, and S. Sundaresan, *The effect of static electrification on gas-solid flows in vertical risers.* Industrial & engineering chemistry research, 2002. **41**(25): p. 6224-6234.
34. Glor, M., *Hazards due to electrostatic charging of powders.* Journal of Electrostatics, 1985. **16**(2-3): p. 175-191.
35. Nifuku, M., T. Ishikawa, and T. Sasaki, *Static electrification phenomena in pneumatic transportation of coal.* Journal of Electrostatics, 1989. **23**: p. 45-54.
36. Pai, D.M. and B.E. Springett, *Physics of electrophotography*. Reviews of Modern Physics, 1993. **65**(1): p. 163.
37. Barry, C.R., N.Z. Lwin, W. Zheng, H.O. Jacobs, *Printing nanoparticle building blocks from the gas phase using nanoxerography.* Applied Physics Letters, 2003. **83**(26): p. 5527-5529.
38. Kelly, E. and D. Spottiswood, *The theory of electrostatic separations: A review Part I. Fundamentals.* Minerals Engineering, 1989. **2**(1): p. 33-46.
39. Tilmatine, A., S. Bendimerad, M. Younes, L. Dascalescu, *Experimental analysis and optimisation of a free-fall triboelectric separator of granular plastic particles.* International Journal of Sustainable Engineering, 2009. **2**(3): p. 184-191.

40. Tilmatine, A., K. Medles, S. Bendimerad, F. Boukholda, L. Dascalescu, *Electrostatic separators of particles: Application to plastic/metal, metal/metal and plastic/plastic mixtures.* Waste management, 2009. **29**(1): p. 228-232.
41. Eden, H.F. and B. Vonnegut, *Electrical breakdown caused by dust motion in low-pressure atmospheres: Considerations for Mars.* Science, 1973. **180**(4089): p. 962-963.
42. Thomas, P. and P.J. Gierasch, *Dust devils on Mars.* Science, 1985. **230**(4722): p. 175-177.
43. Gierasch, P.J., *Martian dust storms.* Reviews of Geophysics, 1974. **12**(4): p. 730-734.
44. Forward, K.M., D.J. Lacks, and R.M. Sankaran, *Triboelectric charging of lunar regolith simulant.* Journal of Geophysical Research: Space Physics, 2009. **114**(A10).
45. Forward, K.M., D.J. Lacks, and R.M. Sankaran, *Particle-size dependent bipolar charging of Martian regolith simulant.* Geophysical Research Letters, 2009. **36**(13).
46. Mehrotra, A., F.J. Muzzio, and T. Shinbrot, *Spontaneous separation of charged grains.* Physical review letters, 2007. **99**(5): p. 058001.
47. Pu, Y., M. Mazumder, and C. Cooney, *Effects of electrostatic charging on pharmaceutical powder blending homogeneity.* Journal of pharmaceutical sciences, 2009. **98**(7): p. 2412-2421.
48. Pingali, K.C., S.V. Hammond, F.J. Muzzio, T. Shinbrot, *Use of a static eliminator to improve powder flow.* International journal of pharmaceutics, 2009. **369**(1): p. 2-4.
49. Watanabe, H., M. Ghadiri, T. Matsuyama, Y.L. Ding, K.G. Pitt, H. Maruyama, S. Matsusaka, H. Masuda, *Triboelectrification of pharmaceutical powders by particle impact.* International journal of pharmaceutics, 2007. **334**(1): p. 149-155.
50. Murtomaa, M., V. Mellin, P. Harjunen, T. Lankinen, E. Laine, V. Lehto, *Effect of particle morphology on the triboelectrification in dry powder inhalers.* International journal of pharmaceutics, 2004. **282**(1): p. 107-114.
51. Lacks, D.J. and R.M. Sankaran, *Contact electrification of insulating materials.* Journal of Physics D: Applied Physics, 2011. **44**(45): p. 453001.
52. Harper, W., *Electrification following the contact of solids.* Contemporary Physics, 1961. **2**(5): p. 345-359.
53. Lowell, J. and W. Truscott, *Triboelectrification of identical insulators. II. Theory and further experiments.* Journal of Physics D: Applied Physics, 1986. **19**(7): p. 1281.
54. Randall, J. and M. Wilkins. *Phosphorescence and electron traps. ii. the interpretation of long-period phosphorescence.* in *Proceedings of the Royal Society of London A: Mathematical, Physical and Engineering Sciences*. 1945. The Royal Society.
55. Kron, A., T. Reitberger, and B. Stenberg, *Luminescence from γ-and β-irradiated HDPE and LLDPE.* Polymer international, 1997. **42**(2): p. 131-137.
56. Aitken, M.J., *Luminescence dating,* in *Chronometric dating in archaeology*. 1997, Springer. p. 183-216.

57. Meunier, M. and N. Quirke, *Molecular modeling of electron trapping in polymer insulators.* The Journal of Chemical Physics, 2000. **113**(1): p. 369-376.
58. Meunier, M., N. Quirke, and A. Aslanides, *Molecular modeling of electron traps in polymer insulators: Chemical defects and impurities.* The Journal of Chemical Physics, 2001. **115**(6): p. 2876-2881.
59. Cubero, D., N. Quirke, and D.F. Coker, *Electronic transport in disordered n-alkanes: From fluid methane to amorphous polyethylene.* The Journal of chemical physics, 2003. **119**(5): p. 2669-2679.
60. Yu, Z.-Z. and P. Watson, *Contact charge accumulation and reversal on polystyrene and PTFE films upon repeated contacts with mercury.* Journal of Physics D: Applied Physics, 1989. **22**(6): p. 798.
61. Yu, Z.-Z.G. and K. Watson, *Two-step model for contact charge accumulation.* Journal of Electrostatics, 2001. **51**: p. 313-318.
62. Hays, D.A., *ELECTRIFICATION DUE TO THE SEPARATION OF MATERIALS.* Digest of Literature on Dielectrics, 1979. **41**: p. 379.
63. Fuhrmann, J., *Contact electrification of dielectric solids.* Journal of Electrostatics, 1978. **4**(2): p. 109-118.
64. Diaz, A.F., J. Guay, *Contact Charging of Organic Materials: Ion vs Electron Transfer.* J. Res. Develop, 1993. **37**(2): p. 249-259.
65. McCarty, L.S. and G.M. Whitesides, *Electrostatic charging due to separation of ions at interfaces: contact electrification of ionic electrets.* Angewandte Chemie International Edition, 2008. **47**(12): p. 2188-2207.
66. Baytekin, H., A.Z. Patashinski, M. Branicki, B. Baytekin, S. Soh, B.A. Gryzbowski, *The mosaic of surface charge in contact electrification.* Science, 2011. **333**(6040): p. 308-312.
67. Salaneck, W., A. Paton, and D. Clark, *Double mass transfer during polymer-polymer contacts.* Journal of Applied Physics, 1976. **47**(1): p. 144-147.
68. Piperno, S., H. Cohen, T. Bendikov, M. Lahav, I. Lubomirsky, *The absence of redox reactions for Palladium (II) and Copper (II) on electrostatically charged teflon: Relevance to the concept of "Cryptoelectrons".* Angewandte Chemie International Edition, 2011. **50**(25): p. 5654-5657.
69. Sakaguchi, M., S. Shimada, and H. Kashiwabara, *Mechanoions produced by mechanical fracture of solid polymer. 6. A generation mechanism of triboelectricity due to the reaction of mechanoradicals with mechanoanions on the friction surface.* Macromolecules, 1990. **23**(23): p. 5038-5040.
70. Sakaguchi, M., Y. Miwa, S. Hara, Y. Sugino, K. Yamamoto, S. Shimada, *Triboelectricity in polymers: effects of the ionic nature of carbon–carbon bonds in the polymer main chain on charge due to yield of mechano-anions produced by heterogeneous scission of the carbon–carbon bond by mechanical fracture.* Journal of electrostatics, 2004. **62**(1): p. 35-50.
71. Wang, D., A.K. Klaassen, G.E. Janssen, E. Boer, R.J. Meier, *The detection of radicals in strained, high-modulus polyethylene fibres.* Polymer, 1995. **36**(22): p. 4193-4196.
72. Kaalund, C. and D. Haneman, *Positive ion and electron emission from cleaved Si and Ge.* Physical review letters, 1998. **80**(16): p. 3642.
73. Zimmerman, K., S.C. Langford, J.T. Dickinson, R.P. Dion, *Electron and photon emission accompanying deformation and fracture of polycarbonate.*

Journal of Polymer Science Part B: Polymer Physics, 1993. **31**(9): p. 1229-1243.
74. Wang, Z.L., *Triboelectric nanogenerators as new energy technology for self-powered systems and as active mechanical and chemical sensors.* ACS nano, 2013. **7**(11): p. 9533-9557.
75. Gundlach, R.W., *Electrostatic generator*. 1986, Google Patents.
76. Zhang, H., Y. Yang, Y. Su, J. Chen, C. Hu, Z. Wu, Y. Liu, C.P. Wong, Y. Bando, Z.L. Wang, *Triboelectric nanogenerator as self-powered active sensors for detecting liquid/gaseous water/ethanol.* Nano Energy, 2013. **2**(5): p. 693-701.
77. Zhu, G., C. Pan, W. Guo, C. Chen, Y. Zhou, R. Yu, Z.L. Wang, *Triboelectric-generator-driven pulse electrodeposition for micropatterning.* Nano letters, 2012. **12**(9): p. 4960-4965.
78. Zhu, G., Z. Lin, Q. Jing, P. Bai, C. Pan, Y. Yang, Y. Zhou, Z.L. Wang, *Toward large-scale energy harvesting by a nanoparticle-enhanced triboelectric nanogenerator.* Nano letters, 2013. **13**(2): p. 847-853.
79. Zhu, G., J. Chen, Y. Liu, P. Bai, Y.S. Zhou, Q. Jing, C. Pan, Z.L. Wang, *Linear-grating triboelectric generator based on sliding electrification.* Nano letters, 2013. **13**(5): p. 2282-2289.
80. Zhu, G., B. Peng, J. Chen, Q. Jing, Z.L. Wang, *Triboelectric nanogenerators as a new energy technology: From fundamentals, devices, to applications.* Nano Energy, 2015. **14**: p. 126-138.
81. Zhang, X.-S., M-D. Han, B. Meng, H-X. Zhang, *High performance triboelectric nanogenerators based on large-scale mass-fabrication technologies.* Nano Energy, 2015. **11**: p. 304-322.
82. Zheng, Q., B. Shi, F. Fan, X. Wang, L. Yan, W. Yuan, S. Wang, H. Liu, Z. Li, Z.L. Wang, *In Vivo Powering of Pacemaker by Breathing-Driven Implanted Triboelectric Nanogenerator.* Advanced Materials, 2014. **26**(33): p. 5851-5856.
83. Gowariker, V.R., N. Viswanathan, and J. Sreedhar, *Polymer science*. 1986: New Age International.
84. Shimizu, J., N. Okui, and T. Kikutani, *Simulation of dynamics and structure formation in high-speed melt spinning.* High Speed Fiber Spinning, Wiley/Interscience, New York, 1985: p. 173-201.
85. Kothari, V. and V. Gupta, *Manufactured Fiber Technology*. 1997, Published by Chapman & Hall. p.
86. Sperling, L.H., *Introduction to physical polymer science*. 2005: John Wiley & Sons.
87. Li, W. and D. Li, *On the correlation between surface roughness and work function in copper.* The Journal of chemical physics, 2005. **122**(6): p. 064708.
88. Galembeck, F., et al., *Friction, tribochemistry and triboelectricity: recent progress and perspectives.* RSC Advances, 2014. **4**(109): p. 64280-64298.
89. Coste, J. and P. Pechery, *Influence of surface profile in polymer-metal contact charging.* Journal of Electrostatics, 1981. **10**: p. 129-136.
90. Ohara, K., I. Nakamura, and M. Kinoshita, *Frictional electrification between flat surfaces of polymers and of Langmuir–Blodgett layers.* Journal of Electrostatics, 2001. **51**: p. 351-358.

91. Tripathi, D., *Practical guide to polypropylene*. 2002: iSmithers Rapra Publishing.
92. Saunders, K.J., *Organic polymer chemistry: an introduction to the organic chemistry of adhesives, fibres, paints, plastics, and rubbers*. 2013: Springer Science & Business Media.
93. Pethrick, R.A., *Polymer Structure Characterization: From Nano to Macro Organization in Small Molecules and Polymers*. 2013: Royal Society of Chemistry.
94. Ferry, J.D., *Viscoelastic properties of polymers*. 1980: John Wiley & Sons.
95. Karian, H., *Handbook of polypropylene and polypropylene composites, revised and expanded*. 2003: CRC press.
96. Hough, M. and R. Dolbey, *Modern Plastics Compendium, vol. 1—Key Properties and Sources.* Smithers Rapra Technology, 1995: p. 87-124.
97. Callister, W.D. and D.G. Rethwisch, *Fundamentals of materials science and engineering: an integrated approach*. 2012: John Wiley & Sons.
98. OGAWA, H., *Review on Development of Polypropylene Manufacturing Process.*
99. Liu, L., Y. Cai, A-F. Seyam, W. Oxenham, *Static Generation/Dissipation Measurements on Polymeric Films' Surfaces.*
100. McCrone, W.C., L.B. McCrone, and J.G. Delly, *Polarized light microscopy*. 1978: Ann Arbor Science Publishers Inc. and McCrone Research Institute.
101. Oldenbourg, R. and G. Mei, *Polarized light microscopy*. 1996, Google Patents.
102. Rugar, D. and P. Hansma, *Atomic force microscopy.* Physics today, 1990. **43**(10): p. 23-30.
103. Binnig, G., C.F. Quate, and C. Gerber, *Atomic force microscope.* Physical review letters, 1986. **56**(9): p. 930.
104. Quate, C. and C. Gerber, *Atomic Force Microscopy.* 1986.
105. Eaton, P. and P. West, *Atomic force microscopy*. 2010: Oxford University Press.
106. Glatzel, T., M.C. Lux-Steiner, E. Strassburg, A. Boag, Y. Rosenwaks, *Principles of Kelvin probe force microscopy*, in *Scanning probe microscopy*. 2007, Springer. p. 113-131.
107. Nony, L., *Principles of Kelvin Probe Force Microscopy and applications*. 2013, IM2NP-Aix Marseille Université.
108. Cassetta, A., *X-Ray Diffraction (XRD).* 2014.
109. Warren, B.E., *X-ray Diffraction*. 1969: Courier Corporation.
110. Scheirs, J., *Compositional and failure analysis of polymers: a practical approach*. 2000: John Wiley & Sons.
111. Stuart, B.H., *Polymer analysis*. Vol. 30. 2008: John Wiley & Sons.
112. Monasse, B. and J. Haudin, *Growth transition and morphology change in polypropylene.* Colloid and Polymer Science, 1985. **263**(10): p. 822-831.
113. Karger-Kocsis, J., *Polypropylene structure, blends and composites: Volume 3 composites*. 2012: Springer Science & Business Media.
114. Gardiner, D.J., *Introduction to Raman scattering*, in *Practical Raman Spectroscopy*. 1989, Springer. p. 1-12.
115. Bowley, H.J., D.L. Gerrard, JD Louden, G. Turrell, *Practical raman spectroscopy*. 2012: Springer Science & Business Media.

116. Nielsen, A.S., D. Batchelder, and R. Pyrz, *Estimation of crystallinity of isotactic polypropylene using Raman spectroscopy.* Polymer, 2002. **43**(9): p. 2671-2676.
117. Watts, J.F. and J. Wolstenholme, *An introduction to surface analysis by XPS and AES.* An Introduction to Surface Analysis by XPS and AES, by John F. Watts, John Wolstenholme, pp. 224. ISBN 0-470-84713-1. Wiley-VCH, May 2003., 2003: p. 224.
118. Briggs, D. and M.P. Seah, *Practical surface analysis by Auger and X-ray photoelectron spectroscopy.* D. Briggs, & M. P. Seah,(Editors), John Wiley & Sons, Chichester 1983, xiv+ 533, 1983.
119. Favaro, M.M., M.C. Branciforti, and R.E.S. Bretas, *A X-ray study of β-phase and molecular orientation in nucleated and non-nucleated injection molded polypropylene resins.* Materials Research, 2009. **12**(4): p. 455-464.
120. Aurrekoetxea, J., M.A. Sarrionandia, I. Urrutibeascoa, M.L. Maspoch, *Effects of injection moulding induced morphology on the fracture behaviour of virgin and recycled polypropylene.* Polymer, 2003. **44**(22): p. 6959-6964.
121. Mollova, A., R. Androsch, D. Mileva, M. Gahleitner, *Crystallization of Isotactic Polypropylene Containing Beta-Phase Nucleating Agent at Rapid Cooling*. J. European Polymer, 2013. **49**: p. 1057-1065.
122. French, A.D., M.S. Cintron, *Cellulose Polymorphy, Crystallite Size, and the Segal Crystallinity Index.* Springer: Cellulose, 2013. **20**(1): p. 583-588.
123. Jonassen N., Electrostatics, 1998. Springer Science+Business Media Dordrecht.
124. Jewett, J.W. and R.A. Serway, *Physics for scientists and engineers with modern physics*. 2008: Cengage Learning EMEA.
125. Gooding, D.M. and G.K. Kaufman, *Tribocharging and the triboelectric series.* Encyclopedia of Inorganic and Bioinorganic Chemistry, 2014.